Endocannabinoid system and the aging locus coeruleus

Doctoral thesis

to obtain a doctorate (PhD)

from the Faculty of Medicine

of the University of Bonn

Alessandra Gargano
from Rome, Italy
2022

Written with authorization of

the Faculty of Medicine of the University of Bonn

First reviewer: Prof. Dr. Andreas Zimmer

Second reviewer: Prof. Dr. Mauro Maccarrone

Day of oral examination: 23.11.2022

From the Institute of Molecular Psychiatry

Director: Prof. Dr. Andreas Zimmer

For all those who have been part of this journey.

Table of contents

List of abbreviations

2-AG	2-arachidonoylglycerol
5-CSRTT	5-choice serial reaction time test
AD	Alzheimer's disease
BLA	basolateral amygdala
BSA	albumin bovine fraction
BW	body weight
CA1	cornu ammonis 1
CA3	cornu ammonis 3
CB1r	cannabinoid receptor 1
CB2r	cannabinoid receptor 2
CD68	cluster of differentiation 68
CFC	contextual fear conditioning
Cnr1$^{-/-}$	constitutive CB1r knock-out
CNS	central nervous system
CRF	corticotropin-releasing factor
DAB	diaminobenzidine
DAGLα	diacylglycerol lipase alpha
DAGLβ	diacylglycerol lipase beta
DAPI	4',6-diamidino-2-phenylindole dihydrochloride
DBH	dopamine beta-hydroxylase
DG	dentate gyrus
DNA	deoxyribonucleic acid
dNTPs	deoxyribose nucleoside triphosphates
DSE	depolarization-induced suppression of excitation
DSP-4	N-(2-Chloroethyl)-N-ethyl-2-bromobenzylamine hydrochloride
eCBS	endocannabinoid system
eCBs	endocannabinoids
EDTA	ethylenediaminetetraacetic acid
EtBr	ethidium bromide

FI	food intake
GFAP	glial fibrillary acidic protein
HC	hippocampus
Iba1	ionized calcium-binding adaptor molecule 1
IHC	immunohistochemistry
ISH	*in situ* hybridization
ITI	inter-trial interval
LC	locus coeruleus
LH	limited hold time
Mb HY	mediobasal hypothalamus
NET	noradrenaline transporter
Pa CTX	parietal cortex
PB	phosphate buffer
PBS	phosphate-buffered saline
PCR	polymerase chain reaction
PD	Parkinson's disease
PFA	paraformaldehyde
PUbiquitin	serine 65-phosphorylated ubiquitin
RNA	ribonucleic acid
ROIs	regions of interests
SD	stimulus duration
SDS	sodium dodecyl sulphate
SEM	standard error of the mean
SN	substantia nigra
TH	tyrosine hydroxylase
TNFα	tumor necrosis factor alpha
VTA	ventral tegmental area
WT / Cnr1$^{+/+}$	wild-type

1. Introduction

1.1. Locus coeruleus: anatomy and functions

The locus coeruleus (LC), from Latin “blue spot”, is a small nucleus located in the pons of the brainstem, adjacent to the IVth ventricle, identifiable by a dark pigmentation due to neuromelanin granules within the neurons (**Figure 1**). The LC represents the major source of noradrenaline (NE) in the central nervous system (CNS).

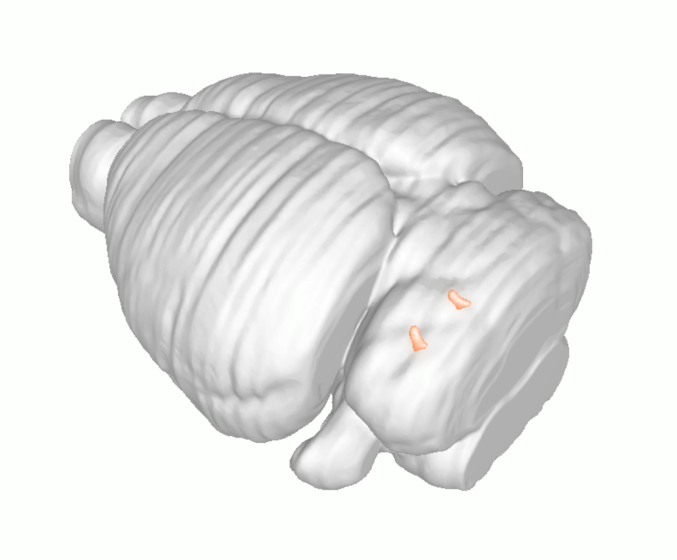

Figure 1: Locus coeruleus in a 3D model of a mouse brain.
3D reconstruction of a mouse brain with the LC nuclei highlighted using the EPFL’s Blue Brain Cell Atlas (EPFL, 2022: Blue Brain Cell Atlas. https://bbp.epfl.ch/nexus/cell-atlas/. Data accessed: 20.05.2022).

The overall number of LC noradrenergic neurons is surprisingly small: the most recent estimate counts 45–50 thousand neurons in a healthy young adult human (Sharma et al., 2010) and roughly 1500 in adult mice (Sturrok and Rao, 1985). Nevertheless, their projections reach far and wide: noradrenergic terminals richly innervate the cortex, mainly somatosensory and motor cortex (Gaspar et al., 1989), hippocampus, amygdala, hypothalamus and brainstem itself (Gaspar et al., 1989; Ginsberg et al., 1993; Radley et al., 2008; Sadikot and Parent, 1990; Westlund and Dan Coulter, 1980). The LC also receives a sizable number of afferents from the cortex, amygdala and spinal cord (Arnsten and Goldman-Rakic, 1984; Pammer et al., 1990; Westlund and Craig, 1996) (**Figure 2 A**).

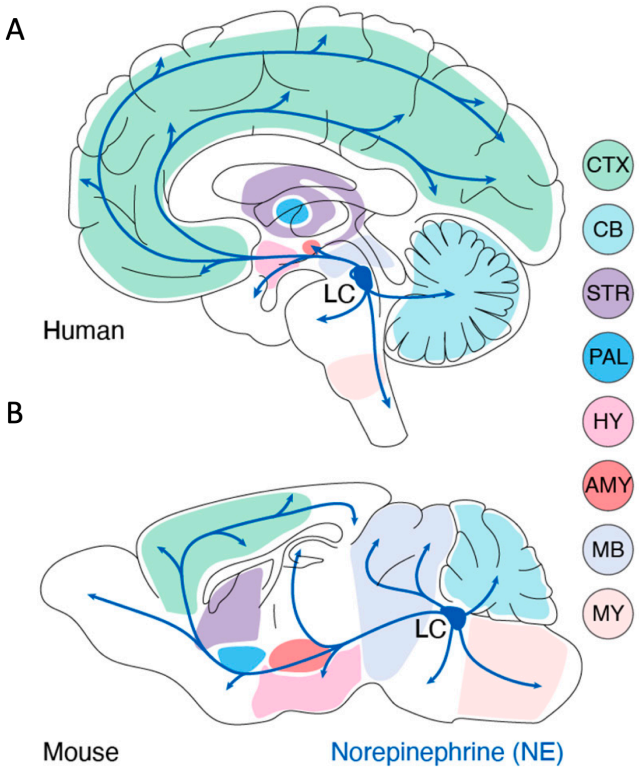

Figure 2: LC-NE system in humans and mice.
Anatomy of LC-NE efferents: comparison between a human **(A)** and a mouse **(B)** brain. Cortex (CTX), cerebellum (CB), striatum (STR), pallidum (PAL), hypothalamus (HY), amygdala (AMY), midbrain (MB) and medulla (MY). Adapted from Breton-Provencher et al. (2021).

Interestingly, this brain region appears to be well preserved among species: properties such as homogeneity in cell types and modularity in projection patterns are much comparable between humans and mice (**Figure 2 A – B**). Nevertheless, along the evolutionary path, more evolved species developed more LC cells, probably due to the need of modulating more complex behavioral responses (Wang et al., 2022).

Indeed, the LC plays a crucial role in modulating numerous cognitive functions such as attention, memory, the regulation of sleep/wake states and stress response (Berridge and Waterhouse, 2003). The peculiarity of LC noradrenergic neurons is an autonomic double-firing mode that changes according to the degree of attention required for a certain task: a tonic firing mode is associated with a low-attention state, while the shift toward a phasic firing mode represents a response to an attention-demanding stimulus (Aston-Jones and Cohen, 2005; Poe et al., 2020; Sara, 2009). Therefore, LC neurons function as an actual

cognitive “attention filter” as they facilitate the performances by releasing NE in the cortex and setting the optimal arousal level for task-relevant situations (Aston-Jones et al., 1991, 1994; Sara, 2009).

1.2. Locus coeruleus and age-related neurodegeneration

It has been widely demonstrated that the LC undergoes structural and functional changes in patients suffering from neurodegenerative diseases such as Parkinson’s disease (PD) and Alzheimer’s disease (AD) (Braak et al., 2003, 2011). The neuronal loss is massive in the LC of AD patients, being higher that the loss of cholinergic neurons in the nucleus basalis (67.9 % vs. 41.1%) (Ordureau et al., 2015) and also in PD patients being more severe than in the substantia nigra (83.2 % vs 77.8 %) (Hou et al., 2018). These changes are already observable in patients with just mild cognitive impairment (Reddy and Oliver, 2019).

However, although it seems well-known that the disruption of the noradrenergic system is linked to the onset and progression of neurodegenerative diseases, whether or not LC neurons are also lost during physiological aging is still debated (Flood and Coleman, 1988). Manaye et al. (1995) reported in a human postmortem study an age-related decrease in LC neuronal number of about 20-40 %, while other studies did not confirm such a reduction (Mouton et al., 1994; Ohm et al., 1997). Nevertheless, a recent in vivo human study, based on a sophisticated magnetization transfer weighted imaging technique, showed a correlation between LC signal intensity values and age, revealing for the first time an age-related decline in LC signal intensity values from the age of 60. In this study it was also shown that the age-related decline is not homogenous: it is significant in the rostral but not in the caudal regions of the LC (Liu et al., 2019). This last information is important as it shows how the LC, which had been thought to contain neurons whose axons indiscriminately innervate different regions, is not homogeneous at all and how distinct subpopulations innervate anatomically and functionally distinct targets (Poe et al., 2020). Several animal studies have indicated that the rostral LC projects to the cerebral cortex and forebrain, including the hippocampus, whereas the caudal LC innervates spinal cord and cerebellum, which suggests that a decrease in noradrenergic neuronal number in the LC could differently affects anterior and posterior brain regions (Morrison et al., 1979; Sanchez-Padilla et al., 2014).

While these findings support the hypothesis of an age-related loss of noradrenergic neurons in the human LC, for mice the results are controversial. For example, different studies conducted on CFW, ASH/TO and C57BL/6J mice reported that the mean LC cell number decreased with age and that this change inversely correlated with the memory performance of animals (Leslie et al., 1985; Sturrok and Rao, 1985; Tatton et al., 1991). Other studies, however, failed in replicating these data (Szot et al., 2009). Therefore, whether an age-related decline in the number of LC neurons is present in mice is still controversial. The discrepancies in the results obtained from the different studies may be attributed in part to the fact that different mouse strains have been used and in part to the fact that they did not use unbiased stereological counting.

Nonetheless, all together these data suggest that the LC cell population is particularly sensitive to age-related changes, although a unique explanation for this has not yet been identified. Several features of these neuronal population that could predispose them to such vulnerability have been considered. Firstly, the cytoarchitecture and high arborization of these cells: LC neurons have extremely long axons that have poor myelination, and this forces the cells to increase their energy production to perform efficiently, leading to an increase intracellular oxidative stress (Theofilas et al., 2015). Noradrenergic neurons are in fact known for their high bioenergetic need, which may exacerbate the vulnerability of these neurons (Weinshenker, 2018). In order to preserve their physiological function and their double-firing mode, LC neurons sustain their spiking rate with autonomous mitochondrial activity which inevitably leads to a raise in ROS production (Sanchez-Padilla et al., 2014), and eventually to a final global energetic failure. Another important remark concerns the exposure of LC neurons to environmental toxins and heavy metals. LC neurons are, in fact, particularly exposed to environmental toxins from both blood (innervating roughly 20 m of capillaries) and cerebrospinal fluid (the LC being in close proximity to the IVth ventricle) (Kisler et al., 2017; Pamphlett, 2014; Satoh and Iijima, 2019). Thus, all together these characteristics support the hypothesis that the survival capacity of noradrenergic neurons to aging is very different from any other neuronal type and that it strongly depends on the fine balance between neurodegenerative and neuroprotective processes.

1.3. Endocannabinoid system

In 1964, Δ9-tetrahydrocannabinol (THC), the psychoactive component of *Cannabis sativa*, was isolated for the first time (Gaoni and Mechoulam, 1964). Only three decades later the endogenous system interacting with THC was discovered and named the endocannabinoid system (eCBS).

The eCBS is an important neuromodulatory system composed of small lipophilic molecules called endocannabinoids (eCBs), their receptors (CBr), and the respective synthesizing and degrading enzymes.

The most abundant eCBs are 2-arachidonoylglycerol (2-AG) and anandamide (AEA). 2-AG and AEA are synthesized from membrane phospholipids by the enzymes diacylglycerol lipase alpha and beta (DAGLα/β) and N-acyl phosphatidylethanolamine phospholipase D (NAPE-PLD) (Devane et al., 1992; Mechoulam et al., 1995) and degraded by the enzyme monoacyl glycerol lipase (MAGL) and fatty acid amide hydrolase (FAAH), respectively, into arachidonic acid and glycerol or ethanolamine.

The first cannabinoid receptor was identified in humans in 1988 and named cannabinoid receptor 1 (CB1r); CB1r is encoded by the *Cnr1* gene, located on the chromosome 6 (6q15) (Devane et al., 1988; Matsuda et al., 1990). Subsequently, in 1993 in humans the second receptor was identified, named cannabinoid receptor 2 (CB2r), encoded by the *Cnr2* gene, located on the chromosome 1 (1p36.11) (Munro et al., 1993). Both CB1r and CB2r are G-protein-coupled receptors (GPCRs). CB1r is richly expressed in the central nervous system, on both GABAergic and glutamatergic neurons (Kawamura et al., 2006; Uchigashima et al., 2007), representing one of the most abundant GPCRs in the brain. It is indeed highly expressed in the hippocampus, cerebellum and cortex, where it seems to play an essential role in cognition, movement and emotional behavior (Eggan and Lewis, 2007; Herkenham et al., 1990; Mechoulam and Parker, 2013).

Although CB1r was thought to be localized specifically on the cell membrane, its expression has also been detected on mitochondria where it seems to play an essential role in neuronal energy metabolism (Bénard et al., 2012). Moreover, CB1r may also play an important role also in the communication between neurons and glia cells since it has also been found on both astrocytes and microglia (Castillo et al., 2012; Stella, 2009). Our

lab indeed showed that CB1r on GABAergic neurons influence neuron–microglia interaction through fractalkine/CX3CR1 signalling (Ativie et al., 2018).

In the CNS the eCBS acts as a brake. Indeed, the main function of the CB1r is to regulate the synaptic transmission by stopping the release of the neurotransmitter from the presynaptic terminal. Endocannabinoid production is triggered by the release of neurotransmitter, through the activation of Gq/11-coupled metabotropic receptors or the mobilization of Ca^{2+} in the postsynapse. Endocannabinoids are then released into the synaptic cleft and in a retrograde fashion bind to the presynaptic CB1r leading to a decrease in neurotransmitter release from the presynapse itself (**Figure 3**). This is possible because the CB1r is linked to Gi/o protein, inducing the inhibition of the adenyl cyclase activity with the subsequent downregulation of the cyclic adenosine monophosphate/protein kinase A (cAMP/PKA) pathway within the presynaptic neuron (Chevaleyre et al., 2007; Heifets and Castillo, 2009; Howlett et al., 2002; Kano et al., 2009; Mechoulam and Parker, 2013).

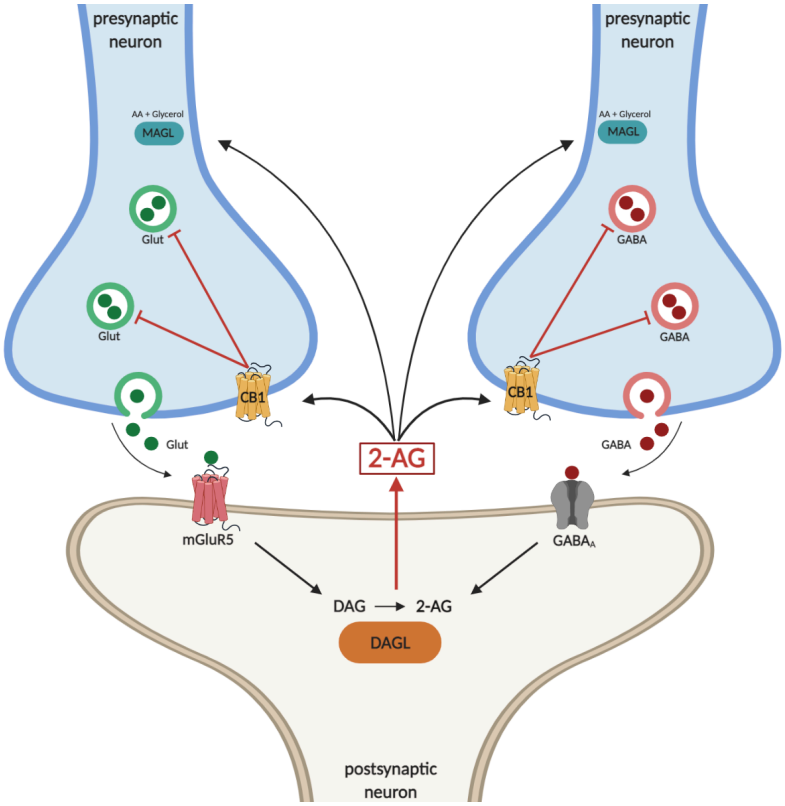

Figure 3: Overview of the eCBS.
Overview of the mechanism of action of the eCBS in both pre- and postsynaptic neurons.

Although this thesis will focus on the brain, it is important to mention that the eCBS is a key mediator in many peripheric systems such as cardiovascular, gastrointestinal and immune systems and it plays also a role in physiological processes such as bone formation and resorption, skeletal muscle formation and pregnancy (Maccarrone et al., 2015; Rossi et al., 2019).

1.3.1. Endocannabinoid system and brain aging

Many studies over the years have confirmed the pleiotropic nature of the eCBS and associated it with anti-inflammatory, neuromodulatory, and neuroprotective functions. The eCBS is indeed activated on demand in order to modulate many physiological functions, often after perturbations of the homeostasis, to restore the physiological state of the organisms (Di Marzo et al., 2004). By definition, aging is associated with a reduced capacity to respond to various challenges, therefore with an impairment in reestablishing homeostasis. The molecular and cellular hallmarks of aging have been cataloged in three main categories: a) primary hallmarks as causes of damage, b) antagonistic hallmarks as responses to damage and c) integrative hallmarks as culprits of the phenotype (López-Otín et al., 2013). The principal hallmarks from the first category includes telomere attrition, epigenetic modifications, genomic instability and impairment in proteostasis. The second group includes cellular senescence, deregulated nutrient sensing and mitochondrial dysfunction. The last classification includes inflammation, stress response, stem cell exhaustion, and altered intracellular communication. Interestingly, numerous studies have shown that the eCBS is involved in the modulation of many of the hallmarks of aging (Bilkei-Gorzo, 2012a). Some of the most important aspects are discussed in this paragraph.

In the first place, several data indicate that the eCBS is able to regulate ROS production and levels via different intracellular pathways. The first evidence supporting this hypothesis is an in vitro study showing that 2-AG is able to inhibit the production of ROS (Gallily et al., 2000). To explain this phenomenon in vivo, the cellular localization of the CB1r has been considered. Indeed, it has been shown that the majority of CB1r is not localized on the cell surface but instead it has an intracellular localization, on lysosomes and late endosomes (Brailoiu et al., 2011; Rozenfeld and Devi, 2008). Therefore, endocannabinoids can increase lysosomal stability and integrity, reducing the amount of

ROS by influencing the elimination of damaged macromolecules through these organelles. Supporting this evidence, data from our lab showed that mice knock-out for the CB1r ($Cnr1^{-/-}$ mice) have an impaired autophagosomal and lysosomal turnover, as well as a general increase in oxidative stress with an additional formation of lipofuscin-like aggregates in both neurons and microglial cells from aged animals (Bilkei-Gorzo et al., 2012b).

With regard to glia cells, it is important to mention that both astrocytes and microglia express CB1r and CB2r in an activity-dependent manner, therefore it was hypothesized that the eCBS could play an important role in neuron–glia communication and inflammation. It was indeed shown that endocannabinoids can modulate glial activity directly or indirectly by binding the glial endocannabinoid receptors (Eljaschewitsch et al., 2006; Navarrete and Araque, 2008; Stella, 2009) or by modulating neuronal activities (Albayram et al., 2011). Supporting this hypothesis, the eCBS appears generally upregulated in brain inflammation, as in multiple sclerosis (Eljaschewitsch et al., 2006), AD (Mulder et al., 2011), where it could counteract inflammation, confirming the studies in vitro showing that the elevation of anandamide levels or activation of the cannabinoid receptors by synthetic agonists inhibits the production of pro-inflammatory mediators and reduces microglial migration (Ortega-Gutiérrez et al., 2005; Romero-Sandoval et al., 2009; Tham et al., 2007).

The eCBS also seems to play a crucial role also in adult neurogenesis. Schuele et al. (2022) recently showed that the eCBS modulates adult hippocampal neurogenesis by promoting the proliferation and survival of neural stem and progenitor cells (NSPCs) and that Daglα in NSPCs from the dentate gyrus or astrocytes is an essential regulator of this process.

Lastly, one of the major highlights regarding the eCBS of the last few years is its role in mitochondria regulation. As mentioned above, aging is characterized by a massive mitochondrial dysfunction, leading to an increased intracellular oxidative stress. Recently, several lines of evidence revealed how much the eCBS, especially the CB1r signalling, influences mitochondrial activity. Indeed, Bénard et al. (2012) showed that CB1r is present at the membranes of neuronal mitochondria (mtCB1r), where it directly modulates cellular respiration and energy production. Furthermore, through the activation of mtCB1r, cyclic AMP concentration, protein kinase A activity, complex I enzymatic activity and respiration

in neuronal mitochondria are decreased, emphasizing the essential role played by the CB1r in the regulation of neuronal energy metabolism.

Overall, these data support the hypothesis of an important role of the eCBS in brain aging; however, several lines of evidence indicate that also the eCBS undergoes changes during lifetime (Di Marzo et al., 2015). For example, in rodents CB1r mRNA levels are elevated during adolescence, stay stable during adulthood, but decline in different brain areas in old animals (Berrendero et al., 1998). In the same way, the mRNA level of NAPE-PLD increase during aging, whereas DAGLα peaks in young adults and drops in older individuals in both hippocampus and prefrontal cortex. FAAH mRNA shows only a slight increase with aging, while MAGL mRNA levels are highest during childhood and decrease thereafter (Long et al., 2012; Piyanova et al., 2015). These changes might be responsible for some of the age-specific alterations in behavioral tests following cannabinoid exposure. A great example of these age-specific differences is the study from Bilkei-Gorzo et al. (2017) showing for the first time that a low dose of THC can reverse the age-related decline in cognitive performance in old mice tested with the Morris water maze task. This behavioral effect also was accompanied by an enriched expression of synaptic markers and hippocampal spine density. However, young mice treated with the same low dose of THC performed significantly worse compared to age-matched vehicle treated controls, indicating a different endogenous cannabinoid tone regulating the whole process. The evidence that the eCBS undergoes changes during its lifetime could also explain why young $Cnr1^{-/-}$ mice performed as well as wild-type mice in behavioral models of skill-learning, partner recognition, and operant conditioning, while the performance of mature $Cnr1^{-/-}$ mice was much worse. In fact, in most of the tests, mature $Cnr1^{-/-}$ mice performed at the same level as old animals, additionally showing a loss of neurons in the CA1 and CA3 regions of the hippocampus (Bilkei-Gorzo et al., 2005).

Overall, these studies indicate that the disruption of the endocannabinoid signalling enhances an age-related decline in brain (and a number of tissues in which they have important physiological functions) and link the eCBS in the control of the aging process.

1.4. Endocannabinoid signalling in LC-NE system

LC neurons express receptors for a wide variety of transmitters and neuromodulators including endocannabinoid receptors. There are several pieces of evidence indicating a

prominent endocannabinoid modulation of the LC neuronal properties. First of all, CB1r were also identified on noradrenergic axon terminals in the frontal cortex, one of the main projection areas of the LC. In general, CB1r-immunoreactivity was localized pre- and post-synaptically. Of the immunoreactive structures, 66 % are somatodendritic structures, 22 % are axon terminals, and 12 % are structures associated with glial and small unmyelinated axon (Scavone et al., 2011) confirming a heterogeneous distribution of CB1r in LC neurons. Although CB1r can influence both inhibitory and excitatory signaling, most of the axonal CB1r in the LC are on inhibitory synapses. Consistent with these findings, the administration of WIN55,212-2, a strong CB1r agonist, has been shown to increase forebrain NE release as well as a general noradrenergic activity (Oropeza et al., 2005; Páldy et al., 2008).

Wyrofsky et al. (2017), through immunofluorescence and high-resolution immunoelectron microscopy, showed that in noradrenergic neurons the CB1r directly co-localize with the corticotropin-releasing factor (CRF), a primary mediator of stress-induced activation of noradrenergic neurons; the functional interaction between them supported the idea that the eCBS is poised to directly modulate stress response through the LC-NE system. Furthermore, to determine whether the deletion of CB1r altered LC signaling, they applied whole-cell patch-clamp to LC neurons of both wild-type and $Cnr1^{-/-}$ mice, finding that CB1r deletion caused a global disruption in LC-NE signaling. In detail, CB1r deletion caused a significant increase in LC-NE excitability and input resistance, a significant increase in cortical NE levels, tyrosine hydroxylase and CRF levels in the LC compared to wild-type controls, and a significant increase in LC α2-AR levels (only in females). Interestingly, LC neurons from $Cnr1^{-/-}$ mice also seemed unresponsive to CRF, a strong activator of LC neurons, compared to wild-type mice (Wyrofsky et al., 2019). Altogether, these results strongly support the hypothesis of a basal endocannabinoid regulation of LC-NE activity.

As mentioned above, during the lifetime LC noradrenergic neurons may become particularly dependent on the activity of neuroprotective mechanisms because of their high vulnerability; besides, the factors contributing to this vulnerability (increased oxidative stress, pacemaking activity, impaired proteostasis due to the high arborization, high load on mitochondria due to the big energetic need) are all influenced by the endocannabinoid system. The eCBS, indeed, not only seems to influence generally the development of brain aging, but may also influence neuronal survival as for hippocampal neurons (Bilkei-

Gorzo et al., 2005). Nevertheless, whether the eCBS takes on a neuroprotective role in LC noradrenergic neurons throughout aging (as seen for the hippocampus) is still not known.

1.5. Aim of the study

LC neurons represent the main source of noradrenaline in the brain. However, this brain region is known to be vulnerable to age-related changes in humans. The primary aim of this study was to investigate how the ECS, and especially the CB1r, affected the survival capacity of LC noradrenergic neurons to aging. To do so, we compared the age-related decline in the number of noradrenergic neurons, using stereological counting, and the density of noradrenergic axon terminals in the main efferent areas of LC, using IHC, between wild-type and $Cnr1^{-/-}$ mice. Moreover, to understand the mechanism through which CB1r influences the survival of LC neurons, we compered histological signs of neuroinflammation and mitochondrial dysfunction between wild-type and $Cnr1^{-/-}$ mice.
Contextually, we aimed to understand how the ECS itself is influenced by aging in the LC. Therefore, we analyzed the protein and mRNA expression of DAGL enzyme in young and old wild-type mice.
Among the main findings of this thesis, we show that in C57BL/6J mice the LC goes through an age-related neurodegenerative process involving the 20 % of noradrenergic neurons. Our next goal was to investigate whether this age-related decrease of noradrenergic neurons could be responsible for the fear memory and attention impairments observed in old individuals. For that, we first determined the dose of DSP-4 toxin which induces a similar reduction in noradrenergic neuronal numbers as aging. Next, we assessed whether this dose of DSP-4 induced similar deficits in the contextual fear conditioning and in the 5-choice serial reaction time tests in young animals as observed in aged ones.

2. Material and methods

2.1. Chemicals

Chemical	Company (catalog number)
100 bp DNA ladder	Life Technologies (15628-050)
2-Methylbutane/Isopentane	Sigma-Aldrich (320404)
2-Propanol/Isopropanol	Carl Roth (6752.4)
4',6-Diamidino-2-phenylindole dihydrochloride (DAPI)	Sigma-Aldrich (10236276001)
Albumin bovine fraction V, pH = 7.0 (BSA)	Serva (11930.04)
Ammonium nickel sulfate (NH_4Ni-$(SO_4)_2$)	Sigma-Aldrich (A1827)
Citric acid	Promega (H526a)
Diaminobenzidine (DAB)	Sigma-Aldrich (D7304)
dNTP mix (10 mM)	Sigma-Aldrich (D7295)
Ethylenediaminetetraacetic acid (EDTA)	Calbiochem (324503)
Ethanol (EtOH)	VWR (20821.330)
Ethidium bromide solution (10 mg/ml)	Sigma-Aldrich (E1510)
Hydrochloric acid (HCl) 37 %	Carl Roth (X942.1)
Hydrogen peroxide 30 %	TH.GEYER (A1134,0500)
Paraformaldehyde (PFA)	Sigma-Aldrich (P6148)
Phosphate-buffered saline (PBS)	Gibco (18912014)
Proteinase K	NEB (P8107S)
Roti Histokitt II mounting medium	Carl Roth (T160.1)
Sodium chloride (NaCl)	Carl Roth (9265)
Sodium dodecyl sulphate (SDS)	Carl Roth (2326)
Sucrose	Sigma-Aldrich (84100)
Taq polymerase (10x ThermoPol buffer)	NEB (M0267X)
Tris base	Carl Roth (5429)
Tris/HCl	Carl Roth (9090.3)
Triton™ X-100	Sigma-Aldrich (T9284)
TWEEN® 20	Sigma-Aldrich (P9416)

Vectastain Elite ABC-HRP kit (ABC-reagent)	Biozol (VEC-PK-6100)
UltraPure™ agarose	Invitrogen (15510-027)

Table 1: List of chemicals.

2.2. Solutions

2.2.1. Genotyping

Solution/buffer	Composition
Lysis buffer	MilliQ H_2O
	100 mM Tris/HCl pH = 8.0
	5 mM EDTA
	200 mM NaCl
	0.2 % (w/v) SDS
	Proteinase K (1 mg/ml)
EtBr bath	TAE Buffer
	1.5 µg/ml Ethidium bromide
Tris-EDTA (TE) buffer, pH = 7.4	MilliQ H_2O
	10 mM Tris
	1 mM EDTA, pH = 8.0
Tris-acetate-EDTA (TAE) buffer	MilliQ H_2O
	40 mM Tris-acetate
	1 mM EDTA pH = 8.0

Table 2: List of solutions for genotyping.

2.2.2. Immunohistochemistry

Solution/buffer	Composition
PBS 1x pH = 7.4 (500 ml)	500 ml MilliQ H_2O

	1 PBS tablet
0.1M Phosphate Buffer (PB), pH = 7.4	500 ml MilliQ H_2O
	0.02 M Sodium phosphate monobasic
	0.08 M Sodium phosphate dibasic
TBS 10X	1 L MilliQ H_2O
	200 mM Tris
	1.5 M NaCl
4 % formaldehyde	PBS 1x
	4 % (w/v) PFA powder, filtered
Cryoprotectant	PBS 1x
	20 % Sucrose
Stereology – TH staining	
Permeabilization	PBS
	0.5 % Triton X-100
Blocking solution	PBS
	3 % BSA
Antibody solution	PBS
	0.5 % BSA
	0.05 % Triton X-100
ABC-reagent	Avidin-biotin complex
Reagent bath	50 mM Tris pH 7.3
	0.5 mg/mL DAB
	0.5 mg/mL NH4Ni-Sulphate

TH – Iba1 – TNFα – CD68 co-staining	
Permeabilization	PBS
	0.5 % Triton X-100
Blocking solution	PBS
	3 % BSA
	0.05 % Triton X-100
Antibody solution	PBS
	0.3 % BSA
	0.05 % Triton X-100
TH – PUbiquitin – GFAP co-staining	
Permeabilization	PBS
	0.5 % Triton X-100
Blocking solution	PBS
	3 % BSA
	0.05 % Triton X-100
Antibody solution	PBS
	0.5 % BSA
	0.05 % Triton X-100
TH – DAGLα co-staining	
Permeabilization	PB
	0.5 % Triton X-100
Blocking solution	3 % BSA
	0.05 % Triton X-100

Antibody solution	0.3 % BSA
	0.05 % Triton X-100
NET staining	
Antigen retrieval solution – Citrate buffer, pH = 6	1 L MilliQ H_2O
	1 ml TWEEN® 20
	17.5 mM Citric acid
Washing buffer	TBS
	0.5 % Triton X-100
Blocking solution	3 % BSA
	5 % NDS
	5 % NGS
	0.5 % Triton X-100
Antibody solution	*see blocking solution

Table 3: List of solutions for IHC.

2.3. Antibodies

Primary Antibodies					
Name	**Antigen**	**Host**	**Dilution**	**Company**	**Catalog #**
TH	Tyrosine Hydroxylase	Sheep	1:1000	abcam	ab113
Iba1	Ionized calcium-binding adaptor molecule 1	Rabbit	1:1000	FUJIFILM Wako	019-19741
TNFα	Tumor necrosis factor alpha	Mouse	1:100	abcam	Ab1793

CD68	Cluster of differentiation 68	Rat	1:1000	Bio-RAD	AB_322219
PUbiquitin	Ser65	Rabbit	1:500	Millipore	ABS1512-I
DAGLα	Diacylglycerol lipase alpha	Rabbit	1:300	Frontier Institute Japan	AF380
NET	Noradrenaline transporter	Rabbit	1:2000	Synaptic Systems	260003
Secondary Antibodies					
Antigen	**Conjugate**	**Host**	**Dilution**	**Company**	**Catalog #**
Sheep IgG	AF488	donkey	1:1000	Life technologies	A11015
Sheep IgG	Biotin	donkey	1:500	abcam	ab97123
Rabbit IgG	AF647	goat	1:1000	Thermo Fisher Scientific	A21245
Rabbit IgG	AF568	goat	1:1000	Life technologies	A11036
Rabbit IgG	Cy3	goat	1:1000	Merk	AP132C
Mouse IgG	AF647	donkey	1:1000	Invitrogen	A31571
Rat IgG	AF647	goat	1:1000	Life technologies	A21247

Table 4: List of antibodies.

2.4. Anesthesia

Medication	Company	Working solution (ml)
Xylazin (2 %)	Bela-pharm gmbH & Co. KG, Vechta	1
Ketaminhydrochlorid solution for injection	Bela-pharm gmbH & Co. KG, Vechta	2
Saline	Sigma-Aldrich	3

Table 5: List of solutions for anesthesia.

2.5. Animals

We used C57BL/6J wild type (WT) and B6.cg Cnr1tm1Zim (constitutive CB1r knock-out mice, $Cnr1^{-/-}$. MGI:1857762) mice. Cnr1 mutation was created through homologous recombination in MPI2 embryonic stem cells by inserting a neo cassette and replacing amino acids 33-447 of the coding region, corresponding to most of the coding sequence of the gene. $Cnr1^{-/-}$ were bred homozygously and backcrossed with C57BL/6J line every 5-6 generations in order to minimalize the risk of a genetic drift (Zimmer et al., 1999). The mouse strains were housed and bred under specific-pathogen-free conditions in the main animal facility of the University Hospital Bonn (UKB). At the age of 21 days, the pups were weaned and group-housed in standard laboratory cages with automatic ventilation system and *ad libitum* water and food. Normally, all the animals were kept under 12 hour light-dark cycle (lights on at 09:00 am). However, when directed to behavioral studies, the animals were moved to a room with a reversed 12 hour light-dark cycle (lights off at 09:00 am) in order to test them during their active phase. Cages were monitored daily and bedding, water and food were changed weekly. Care of the animals and conduction of the experiments followed the guidelines of the European Communities Directive 86/609/EEC and the German Animal Protection Law regulating animal research. Animal experiments were approved by the Landesamt fuer Natur, Umwelt und Verbraucherschutz Nordrhein-Westfalen (LANUV NRW; 81-02.04.2020.A360; 81-02.04.2019.A423).

2.5.1. Experimental groups

The different cohorts of mice we used throughout the experiments are summarized in **Table 6**.

In order to understand the aging effect on the number of TH-positive cells and DAGLα protein expression within the LC, we used a cohort composed of 14 3- and 22-month-old wild-type mice. To outline the timeline of LC age-related neurodegeneration, we used six different age groups of wild-type mice: 2-3, 4-6, 7-9, 11-13, 14-16 and up to 24 months. Each group consisting of 3-4 animals. Another small cohort of wild-type animals (4 2-month-old and 4 18-month-old) has been used for the RNAscope experiment.

To understand the differences between wild-type and Cnr1$^{-/-}$ animals we used a cohort made of 10 3-and 18-month-old Cnr1$^{-/-}$ and 12 age-matched wild type controls. We used this cohort to establish: number of TH-positive cells, inflammatory (Iba1, TNFα, CD68, microglia morphology) and autophagic/mitophagic (PUbiquitin, Lipofuscin) profile within the LC and noradrenergic axon terminal density in different brain regions (NET).

In order to establish the dose of DSP-4 toxin to use so as to obtain the 20 % of reduction in the number of LC noradrenergic neurons, we used a cohort of 30 wild-type animals that were injected with different toxin concentrations (vehicle, 6.25, 12.5, 25, 50 mg/kg); 6 animals per dose were injected at the age of 5 weeks.

For the behavioral studies comparing young versus old mice, 20 animals (10 3-month-old and 10 20-month-old) for the fear conditioning and 22 (12 3-month-old and 10 19-month-old) for the 5-CSRTT have been used.

For the behavioral studies comparing DSP-4 injected mice versus controls, 20 animals (10 DSP-4 injected and 10 controls) for the fear conditioning and 30 animals (15 DSP-4 injected and 10 controls) for the 5-CSRTT have been used. All the animals used for behavioral studies were also used for the immunohistochemical analysis of NET in prefrontal cortex.

Experiment	Sex	Age (months)	Line/Strain	Genotype	No. of animals
- Aging effect on LC; - DAGLα protein expression within the LC	Males	- 3 - 22	C57BL/6J	WT	14
- Timeline of LC age-related neurodegeneration	Males	- 2-3 - 4-6 - 7-9 - 11-13 - 14-16 - up to 24	C57BL/6J	WT	3-4 per age group
- DAGLα and DAGLβ RNAscope experiment	Males	- 2 - 18	C57BL/6J	WT	8
- Differences between wild-type and $Cnr1^{-/-}$ animals	Males	- 3 - 18	B6.cg Cnr1 tm1Zim	$Cnr1^{+/+}$ $Cnr1^{-/-}$	22
- DSP-4 dose establishment	Males	- 1	C57BL/6J	WT	30
- Fear conditioning: young vs old	Males	- 3 - 20	C57BL/6J	WT	20
- 5-CSRTT: young vs old	Males	- 3 - 20	C57BL/6J	WT	22
- Fear conditioning: DSP-4 vs controls	Males	- 4	C57BL/6J	WT	20
- 5-CSRTT: DSP-4 vs controls	Males	- 5	C57BL/6J	WT	30

Table 6: Experimental groups.

2.6. Genotyping

2.6.1. DNA isolation

Right after weaning, mouse tail tip biopsies were taken. The tissue was lysed in 200 µl of lysis buffer with freshly added 3-5 µl of Proteinase K (1 mg/ml) and placed at 55° C with shaking at 550 rpm overnight. The next day, the samples were centrifuged (13000 x g, 10 min, 4° C) to remove debris, the supernatant was transferred to a new Eppendorf tube and added with 200 µl of isopropanol, gently inverting the tube several times. Afterwards, samples were centrifuged to obtain DNA pellet. Precipitated DNA pellet was washed with 70 % ethanol and air-dried. Finally, the DNA was dissolved in 50-100 µl of TE buffer and stored at 4° C.

2.6.2. DNA amplification by polymerase chain reaction (PCR)

A description and a list of PCR components used are listed below (see **2.6.3** and **0**). For the PCR master mix, first MilliQ water, 10x ThermoPol buffer, deoxyribose nucleoside triphosphates (dNTPs) and primers were mixed, then Taq-Polymerase was added at last and the PCR reaction was distributed to PCR tubes. DNA was added to each tube at last.

2.6.3. Primers

Primer	Sequence
Primer COMM (Fw)	CTC CTG GCA CCT CTT TCT CAG TCA
Primer WT (Rv)	TGT GTC TTC TGC TGG AAC CAA CGG
Primer KO (Rv)	TCT CTC GTG GGA TCA TTG TTT TTC TCT TGA

Table 7: List of primers.

2.6.4. PCR for CB1r knock-out

Mix:	**µl**
H_2O	15.5
10x Buffer	2
Primer COM	0.5
Primer WT	0.3
Primer KO	0.7
dNTPs	0.5
Taq pol	0.5
DNA template	1
	total = 21

Table 8: PCR for CB1r knock-out.

2.6.5. PCR program for CB1r knock-out

Cycle	Temperature	Time (min)
1x	94° C	04:00
35x	94° C 65° C 68° C	00:45 00:45 01:00
1x	68° C	07:00
1x	4° C	∞

Table 9: PCR program for CB1r knock-out.

2.6.6. Gel electrophoresis

Agarose gel 2 % concentrated was prepared by dissolving agarose in TAE buffer and left to harden at room temperature for at least 45 minutes. It was subsequently transferred to the electrophoresis chamber filled with TAE buffer. Each PCR product was added with 10x loading dye. All samples were loaded on the gel into wells. In the first well, 5 µl of 100 bp DNA ladder was loaded to enable the size estimation of the PCR product size. Then, electrophoresis ran at 120 V for 90-100 minutes. The gel was then immerged in a bath

with ethidium bromide for 15 minutes and visualized with ChemiDoc MP imaging system (Bio-Rad Laboratories). Expected band size for homozygous Cnr1$^{-/-}$ mice was 334 bp while homozygous wild-type control band was 284 bp; heterozygous animals showed both.

2.7. DSP-4

DSP-4 (N-(2-Chloroethyl)-N-ethyl-2-bromobenzylamine hydrochloride) is a widely used neurotoxin which is able to pass the blood–brain barrier as a tertiary amine and form quaternary derivatives within the brain. There, it blocks the release of noradrenaline at the nerve terminals, selectively binding neuronal noradrenalin uptake transporter and depletes noradrenaline levels. In rodents, DSP-4 produces a dose dependent degeneration of noradrenergic neurons in the LC. Because of its instability, DSP-4 was dissolved in MilliQ water at pH 5 and freshly prepared before use. The compound was injected intraperitoneally in different concentration (described in the **Result 3.7** section).

2.8. Behavioral studies

2.8.1. Contextual fear conditioning

Fear conditioning (FC) is a Pavlovian behavioral paradigm in which the animal learns to associate a neutral conditioned stimulus with an aversive unconditioned stimulus, showing a conditioned response resulting from the creation of fear memories. In our case, the conditioned stimulus was the context itself (contextual fear conditioning, CFC), the unconditional stimulus was a mild foot shock, and the conditioned response was measured in terms of freezing behavior. We used The UGO BASILE ANY-maze controlled Fear Conditioning System, consisting of: FC-Unit (55 x 60 x 57 cm), FC-Cage with electrified floor (24 x 20 x 30 cm) (**Figure 4**), an individual controller on-board (version 1.1.6), an ANY-maze software (ANY-maze 6.3 ©1999-2021 Stoelting Co.).

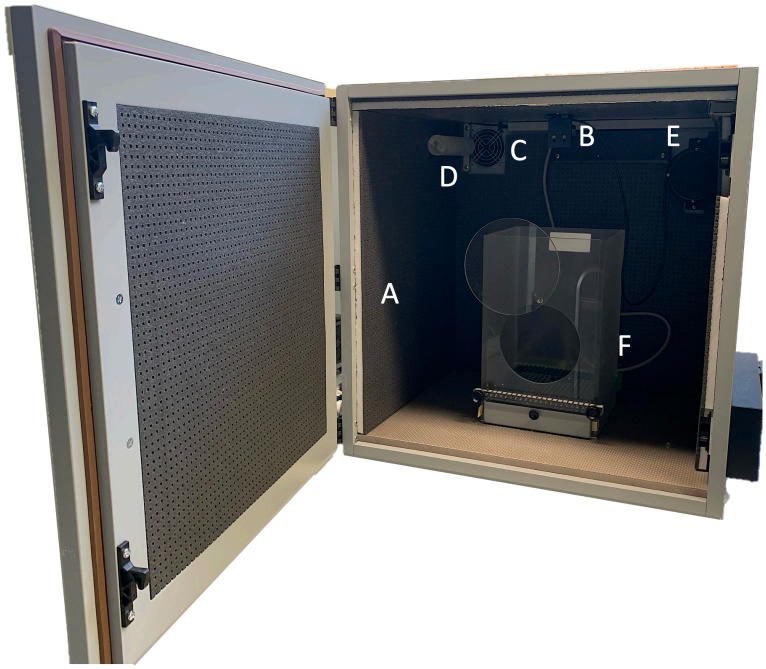

Figure 4: CFC setup.
FC-Unit encompassing a Sound-Attenuating Box **(A)**, a USB-camera **(B)**, ventilating fan **(C)**, a dual (visible/I.R.) light **(D)**, a speaker **(E)** and a FC-Cage **(F)**.

Animals were single caged and kept on a reversed light-dark cycle one week before the beginning of the test. On the first day of test, mice were exposed to the fear conditioning protocol: for the first 3 minutes they were free to explore the FC-Cage (cage light: 30 lux; white noise: 10 units), and afterwards received a 2 seconds foot shock (intensity: 0.8 mA) every minute for a total of three times. From the next day until day 4 the mice were placed daily in the same context for 3 minutes without any unconditioned stimulus, in order to establish the freezing behavior post-conditioning. The detection of freezing was automated and based on video analysis.

2.8.2. 5-Choice serial reaction time test

5-choice serial reaction time test (5-CSRTT) is a behavioral test extensively used to measure attention in rodents. We used the 5-9 Holes Box Operant Conditioning (LE507-76-0001), from Panlab Harvard Apparatus (**Figure 5**) and the PACKWIN software (Panlab, v2.0.07). Animals are trained to respond to a brief, unpredictable visual stimulus

(hole illumination) presented in one of five locations in order to obtain a food reward (reinforcement).

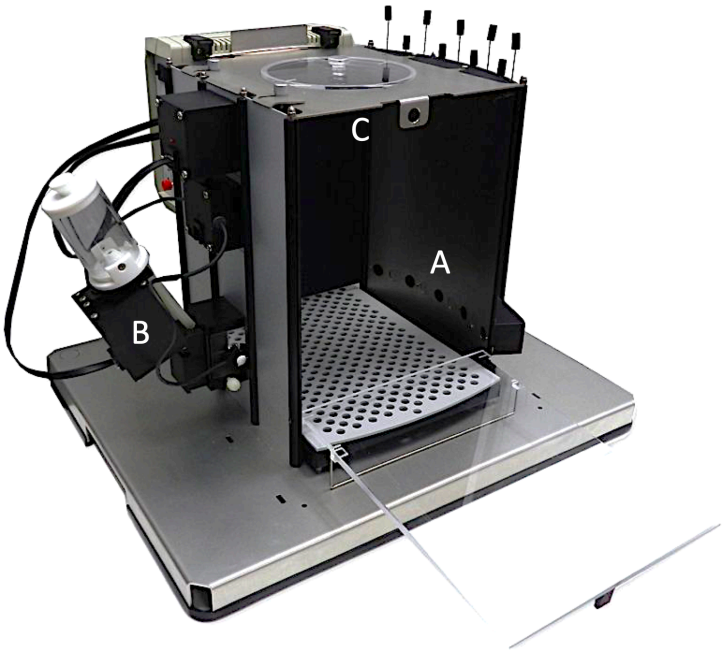

Figure 5: 5-CSRTT Box Operant.
5 illuminable holes **(A)**, food dispenser **(B)**, cage light **(C)**.

Animals were single caged and kept on a reversed light-dark cycle one week before the beginning of the test. For the first five days, food intake (FI) and body weight (BW) were measured for each animal in order to have an average of the food consumed daily in relation with body weight. Afterwards, on day 7, mice were food deprived. On day 8, the 5-CSRTT started. For the whole duration of the test the animals were fed 0.7 - 0.9 % of their normal FI, based on their daily BW.

The test consisted of 6 phases, each stage more challenging than the last. To proceed to each subsequent stage, mice were required to reach the criteria for two consecutive days. Each session lasted 30 minutes.

During the training phase, animals just needed to learn how to correlate the “nose-poke” into any hole to a reinforcement, so all holes were illuminated for the whole session. From the phase 1 on, a free reinforcement pellet was delivered at the start of each testing session and trial began with an inter-trial interval (ITI) characterized by the house-light turned on. At the end of the ITI, the program randomly selected a stimulus location (1 out of 5 holes) and turned on the corresponding light. The light remained on for the stimulus

duration (SD) value set. Therefore, the animal had limited hold time (LH) to nose-poke into the lit hole in order to get a reinforcement. A detailed description of the different phases and the criteria used is summarized below (**Table 10**).

Phase	ITI (sec)	SD (sec)	LH (sec)	Criteria
Training to Phase 1	/	/	/	- 20 reinforcements + 20 detection at the food dispenser (for 3 days) OR - >25 reinforcements + >25 detection at the food dispenser (for 2 days)
Phase 1 to Phase 2	5	20	10	>20 correct answers, 20 % total trials* (for 2 days)
Phase 2 to Phase 3	5	10	10	>30 correct answers, 30 % total trials (for 2 days)
Phase 3 to Phase 4	5	8	10	>40 correct answers, 80 % accuracy* (for 2 days)
Phase 4 to Phase 5	5	4	5	>40 correct answers, 80 % accuracy (for 2 days)
Phase 5	5	2	5	>45 correct answers, 80 % accuracy (for 2 days)

*total trials = no. correct + incorrect + omitted answers
*accuracy = no. correct anwers / no. correct + incorrect answers

Table 10: 5-CSRTT phases.

After completing phase 5, animals were also exposed to a distractor for 3 days interspersed with 3 more days without it. The distractor consisted of three elements: a sound (loud music), a smell (a cotton swab soaked in lemon extract) and a visual element (stroboscopic light).

The learning capacity was measured in terms of days needed to pass each phase, while choice accuracy was measured in terms of correct, incorrect and omitted answers during the last six days with and without distractor.

2.9. Tissue preparation: transcardial perfusion

Mice were deeply anesthetized with a mixture of ketamine and xylazine (see **2.4**) and then transcardially perfused first with PBS and next, when required, with 4 % formaldehyde. The isolated brains were post-fixed 2 hours in 4 % formaldehyde solution, kept in 20 % sucrose overnight for cryoprotection, snap frozen in dry ice-cooled isopentane and stored in -80° C. Afterwards, 10-18 μm thick coronal slices were serially sectioned using a cryostat (CM3050 S, Leica, Wetzler, Germany) and mounted on glass slides. Glass slides were kept at -80° C until further use.

2.10. Immunohistochemistry (IHC)

2.10.1. Immuno-staining

For a detailed list of the buffers and antibody used for each staining see **2.2.2** and **2.3**.
Frozen sections were dried for 30 min at 37° C on a hot plate. After drying, the slices were framed with a PapPen, washed in washing buffer and permeabilized for 1 h. Nonspecific binding was blocked by incubation in blocking solution for 2 h. Next, slices were incubated overnight at 4° C with the primary antibody diluted in antibody solution. Afterwards, slides were washed three times in washing buffer followed by incubation with the respective secondary antibody diluted in antibody solution, at room temperature for 2 h. Then, slides were washed in washing buffer, briefly immersed in MilliQ water, mounted with DAPI and covered and stored at 4° C.
For light microscopy, the processing of the tissues was identical, but we used a biotinylated secondary antibody. Therefore, after the incubation with the secondary antibody, slides were incubated with ABC-reagent for 30 min and immersed in a reagent bath. The reaction was started with H_2O_2 and stopped by washing the slides in 50 mM Tris. Subsequently, slides were rinsed in MilliQ water, dehydrated with serial incubations in solutions with increasing concentrations of ethanol and xylol and mounted with Roti Histokitt II mounting medium.

2.10.2. Image acquisition

Images from IHC staining were acquired with Leica TCS SP8 confocal microscope (Leica, Wetzler, Germany) and different objective lens. The microscope is equipped with an ultraviolet (UV) diode (emission peak at 405 nm), an Argon laser (emission at 458, 476, 488, 514), a diode-pumped solid-state (DPSS) laser (emission at 561 nm) and two helium-neon (HeNe) lasers (emission at: 594 nm and at 633 nm). Respectively, DAPI was excited with a UV Diode, AF488 with argon laser at 488 nm, AF568 with DPSS laser at 561 nm and AF647 with HeNe at 633 nm. For light microscopy, images were obtained with Axio Imager M2 microscope (Zeiss, Oberkochen, Germany) and 20 x objective lens.

2.11. RNAscope

RNAscope is a novel RNA *in situ* hybridization (ISH) technology with a probe design strategy that allows simultaneously to amplify the signal and to reduce the background; in this way is possible to achieve a single-molecule visualization while preserving the tissue morphology. We used RNAscope® Fluorescent Multiplex Assay (ACD) which allows to visualize up to three different RNA targets per cell in one assay. The assays were conducted according to the manufacturer's protocol. The whole procedure can be summarized in 4 steps, detailed description follows below:

1. Tissue sectioning and pretreatment
2. Hybridization of probes to target RNAs
3. Signal amplification
4. Imaging

2.11.1. Tissue section and preparation

Snap-frozen brains were sectioned at the cryostat in 10 μm thick coronal slices and mounted on cold glass slides in order to keep the RNA intact. On the first day of experiment, sections were fixed with 4 % formaldehyde solution for 15 min, dehydrated in increasingly concentrated ethanol series and pre-treated with RNAscope® Proteinase IV (Cat. No. 322336).

2.11.2. Hybridization to target RNAs and signal amplification

We performed two separate and parallel RNAscope experiments to analyze the mRNA of DAGLα and DAGLβ in TH-positive cells.

Therefore, samples were incubated with three different probes: TH, to identify noradrenergic neurons, DAGLα and DAGLβ. Probes were hybridized with a series of signal amplification molecules, culminating in binding of dye-labeled probes detectable in different fluorescent channels. The detection reagent Amp 4 Alt B-FL was used for the last step. The sections were counterstained with DAPI, immediately mounted with Prolong Gold Antifade Mountant and coverslipped. Details about the probes are listed below (**Table 11: RNAscope probes**).

Probe	Excitation	Emission	Cat. No.
TH	Alexa 488 nm	540 ± 10 nm	317621- C2
DAGLα	Atto 550 nm	580 ± 10 nm	478821
DAGLβ	Atto 550 nm	580 ± 10 nm	497801

Table 11: RNAscope probes.

2.11.3. Imaging

For the process of fluorescent confocal imaging see **2.10.2**.

2.12. Image analysis

2.12.1. Stereological quantification of TH-positive cells

For the stereological quantification of TH-positive cells, every 4th slice of the region of interest was collected for a total of 8–10 slices per sample. Then, we stained for TH immunoreactivity. The total number of TH-positive neurons in both hemispheres was estimated manually using the plugin Cell Counter from Fiji software (Ver. 2.1.0/1.53c, NIH, Bethesda, MD, USA).

2.12.2. IHC staining

All the analyses were performed using Fiji software (version 1.0). The results were then exported and further analyzed with Microsoft Excel (version 16.16.11).
Iba1, CD68, and TNFα signal intensities were analyzed within the Iba1-positive microglia of the LC in both hemispheres. All microglial somas were manually delineated and the obtained regions of interests (ROIs) were used for single microglia soma analysis of Iba1, CD68, TNFα signal intensities.
PUbiquitin and Lipofuscin signal intensities were analyzed within the single TH-positive cell; all TH-positive cells were manually delineated and the obtained ROIs were used for PUbiquitin and Lipofuscin signal intensity analysis.
DAGLα was analyzed as the percentage of DAGLα-covered area within the single TH-positive cell; ROIs of TH-positive cells were obtained in the same way as for PUbiquitin and Lipofuscin analysis.
The density of NET-positive axons, analyzed as percentage of area covered by NET-positive signal, was analyzed in the parietal cortex, basolateral amygdala, CA1, CA3 and dentate gyrus regions of the hippocampus and in the mediobasal hypothalamus in both hemispheres.

2.12.3. MotiQ: 3-dimentional (3D) microglia morphology analysis

Prior to the analysis Iba1 z-stacks were acquired (0.5 μm distance) and pre-processed (size reduction 0.5, smoothing, background subtraction: rolling ball). Followed by automated analysis using a custom-written script 'MotiQ' (Plescher et al., 2018). The plugin consists of two sub scripts: Thresholder and 3D Analyzer. First, microglia area was manually selected. Then, Thresholder was used to obtain binary images from the original stacks and the intensity threshold was determined. Afterwards single cells were detected using 3D Analyzer by signal overlap within the z-stack. Only particles larger than 10,000 voxels were included in the analysis (length calibration: 0.3608 µm / pixel; voxel depth 0.5 µm). Skeleton of the cell was derived from a copy of the input image. Reconstructed cells were inspected visually and cells that were incomplete (cut in x, y or z axes) as well as multiple cells detected as one particle were excluded from the analysis. Measured

parameters included: surface area, volume of the cell, ramification index, number of branches, tree length, average branch length (**Figure 6**).

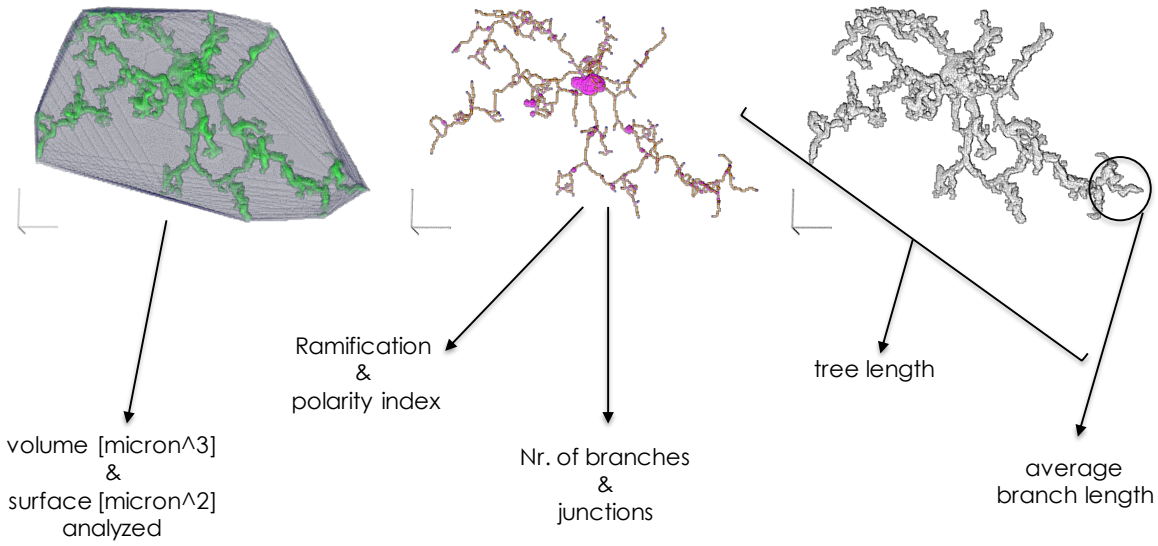

Figure 6: MotiQ: 3-dimentional microglia morphology analysis.
Representative picture of the main parameters analyzed by MotiQ plugin in relation to microglia's structure.

2.12.4. RNAscope

All images were thresholded; the threshold was calculated as an arithmetical average of manually set thresholds for each sample. Noradrenergic neurons were identified thought TH expression and manually delineated in order to obtained ROIs. The single DAGLα and DAGLβ mRNA molecules were automatically quantified within ROIs with the plugin Analyze Particles.

2.13. Determination of Noradrenaline Levels

Noradrenaline levels were quantified in regions representing the main output areas of LC: hippocampus, basolateral amygdala, parietal cortex and mediobasal hypothalamus. 18-month-old male $Cnr1^{+/+}$ and $Cnr1^{-/-}$ mice were used.

Mice were deeply anaesthetized and transcardially perfused with ice-cold PBS. Brains were quickly removed and stored at -80° C until analysis. Brain regions of interest were

isolated using the punch technique from both hemispheres of the frozen brain tissue and homogenized on ice in 0.01 N HCl, 0.15 mM EDTA and 4 mM sodium metabisulfite. Protein concentration was quantified using the Pierce™ BCA Protein Assay Kit (Thermo Fisher Scientific, Waltham, MA, USA). Quantification of noradrenaline was performed using the Mouse/Rat Noradrenaline (Norepinephrine) ELISA Assay Kit (Eagle Biosciences, Inc., Amherst, NH, USA). For extraction, 40 μg of protein per sample were used in a total volume of 400 μl. Extracted samples were eluted in 250 μl 0.025 M HCl and split into 100 μl duplicates for the subsequent enzyme and ELISA procedure. A total of 20 μl of standards and controls were extracted in a total volume of 400 μl and processed in duplicates.

2.14. Statistical analysis and data presentation

Data were collected in Microsoft Excel (version 16.16.11). Statistical analysis and data visualization were performed with GraphPad Prism (version 9.3.1 for MacOS; ©1994 - 2021 GraphPad Software, LLC). Figures were created using both Biorender (app.biorender.com) and Microsoft PowerPoint (version 16.16.11). Data distribution was analyzed using the D'Agostino and Pearson normality test. Based on the result of the data distribution analysis, statistical significance between two independent groups was determined by Student t-test or Mann–Whitney test. For time-related effect, one-way repeated ANOVA was used. Statistical significance between two independent groups with multiple variables (example: age and genotype) was assessed with 2-way ANOVA. Statistical significance was stated when p-value < 0.05. In figures, p-values were reported as * $p < 0.05$, ** $p < 0.01$; *** $p < 0.001$; **** $p < 0.0001$. Significant outliers were identified and excluded by using Grubb's test. All the data are presented with standard error of the mean (SEM).

3. Results

3.1. Age-related neuronal loss in LC of C57BL/6J mice

The first goal was to determine if there was an age-related neuronal loss in the catecholaminergic nuclei of C57BL/6J mice. In order to do that, we used a common marker for dopaminergic and noradrenergic cells, the enzyme tyrosine hydroxylase (TH), and compared the number of TH-positive cells in the locus coeruleus (LC), substantia nigra (SN) and ventral tegmental area (VTA) between 3- (**Figure 7 A**) and 22-month-old (**Figure 7 B**) wild-type mice by stereological counting.
Detailed experimental protocol is explained in **2.9** - **2.10.1** - **2.12.1.**

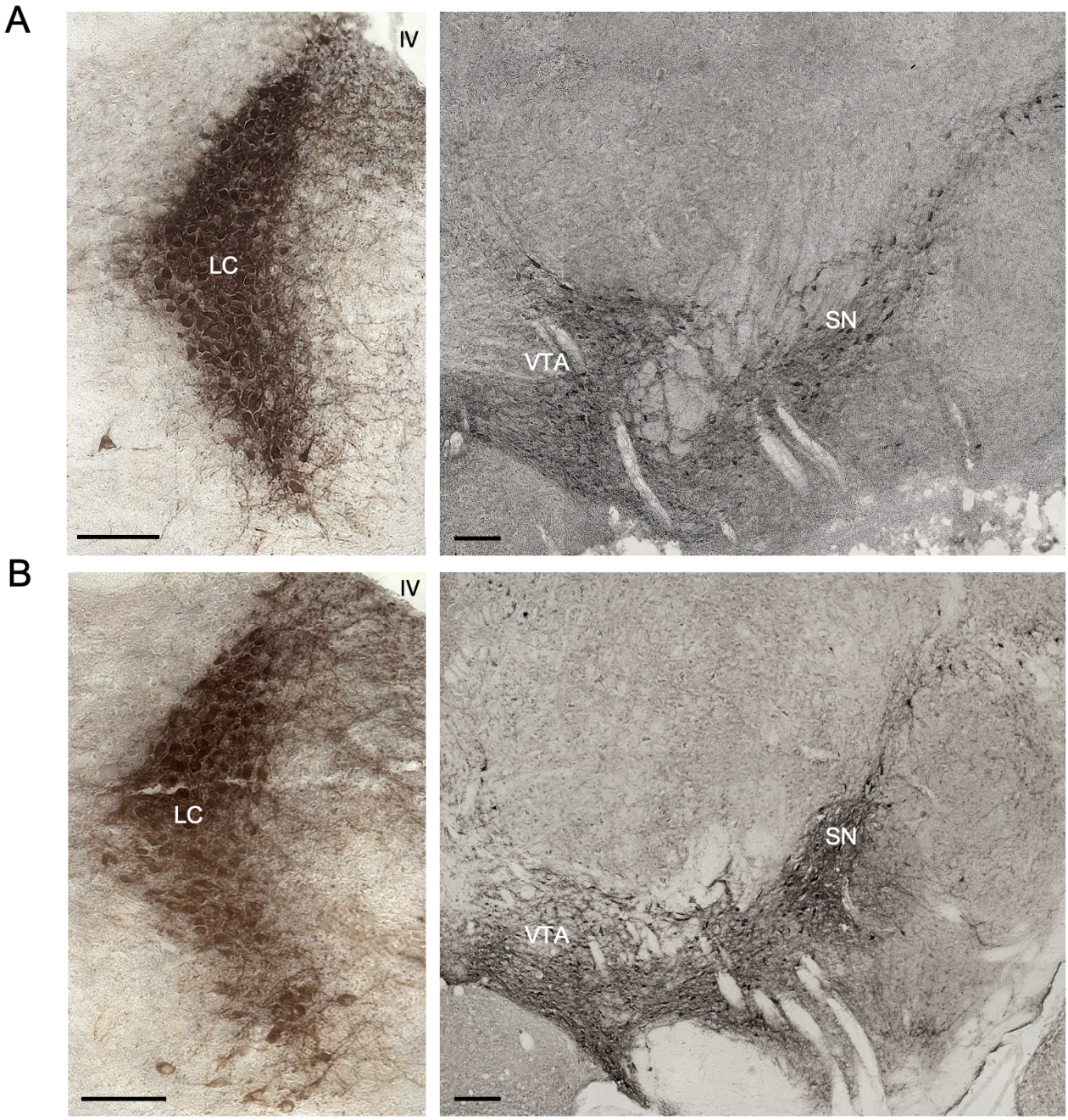

Figure 7: Representative photomicrographs of catecholaminergic nuclei.
Representative photomicrographs of the tyrosine hydroxylase (TH)-positive regions locus coeruleus (LC), substantia nigra (SN) and ventral tegmental area (VTA) in young (3-month-old, **A**) and old (22-month-old, **B**). IV: fourth ventricle. Scalebar: 100 μm.

The number of TH-positive cells in the LC was significantly reduced in old compared to young C57BL/6J mice (t_{12} = 2.560; p = 0.0250) (**Figure 8 A**), whereas neither the SN (t_{12} = 1.425; p = 0.1798) nor the VTA (t_{12} = 1.483; p = 0.1639) showed significant differences between the age groups (**Figure 8 B–C**).

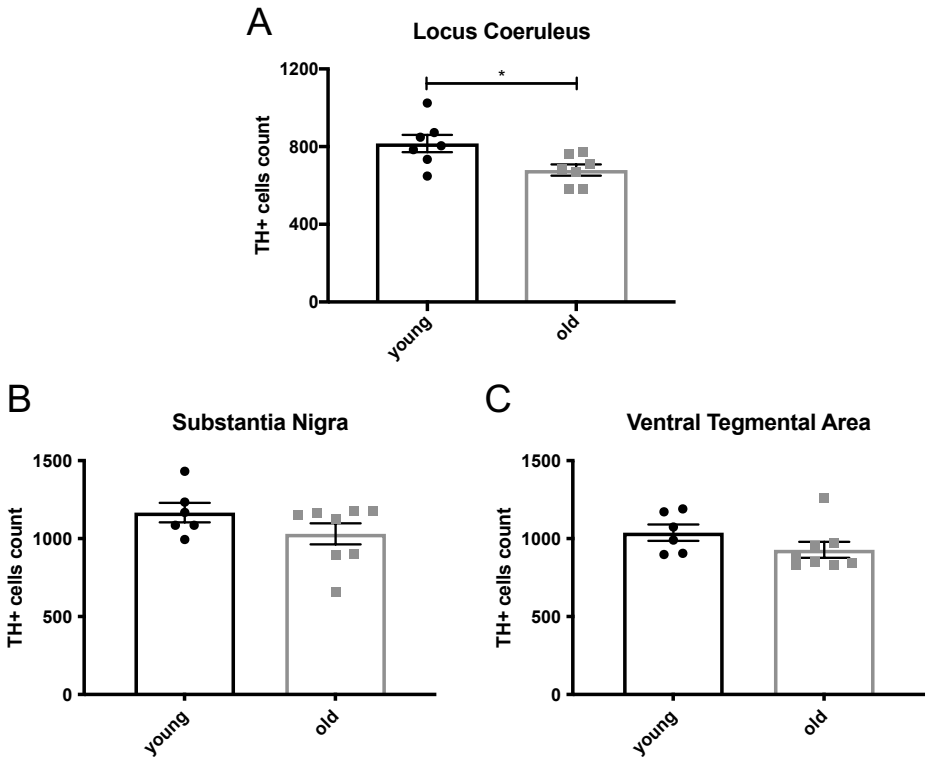

Figure 8: Age-related neuronal loss in LC of C57BL/6J mice.
Quantitative stereological analysis of the total number of tyrosine hydroxylase (TH)-positive cells in the catecholaminergic nuclei LC **(A)**, SN **(B)** and VTA **(C)** of young (3-month-old) and old (22-month-old) C57BL/6J wild-type mice.* $p < 0.05$ according to Student's t-test ($n = 6 – 8$ per age group). Dots represent single animals, columns represent mean values; error bars represent standard error of means (SEM).

3.1.1. Timeline of LC age-related neurodegeneration

Our initial experiment showed that in C57BL/6J mice there was an age-related neurodegeneration in old mice compared to a very young control group. However, we did not know when the neurodegenerative process took place. For this reason, we performed the same stereological counting as in **3.1** to verify the number of TH-positive cells in the LC of mice of different ages: we used six different age groups: 2-3, 4-6, 7-9, 11-13, 14-16 and up to 24-month-old mice. What we found is a prominent decrease in the TH-positive cells number at the age of 7-9-months compared to 2 to 6-months; this number then remained constant until old age ($F_{(5, 16)} = 3.446$, $p = 0.0265$) (**Figure 9**).

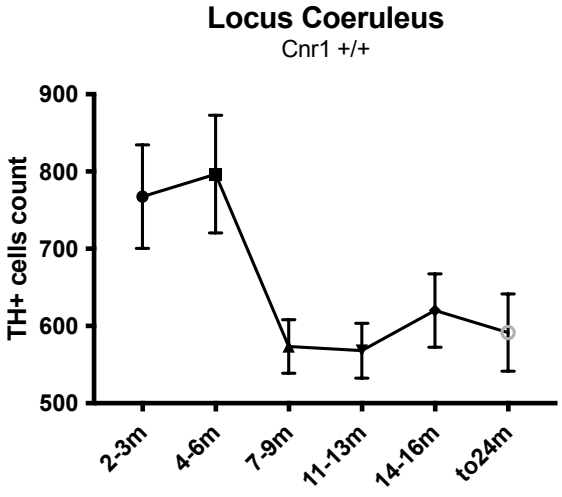

Figure 9: Timeline of LC age-related neurodegeneration.
Quantitative stereological analysis of the total number of tyrosine hydroxylase (TH)-positive cells in C57BL/6J wild-type mice from six different age groups. Data analyzed with Ordinary one-way ANOVA (n = 3 – 4 per age group) Shapes represent mean values; error bars represent standard error of means (SEM).

3.2. Enhanced age-related neuronal loss in the LC of Cnr1$^{-/-}$ mice

To understand the role of CB1r in the survival of noradrenergic cells during aging, we compared the number of TH-positive cells in the LC, SN and VTA between 18-month-old Cnr1$^{-/-}$ mice and wild-type controls (Cnr1$^{+/+}$). Our data show that in the LC the number of TH-positive cells was significantly lower in Cnr1$^{-/-}$ mice compared to age-matched wild-type littermates (t_{10} = 2.663, p = 0.0238) (**Figure 10 A**). Conversely, no genotype effect was found neither for SN nor VTA (t_{10} = 0.3849, p = 0.7084; t_{10} = 1.806, p = 0.1010) (**Figure 10 B–C**). Having used a constitutive knock-out model, we wanted to exclude the possibility that Cnr1$^{-/-}$ mice had a lower number of LC TH-positive cells from birth, regardless from their age. Therefore, we analyzed the number of TH-positive cells in the LC of 3-month-old Cnr1$^{-/-}$ mice and wild-type controls but we did not find any difference between genotypes (t_{11} = 0.971, p = 0.352) (**Figure 10 D**). Thus, these data strongly indicate that the difference observed in old animals is due to an exacerbated age-related cell loss of noradrenergic neurons in mice lacking of the CB1r.

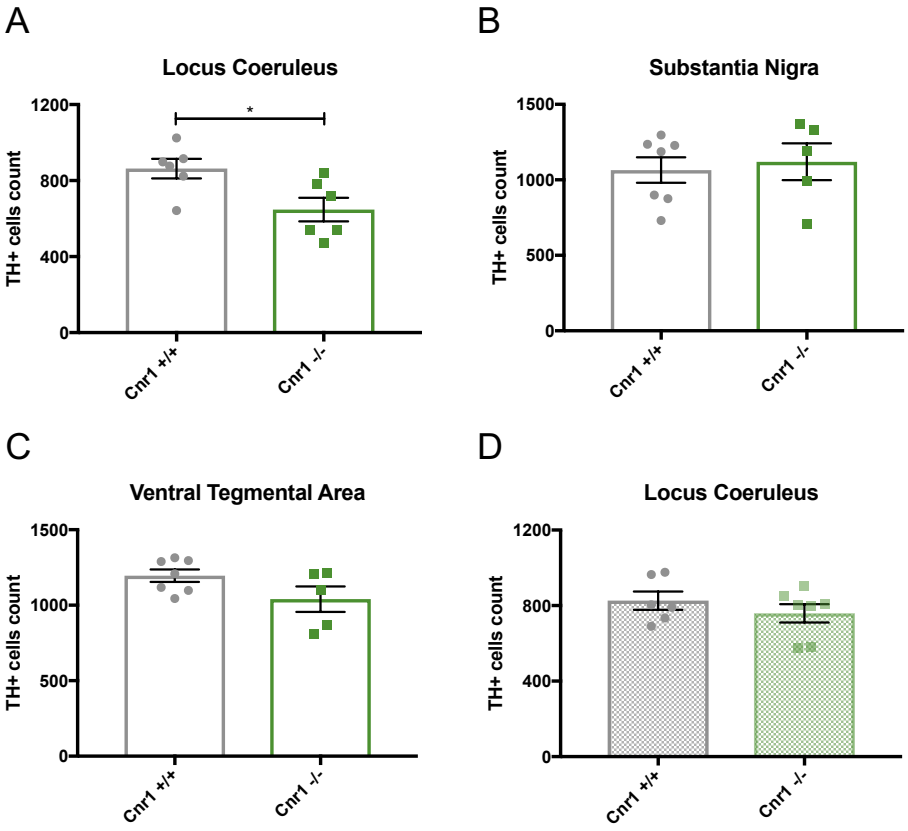

Figure 10: Enhanced age-related neuronal loss in the LC of Cnr1$^{-/-}$ Mice.
Quantitative stereological analysis of the total number of tyrosine hydroxylase (TH)-positive cells in 18-month-old wild-type (Cnr1$^{+/+}$) and Cnr1$^{-/-}$ animals within the LC **(A)**, SN **(B)**, VTA **(C)** and in 3-month-old wild-type (Cnr1$^{+/+}$) and Cnr1$^{-/-}$ animals within the LC **(D)**. * $p < 0.05$ according to Student´s t-test (n = 5 – 7 per genotype). Dots represent single animals, columns represent mean values; error bars represent standard error of means (SEM).

3.3. Reduced density of noradrenergic axon terminals in aged Cnr1$^{-/-}$ mice

Having shown that there was a difference in the number of noradrenergic neurons, our next aim was to determine wheatear old wild-type and Cnr1$^{-/-}$ animals differed in the distribution of noradrenergic axon terminals in the main output regions of LC. So, we analyzed in both genotypes the area covered by the norepinephrine transporter (NET) across the following regions: parietal cortex (Pa CTX), basolateral amygdala (BLA), mediobasal hypothalamus (Mb HY) and hippocampal cornu ammonis 1 (CA1), cornu ammonis 3 (CA3), and dentate gyrus (DG) (**Figure 11**).

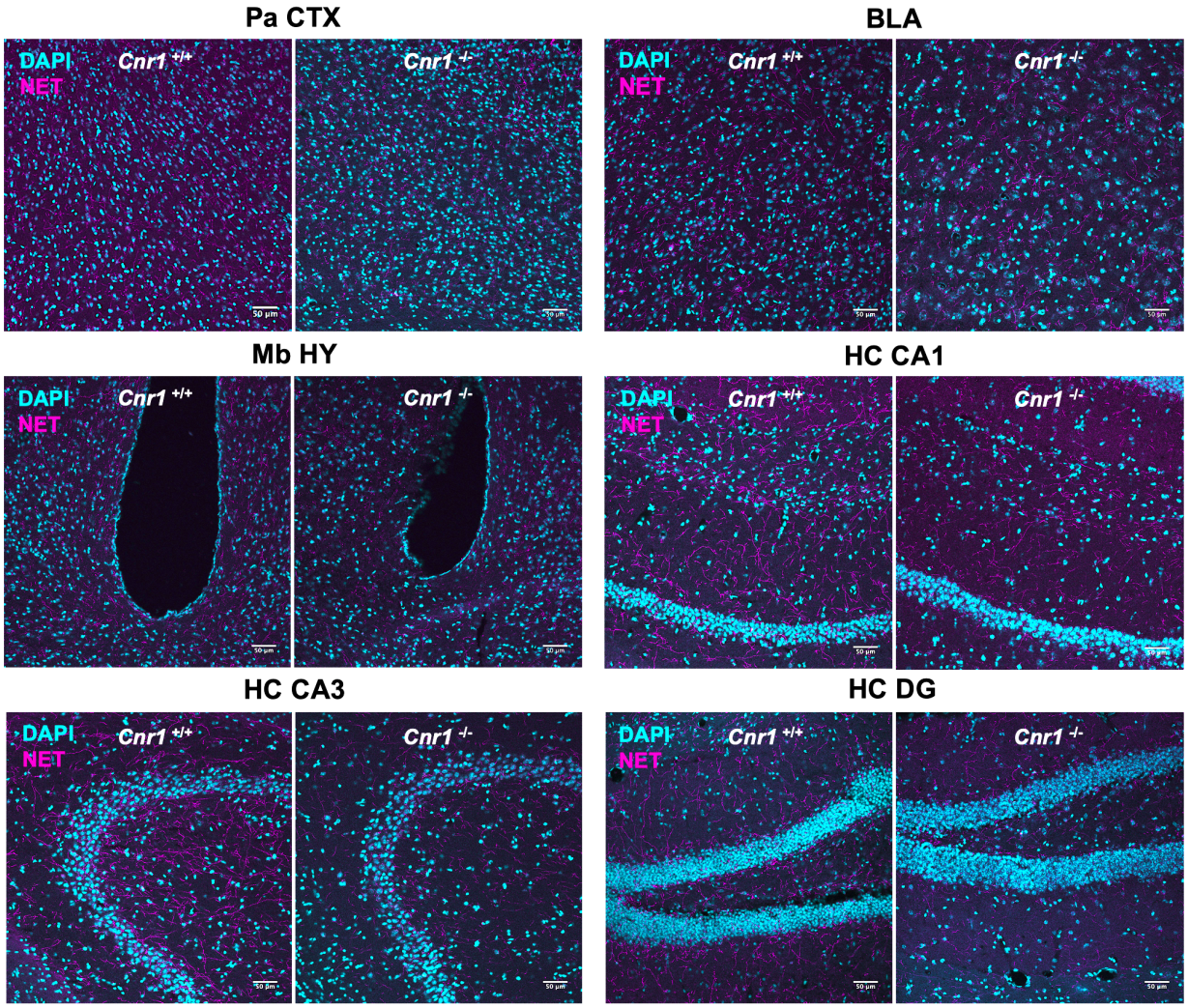

Figure 11: Norepinephrine transporter staining in different brain regions.
Representative photomicrograph of norepinephrine transporter (NET) staining within Pa CTX, BLA, Mb HY and hippocampal CA1, CA3, and DG regions of 18-month-old wild-type ($Cnr1^{+/+}$) and $Cnr1^{-/-}$ animals. Negative controls were stained only with the secondary antibodies. Scalebar: 50 μm.

Our data show that the area covered by NET-positive signal was significantly lower in 18-month-old $Cnr1^{-/-}$ animals (Genotype: $F_{(1, 15)} = 8.104$; $p = 0.0122$) even though the NET signal differed per se based on the brain region, being the lowest in the Mb HY and the highest in the hippocampal CA3 (Area: $F_{(5, 75)} = 5.964$; $p = 0.0001$. Area x genotype: $F_{(5, 75)} = 0.6898$; $p = 0.6327$) (**Figure 12**).

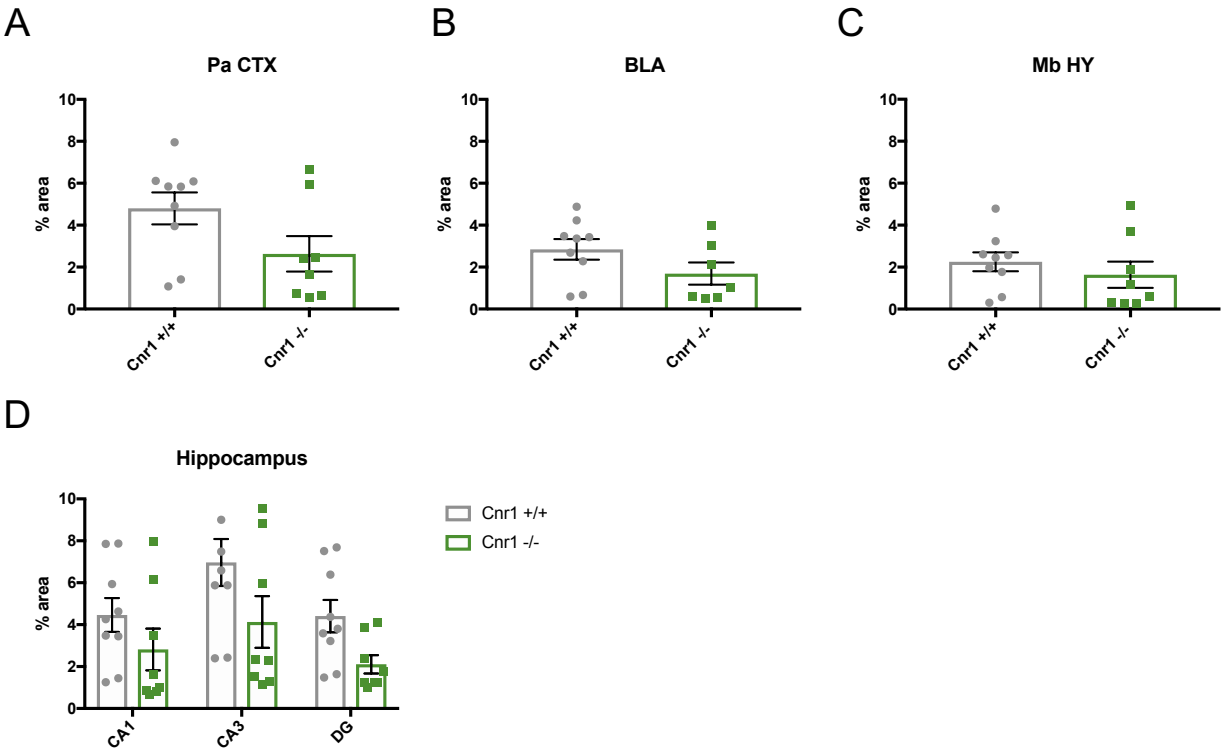

Figure 12: Analysis of noradrenergic axon terminals in 18-month old wild-type (Cnr1$^{+/+}$) and Cnr1$^{-/-}$ animals.
Analysis of the area covered by NET-positive axon terminals in the Pa CTX **(A)**, BLA **(B)**, Mb HY **(C)** and hippocampal CA1, CA3, and DG regions **(D)** of 18-month old wild-type (Cnr1$^{+/+}$) and Cnr1$^{-/-}$ animals. 2way ANOVA (n = 7 – 9 per genotype). Dots represent single animals, columns represent mean values; error bars represent standard error of means (SEM).

To further support that there is no developmental effect in the constitutive Cnr1$^{-/-}$, we repeated the experiment comparing 3-month-old wild-type and Cnr1$^{-/-}$ animals and we could not find neither a difference between genotypes (Genotype: ($F_{(1,9)}$ = 0.005; p = 0.945) nor a difference in NET signal based on the brain region (Area: $F_{(5, 45)}$ = 0.4381; p = 0.8195. Area x genotype: $F_{(5, 45)}$ = 0.1299; p = 0.9848) (**Figure 13**) confirming our previous data.

Note that only groups represented on the same panels in **Figure 12** and **Figure 13** are comparable, because they were stained together in the same staining series. As staining intensities varies between series, results are not comparable between different figures or panels.

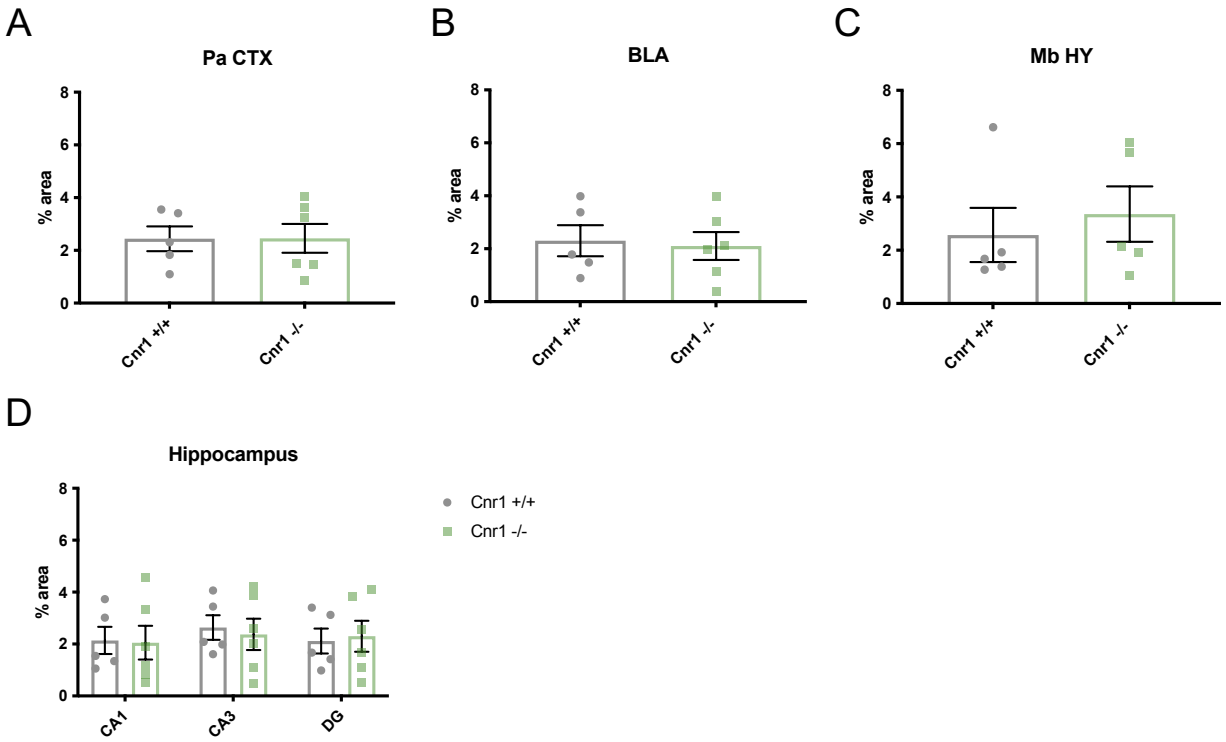

Figure 13: Analysis of noradrenergic axon terminals in 3-month old wild-type (Cnr1$^{+/+}$) and Cnr1$^{-/-}$ animals.
Analysis of the area covered by NET-positive axon terminals in the Pa CTX **(A)**, BLA **(B)**, Mb HY **(C)** and hippocampal CA1, CA3, and DG regions **(D)** of 3-month old wild-type (Cnr1$^{+/+}$) and Cnr1$^{-/-}$ animals. 2way ANOVA (n = 5 – 6 per genotype). Dots represent single animals, columns represent mean values; error bars represent standard error of means (SEM).

Importantly, we found a positive correlation in 18-month-old animals between the number of TH-positive cells and the NET-positive axon densities in both genotypes in the Pa CTX, Mb HY, CA1 and CA3 regions of hippocampus, indicating that a lower TH-cell number was associated with a reduced NET density in these areas (**Figure 14** – **Table 12**). Nevertheless, steady-state noradrenaline levels were not different between the genotypes in any of the brain regions tested: Pa CTX (t_{10} = 0.275; p = 0.789), BLA (t_{10} = 0.787; p = 0.450), Mb HY (t_9 = 1.694; p = 0.125), HC (t_{10} = 0.776; p = 0.4554) (data not shown).

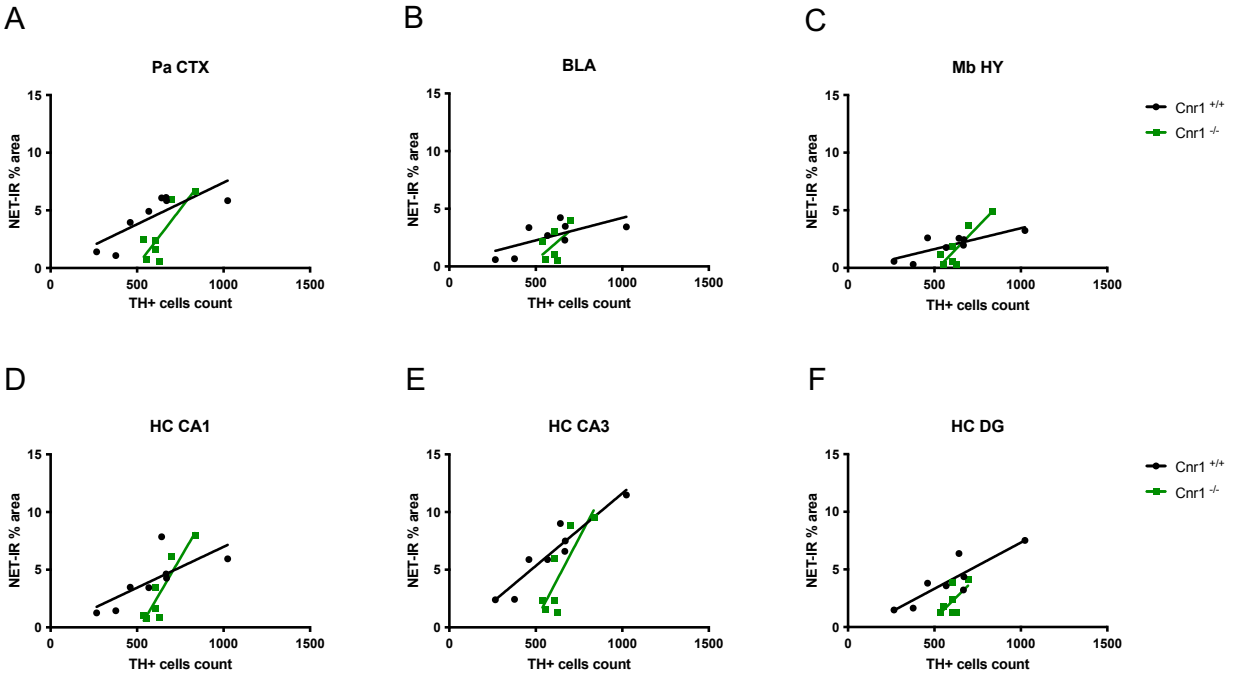

Figure 14: Correlation TH-NET.
Correlation analysis between the number of tyrosine hydroxylase (TH)-positive cells and the area covered by NET-positive axon terminals in the Pa CTX **(A)**, BLA **(B)**, Mb HY **(C)** and hippocampal CA1 **(D)**, CA3 **(E)**, and DG regions **(F)** in wild-type ($Cnr1^{+/+}$) and $Cnr1^{-/-}$ 18-month-old mice.

Brain area	Wild-type		$Cnr1^{-/-}$	
	Correlation (r, Spearman)	Significance	Correlation (r, Spearman)	Significance
Pa CTX	0.6399	0.0171	0.6857	0.0214
BLA	0.4502	0.0685	0.2713	0.2894
Mb HY	0.6643	0.0137	0.7682	0.0096
HC, CA1	0.5527	0.0345	0.8316	0.0042
HC, CA3	0.8863	0.0005	0.6826	0.022
HC, DG	0.7701	0.0042	0.3857	0.1366

Table 12: Statistical analysis of the correlation TH-NET.
Statistical analysis of the correlation between the number of tyrosine hydroxylase (TH)-positive cells and the area covered by NET-positive axon terminals in the Pa CTX, BLA, Mb HY and hippocampal CA1, CA3, and DG regions in wild-type ($Cnr1^{+/+}$) and $Cnr1^{-/-}$ 18-month-old mice.

3.4. Inflammatory profile of the LC in Cnr1$^{-/-}$ mice

3.4.1. Enhanced microglia density in the LC of aged Cnr1$^{-/-}$ mice

To assess the inflammatory profile within the LC of 18-month-old wild-type and Cnr1$^{-/-}$ mice, we investigated different parameters starting with the density of ionized calcium-binding adapter molecule 1 (Iba1)-positive microglia and the level of tumor necrosis factor alpha (TNFα) (**Figure 15**). Details about the analysis in **2.12.2**.

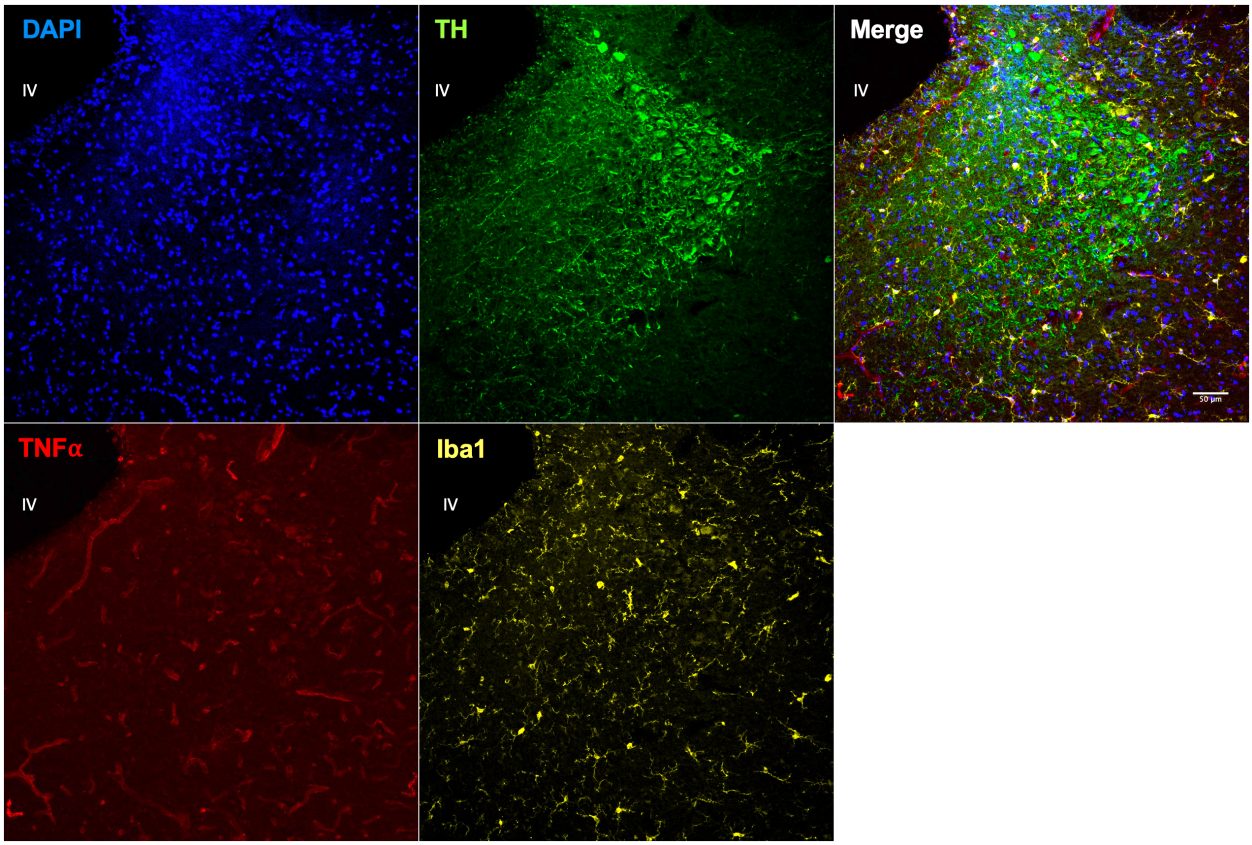

Figure 15: Tumor necrosis factor and ionized calcium-binding adapter molecule 1 staining in LC.
Representative photomicrograph of tumor necrosis factor (TNFα), tyrosine hydroxylase (TH) and ionized calcium-binding adapter molecule 1 (Iba1) staining within the LC of an 18-month-old wild-type animal. Negative controls were stained only with the secondary antibodies. IV: fourth ventricle. Scalebar: 50 µm.

We found that there was an increase of +66 % in Iba1-positive microglia density within the TH-positive area in Cnr1$^{-/-}$ animals (t_{11} = 2.602; p = 0.0246). However, we did not find any

genotype differences in other neuroinflammation markers: Iba1 (t_{192} = 0.984; p = 0.326), TNFα (U = 28924; p = 0.167) (**Figure 16**).

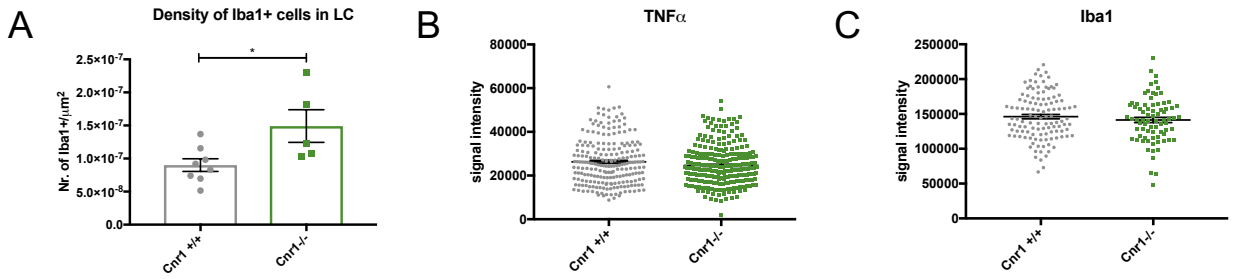

Figure 16: Enhanced microglia density in the LC of aged Cnr1$^{-/-}$ mice.
Density of Iba1-positive microglia within the LC of 18-month-old wild-type (Cnr1$^{+/+}$) and Cnr1$^{-/-}$ animals. * p < 0.05 according to Student´s t-test (n = 5 – 8 per genotype). Dots represent single animals, columns represent mean values, error bars represent standard error of means (SEM) **(A)**. Analysis of TNFα **(B)** and Iba1 **(C)** signal intensity in microglia cells within the LC of 18-month-old wild-type (Cnr1$^{+/+}$) and Cnr1$^{-/-}$ animals. Data analyzed with Student´s t-test and Mann-Whitney test (n = 224 – 291 per genotype). Dots represent individual values; error bars represent standard error of means (SEM).

3.4.2. Microglia morphology in the LC of aged Cnr1$^{-/-}$ mice

To investigate better the role of microglia in the LC age-related neurodegeneration, we analyzed the morphology of Iba1-positive cells in 18-month-old wild-type and Cnr1$^{-/-}$ animals. For detailed information about the plugin MotiQ and the analysis see **2.12.3**.
Our analysis evaluated different parameters of microglia morphology, possibly attributable to a pro-inflammatory status, as cell dimensions and branching (see **Figure 6**). As shown in **Figure 17**, we did not find any genotype difference in terms of cell volume (**Figure 17 A**) (U = 3798; p = 0.299), surface (**Figure 17 B**) (U = 3988; p = 0.611), polarity and ramification index (**Figure 17 C**–**D**) (t_{180} = 1.404; p = 0.1621. U = 3896; p = 0.444) and total tree length (**Figure 17 E**) (U = 3321; p = 0.0678). Nevertheless, in Cnr1$^{-/-}$ mice we detected a significantly lower average branch length (**Figure 17 F**) (t_{182} = 6.421; p = < 0.0001) as well as an increased number of microglia branches and junctions (**Figure 17 G, H**) (U = 2739; p = 0.0004. U = 2840; p = 0.0008).

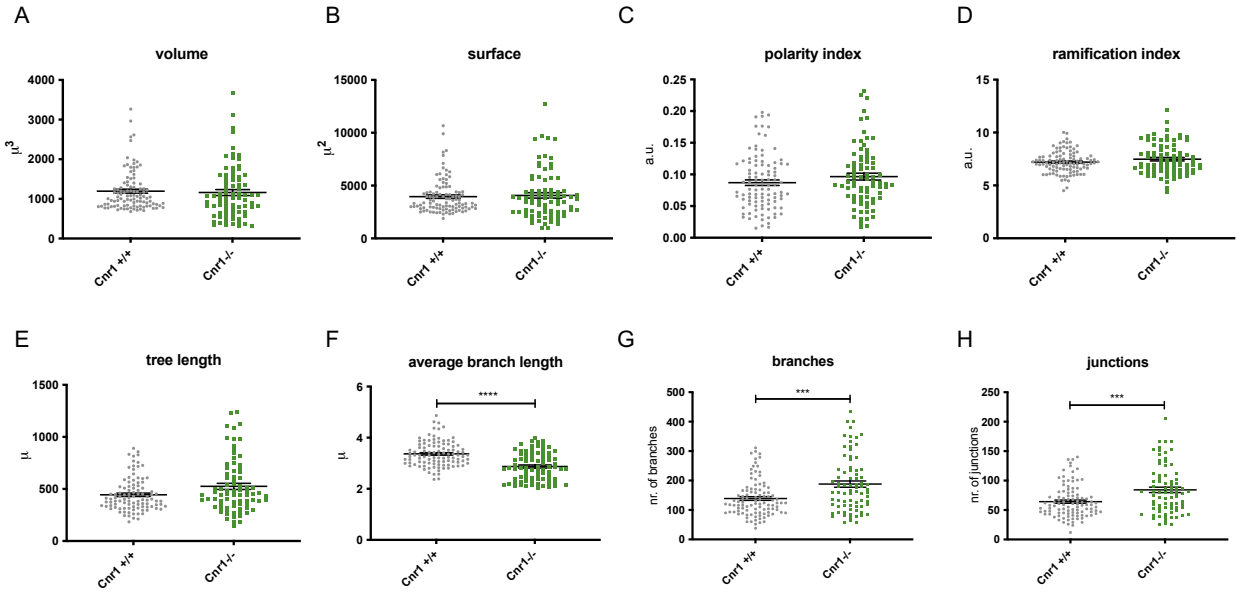

Figure 17: Microglia morphology in the LC of aged Cnr1$^{-/-}$ mice.
Parameters of microglia morphology analyzed with MotiQ plugin for Fiji in 18-month-old wild-type (Cnr1$^{+/+}$) and Cnr1$^{-/-}$ animals: volume **(A)**, surface **(B)**, polarity index **(C)**, ramification index **(D)** tree length **(E)**, average branch length **(F)**, number of branches **(G)** and number of junctions **(H)**. **** $p < 0.0001$ according to Student´s t-test, *** $p = 0.0004$, 0.0008 according to Mann-Whitney test (n = 103 – 81 per genotype). Dots represent single cells; error bars represent standard error of means (SEM).

3.4.3. Microglia's phagocytic activity in the LC of Cnr1$^{-/-}$ mice

To further understand the role of microglia in the age-related neurodegeneration of LC, we investigated its phagocytic activity around the crucial time point found in **3.1.1**. Therefore, we analyzed the level of the glycoprotein cluster of differentiation 68 (CD68) in Iba1-positive microglia cells within the LC of wild-type and Cnr1$^{-/-}$ animals of three different ages: 2-3, 4-6 and 7-9-months. CD68 is a widely used phagocytic marker expressed in a very specific manner by Iba1-positive microglia cells, as shown in **Figure 18.**

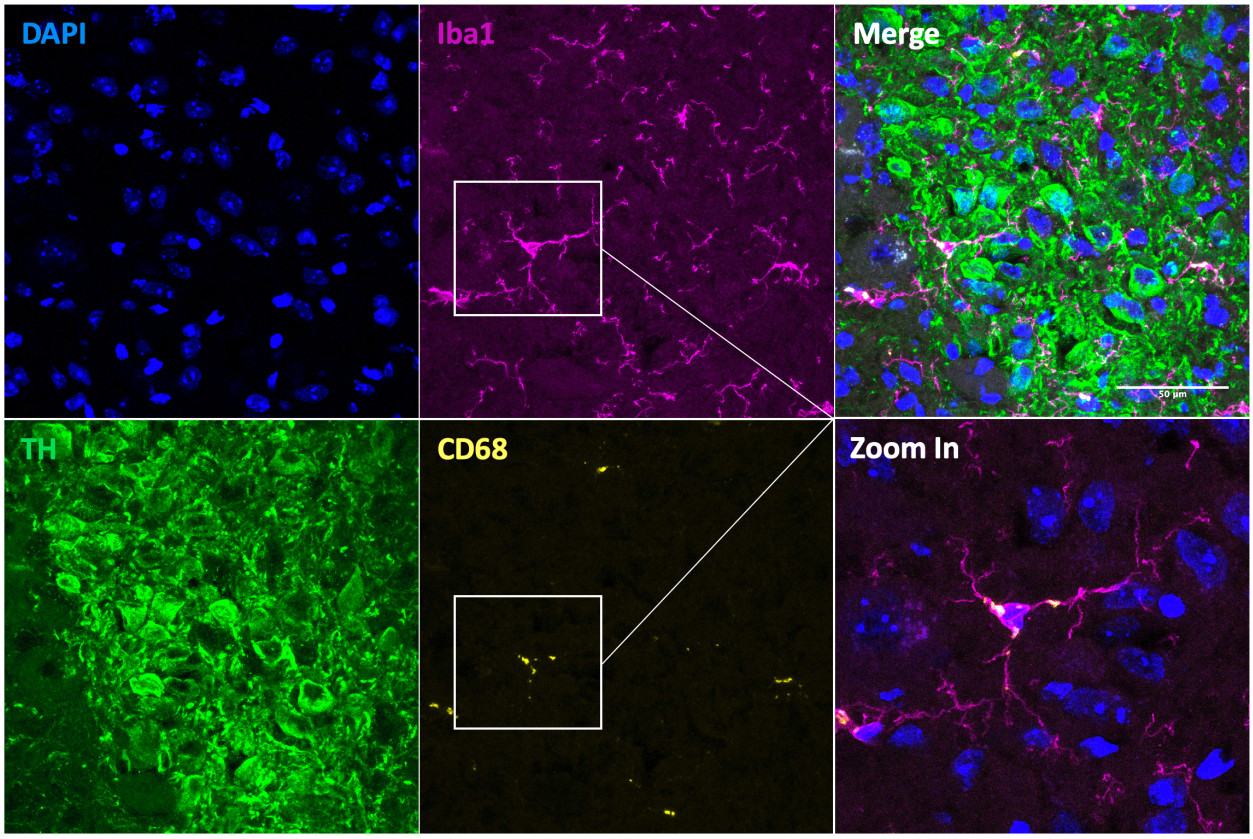

Figure 18: Cluster of differentiation 68 staining in LC.
Representative photomicrograph of cluster of differentiation 68 (CD68), tyrosine hydroxylase (TH) and ionized calcium-binding adapter molecule 1 (Iba1) staining within the LC of a 2-3-month-old wild-type animal. Negative controls were stained only with the secondary antibodies. Scalebar: 50 µm.

From the analysis of CD68 we found a statistically significant increase in signal intensity for both genotypes when comparing 2-3 and 7-9-month-old animals (wild-type, $p = < 0.0001$; $Cnr1^{-/-}$, $p = 0.0130$). $Cnr1^{-/-}$ animals showed a lower CD68 signal intensity for both 4-6- and 7-9-month groups when compared with wild-type controls ($p = 0.0050$; $p = 0.0009$) (**Figure 19 A**).

We also found that the area of Iba1-positive cells was increased in $Cnr1^{-/-}$ animals only when comparing 2-3 and 7-9-month-old animals (wild-type, $p = 0.9097$; $Cnr1^{-/-}$, $p = 0.0158$). The area of Iba1-positive cells was also increased in 2-3 and 4-6-month-old $Cnr1^{-/-}$ animals compared to wild-type controls ($p = 0.0005$; $p = 0.0067$), but not in 7-9-month-old animals ($p = 0.9420$) (**Figure 19 B**).

From the analysis of the Iba1 signal intensity we found a significant decrease in wild-type animals only when comparing 2-3 and 7-9-month-old animals (wild-type, p = 0.0044; $Cnr1^{-/-}$, p = 0.2103). Furthermore, we detected a significant decrease of Iba1 signal intensity in 4-6-month-old $Cnr1^{-/-}$ mice compared to wild-type controls (p = < 0.0001) (**Figure 19 C**). Finally, we analyzed the density of microglia cells within the LC TH-positive area and also in this case we found a significant age-related increase when comparing 2-3 and 7-9-month-old animals only in in $Cnr1^{-/-}$ animals (wild-type, p = 0.9937; $Cnr1^{-/-}$, p = 0.047). No other significant genotype-related differences were found (**Figure 19 D**).

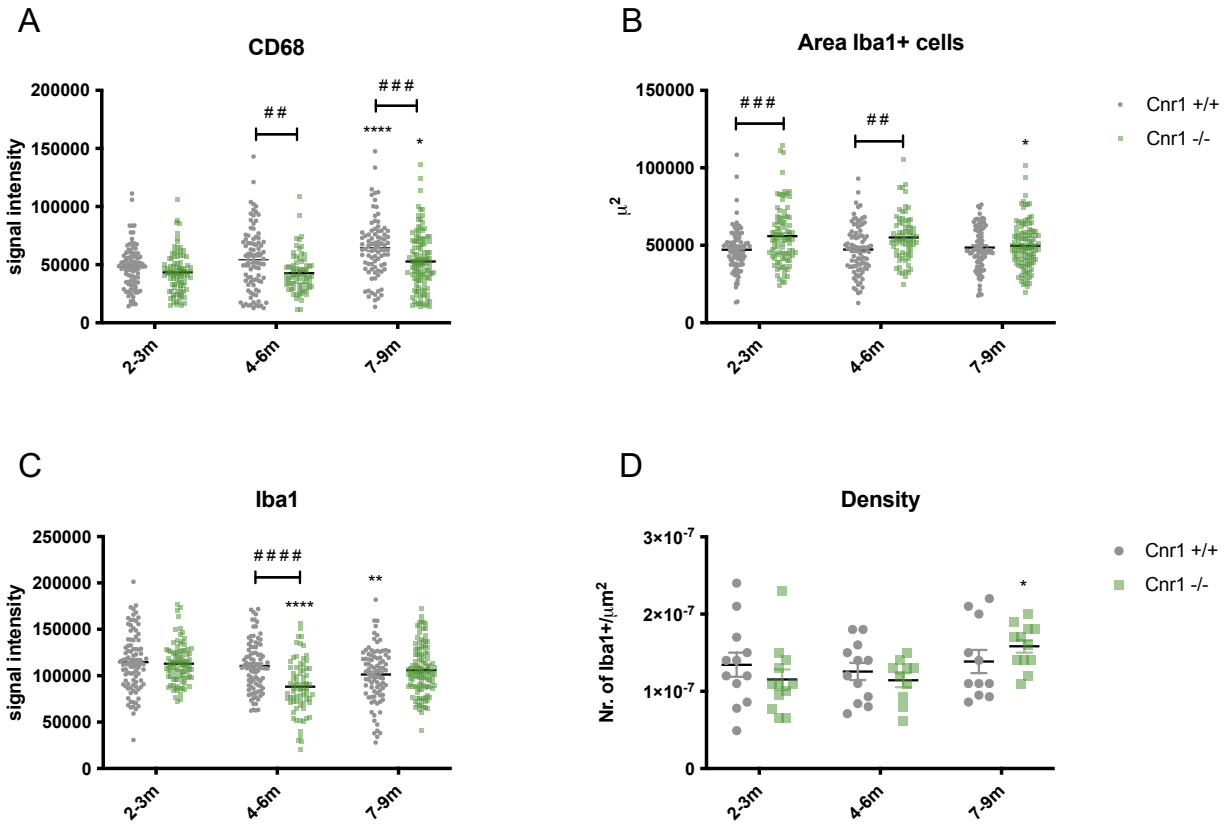

Figure 19: Microglia's phagocytic activity in the LC of $Cnr1^{-/-}$ mice.
CD68 signal intensity **(A)**, area **(B)** and Iba1 signal intensity **(C)** of microglia cells within the LC of wild-type ($Cnr1^{+/+}$) and $Cnr1^{-/-}$ animals from three different age groups (n = 70 – 112 per genotype and age group). Dots represent individual values; error bars represent standard error of means (SEM). Density of Iba1-positive microglia within the LC of wild-type ($Cnr1^{+/+}$) and $Cnr1^{-/-}$ animals from three different age groups **(D)** (n = 10 – 12 per genotype and age group). Dots represent single images; error bars represent standard error of means (SEM). * p < 0.05 according to Šidák's multiple comparisons test. * refers to the comparison between 2-3-months-old animals and the other age groups of the same genotype. # refers to the comparison between wild-type ($Cnr1^{+/+}$) and $Cnr1^{-/-}$ animals.

3.5. Altered mitophagy in the LC of aged Cnr1$^{-/-}$ mice

Autophagy is described as the major turnover pathway by which cellular components are delivered into the lysosomes for degradation. The autophagic activity has been found to decrease with age, contributing to the accumulation of damaged macromolecules within cells. Similarly, mitophagy is the process leading to the degradation of unfunctional mitochondria in order to reduce intracellular ROS levels. In the same way as autophagy, a decline in mitophagy has been described in aging.

Therefore, we analyzed Phospho-Ubiquitin (Serine 65-phosphorylated ubiquitin, Ser65), a marker for mitophagy, and Lipofuscin, a marker for autophagy, within LC noradrenergic neurons of wild-type and Cnr1$^{-/-}$ animals. Lipofuscin is an intracellular granular product composed of lipid-containing residues of lysosomal digestion, particularly pronounced in aged tissues. Lipofuscin is auto fluorescent and clearly visible under the confocal microscope (visible light range, 488 λ nm) (**Figure 20).** For detailed information about the analysis see **2.12.2**.

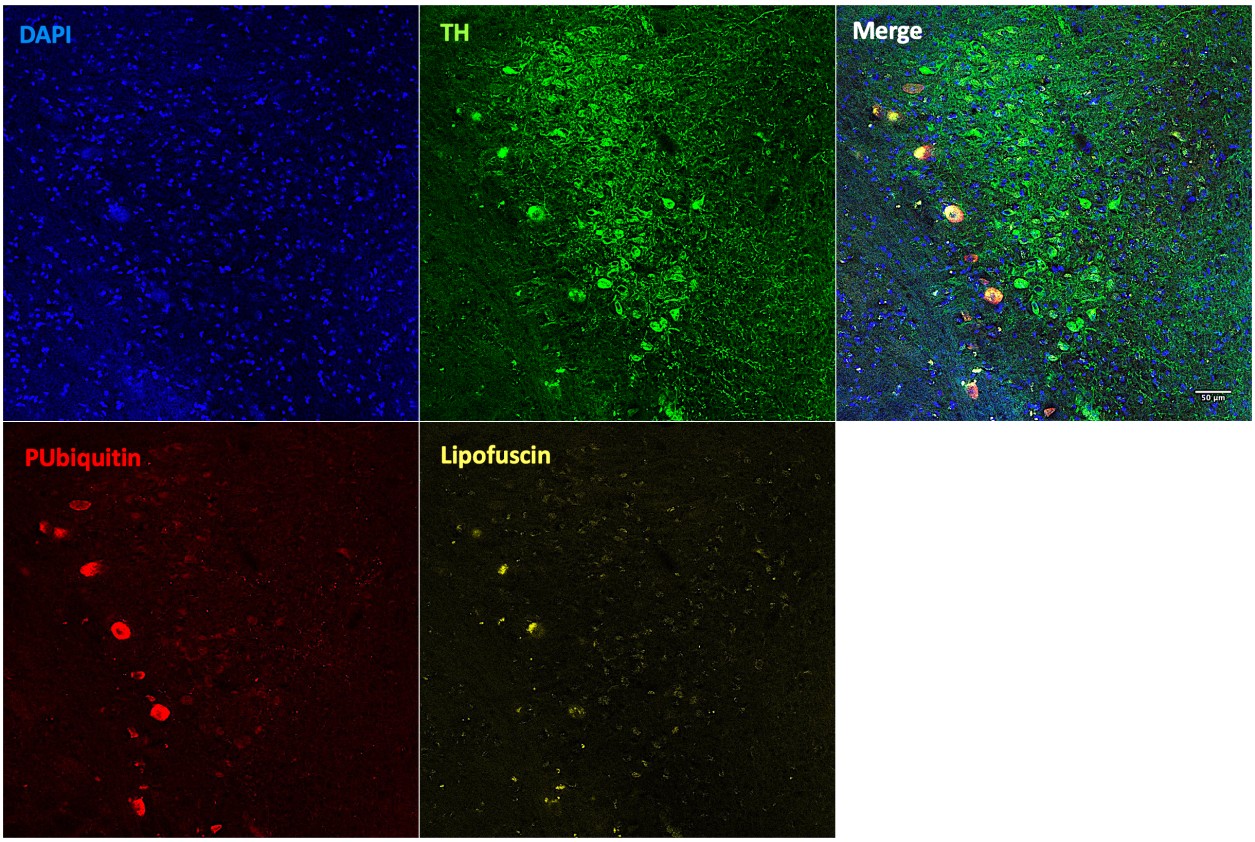

Figure 20: Phospho-Ubiquitin and Lipofuscin staining in LC.
Representative photomicrograph of Phospho-Ubiquitin (PUbiquitin), tyrosine hydroxylase (TH) and Lipofuscin staining within the LC of an 18-month-old wild-type animal. Negative controls were stained only with the secondary antibodies. Scalebar: 50 µm.

Although we did not find any genotype effect regarding Lipofuscin (t_{1267} = 0.3755; p = 0.707), we found a significantly lower Phospho-Ubiquitin signal in Cnr1$^{-/-}$ animals compared to wild-type controls (U = 23195; p = < 0.0001) indicating a possible alteration in the mitophagy process (**Figure 21**).

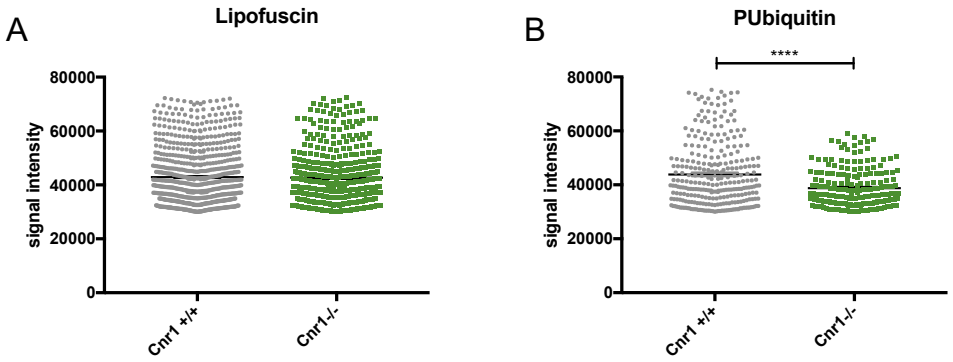

Figure 21: Altered mitophagy in the LC of aged Cnr1$^{-/-}$ mice.
Analysis of Lipofuscin **(A)** and PUbiquitin **(B)** signal intensity in tyrosine hydroxylase (TH)-positive cells within the LC of 18-month-old wild-type (Cnr1$^{+/+}$) and Cnr1$^{-/-}$ animals. **** $p < 0.0001$ according to Mann-Whitney test (n = 313 – 244 for PUbiquitin and 930 – 526 for Lipofuscin, per genotype). Dots represent single values; error bars represent standard error of means (SEM).

3.6. DAGL in the aging LC

3.6.1. DAGLα age-related increase in noradrenergic neurons

To better understand the role of the endocannabinoid system in the aging process of LC, we analyzed the diacylglycerol lipase alpha (DAGLα) protein expression within noradrenergic neurons from young (3-month-old, **Figure 22 A**) and old (22-month-old, **Figure 22 B**) wild-type animals.
For detailed information about the experimental protocol and the analysis see **2.10.1** and **2.12.2**.

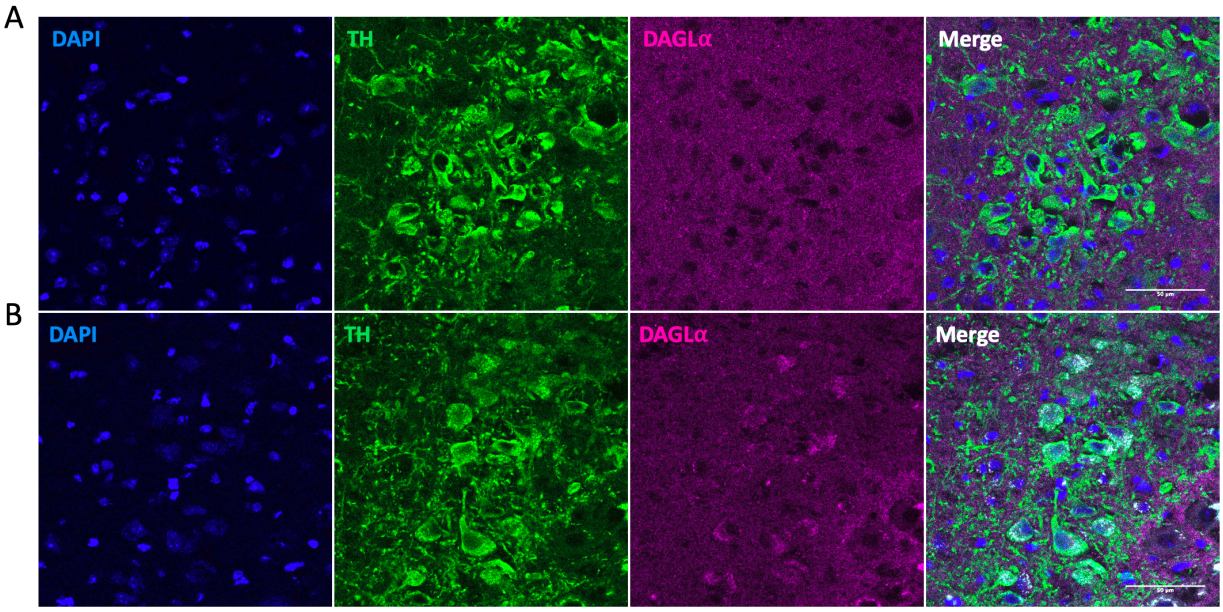

Figure 22: Diacylglycerol lipase alpha staining in LC.
Representative photomicrograph of diacylglycerol lipase alpha (DAGLα), and tyrosine hydroxylase (TH) staining within the LC of 3-month-old **(A)** and 18-month-old **(B)** wild-type animals. Negative controls were stained only with the secondary antibodies. Scalebar: 50 μm.

As it is possible to see in **Figure 22**, we could detect a clear accumulation of DAGLα protein within noradrenergic neurons of old animals compared to young ones. This rise seems to begin gradually from 11-13-months of age, as it is possible to notice from **Figure 23**, becoming prominent in later timepoints.

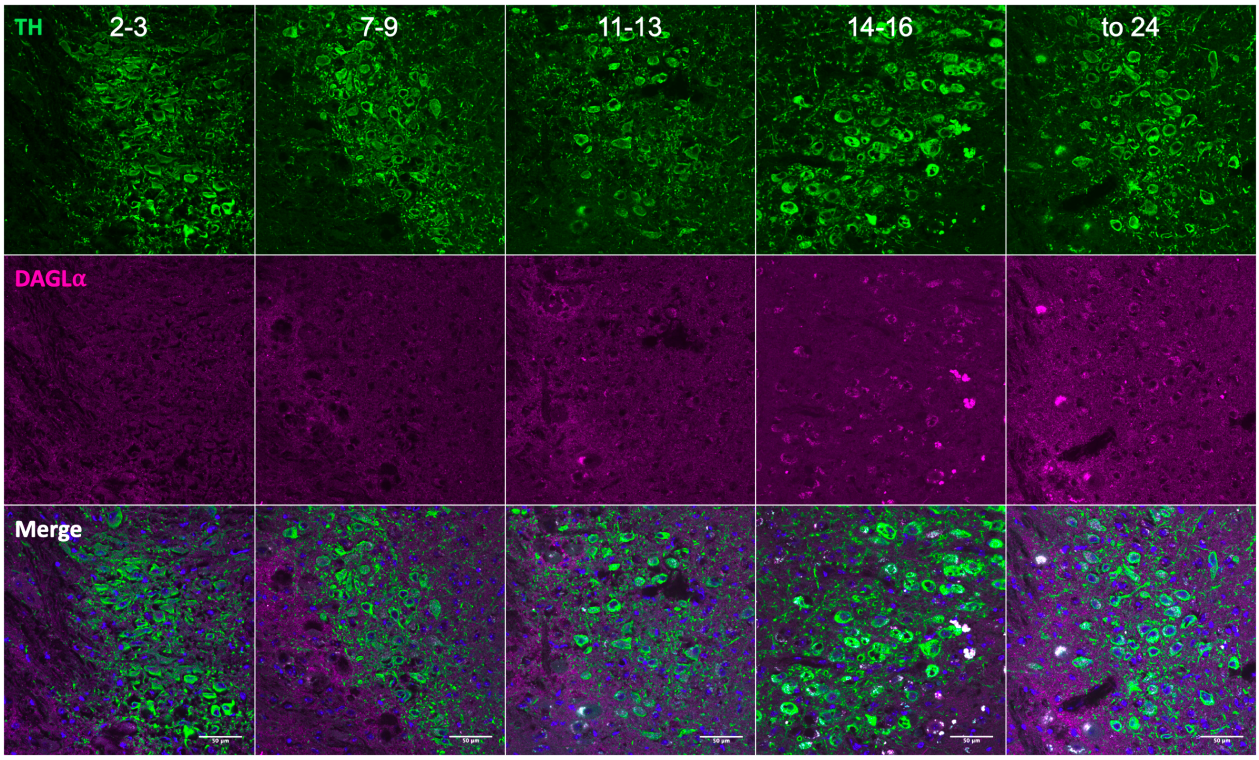

Figure 23: Timeline of Diacylglycerol lipase alpha accumulation in LC.
Representative photomicrograph of diacylglycerol lipase alpha (DAGLα), and tyrosine hydroxylase (TH) staining within the LC from different age groups (2-3, 7-9, 11-13, 14-16 and up to 24-months). Negative controls were stained only with the secondary antibodies. Scalebar: 50 μm.

To understand if it was a process shared with the other catecholaminergic neurons, we analyzed in addition to LC also SN and VTA. Interestingly, we could not see the same pattern in old animals as in LC in neither SN or VTA (**Figure 24**).

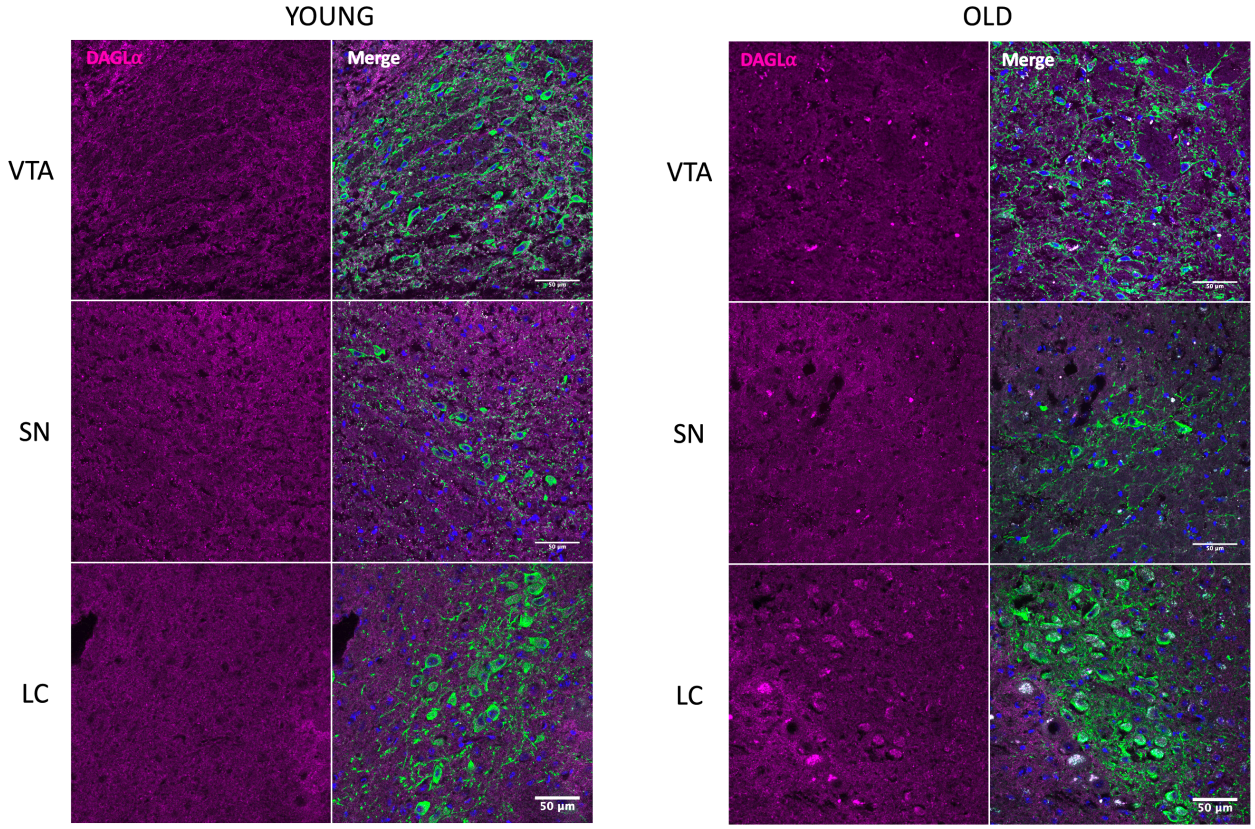

Figure 24: Diacylglycerol lipase alpha staining in LC, SN and VTA.
Representative photomicrograph of diacylglycerol lipase alpha (DAGLα) staining comparing the LC, SN and VTA of young (3-month-old) and old (22-month-old) wild-type animals. Negative controls were stained only with the secondary antibodies. Scalebar: 50 µm.

These data were also confirmed by the subsequent quantifications of DAGLα, which showed a statistically significant increase of DAGLα protein in old animals compared to young controls in LC (U = 1; p = 0.0003) (**Figure 25 A**) but not in VTA (t_9 = 0.4181, p = 0.6857) or SN (t_{17} = 0.2733, p = 0.7879) (**Figure 25 B–C**). Note that only groups represented on the same panels in **Figure 25 B** and **Figure 25 C** are comparable, because they were stained together in the same staining series.

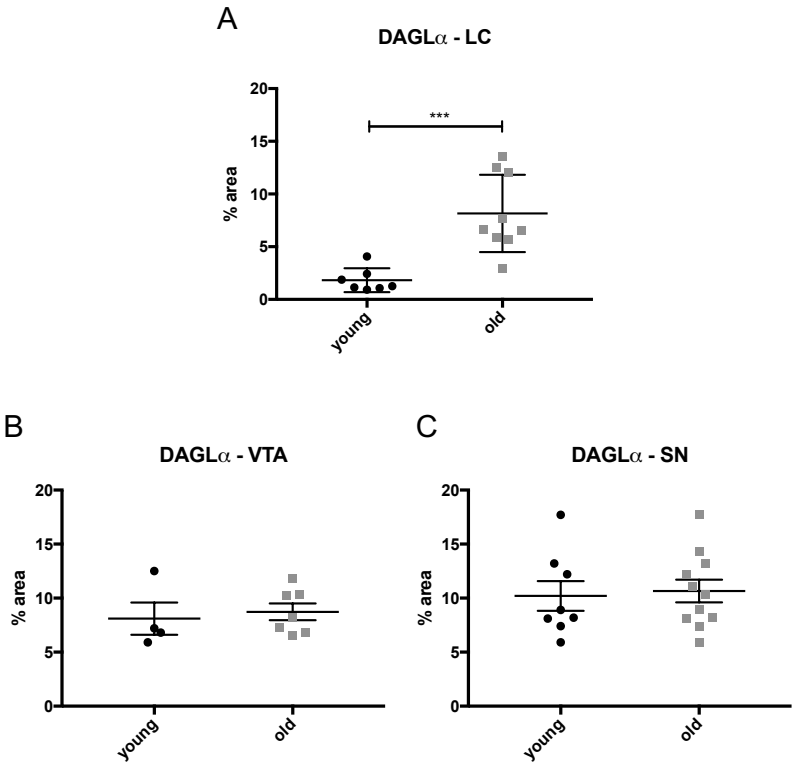

Figure 25: DAGLα age-related increase in noradrenergic neurons.
Analysis of DAGLα protein in the catecholaminergic nuclei LC **(A)**, VTA **(B)** and SN **(C)** of young (3-month-old) and old (22-month-old) C57BL/6J wild-type mice. *** p = 0.0003 according to Mann-Whitney test (n = 4 – 11 per age group). Dots represent single animals; error bars represent standard error of means (SEM).

3.6.2. DAGL gene expression in noradrenergic neurons during aging

To better comprehend the variations of DAGL enzyme throughout the aging process of the LC, we analyzed the RNA level of both DAGLα (**Figure 26**) and DAGLβ (**Figure 27**) in young (2-month-old) and old (18-month-old) wild-type animals. For the detailed procedure and analysis see **2.11** and **2.12.4**.

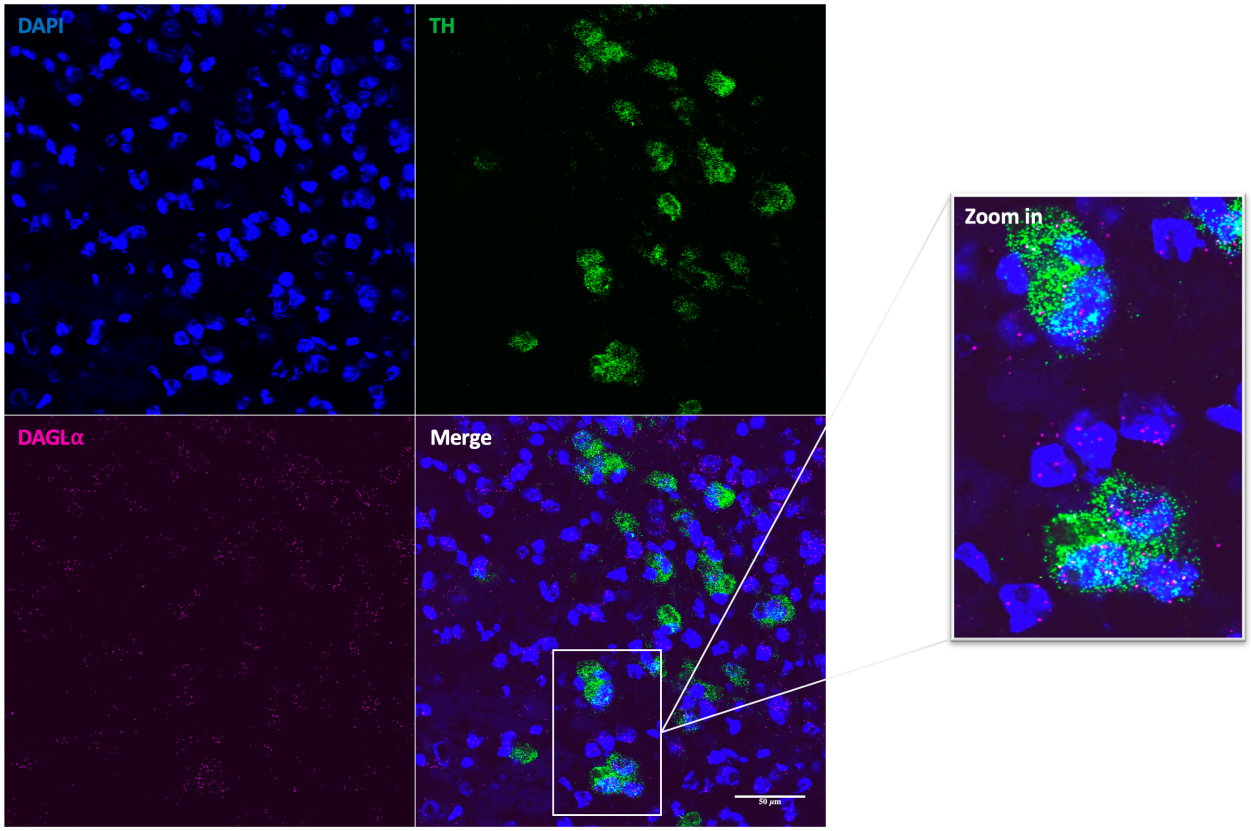

Figure 26: RNAscope for DAGLα in LC.
Representative photomicrograph of diacylglycerol lipase alpha (DAGLα) and tyrosine hydroxylase (TH) RNAscope within the LC of a young (2-month-old) wild-type animal. Scalebar: 50 μm.

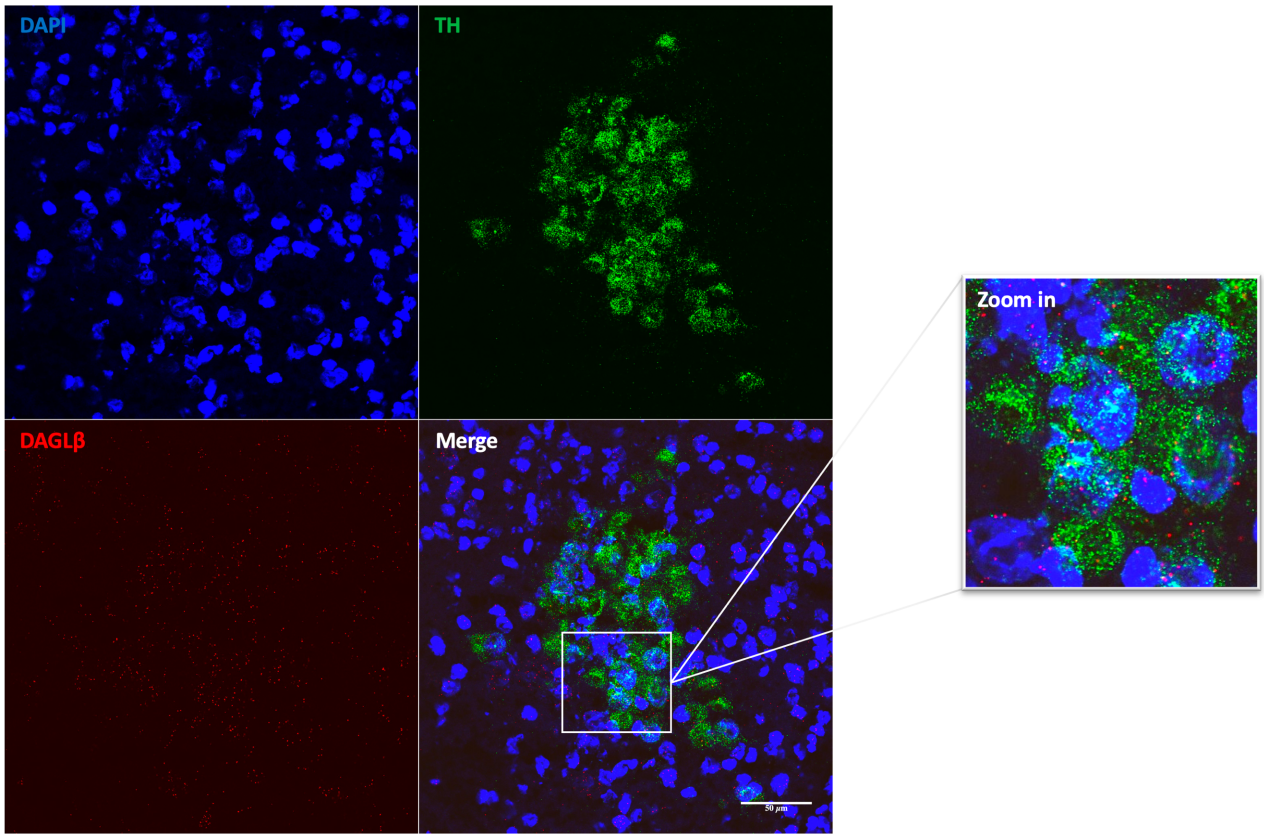

Figure 27: RNAscope for DAGLβ in LC.
Representative photomicrograph of diacylglycerol lipase beta (DAGLβ) and tyrosine hydroxylase (TH) RNAscope within the LC of a young (2-month-old) wild-type animal. Scalebar: 50 μm.

Surprisingly, we did not find an age-related difference for DAGLα (t_{58} = 0.9324; p = 0.355) (**Figure 28 A),** indicating that the increase of DAGLα protein was not due to an increase at the gene expression level.

However, we found an unexpected statistically significant increase of DAGLβ (t_{49} = 2.138; p = 0.0375) in old animals compared to young controls (**Figure 28 B**).

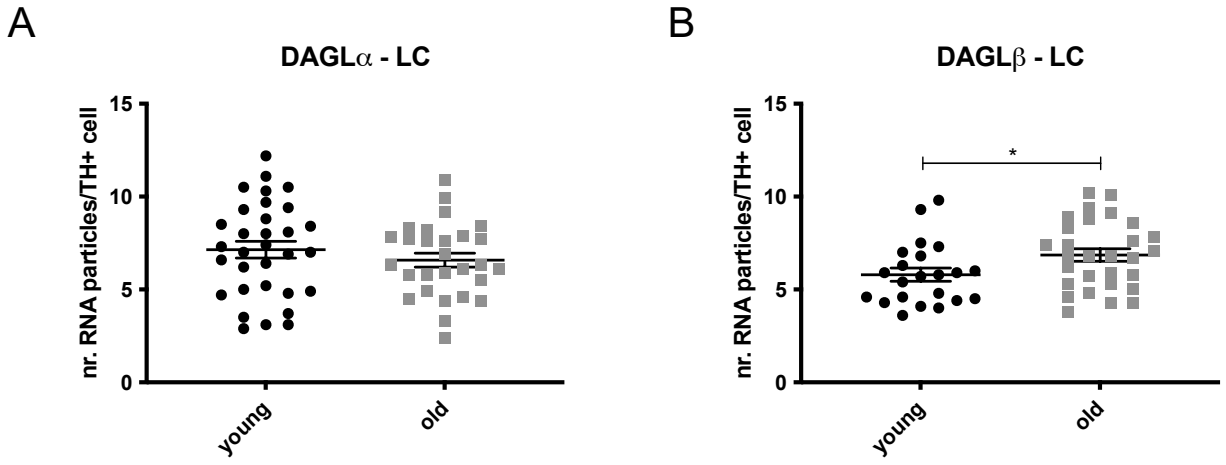

Figure 28: RNAscope for DAGLα and DAGLβ in noradrenergic neurons during aging.
Quantification of DAGLα **(A)** and DAGLβ **(B)** particles within tyrosine hydroxylase (TH)-positive cells from young (2-month-old) and old (18-month-old) wild-type mice. * $p < 0.05$ according to Student´s t-test (n = 32 – 28 for DAGLα and 24 – 29 for DAGLβ, per age group). Dots represent single cells; error bars represent standard error of means (SEM).

3.7. Reduced noradrenergic signalling contributes to age-related cognitive deficits

3.7.1. DSP-4-induced simulation of age-related neurodegeneration of LC neurons

As can be seen from the results shown in paragraph **3.1**, we found that during aging the LC undergoes a neurodegeneration of about 20 % of neurons. Therefore, we aimed to understand the importance of this percentage and how much this neuronal loss affects some aspects of the behavioral sphere in aging.

In order to do so, we used the DSP-4 toxin to simulate in young mice the LC age-related neuronal loss. For a description of the toxin and its preparation see **2.7**.

Despite being a widely used toxin, the most common dose used in literature is 50 mg/kg which, used in acute form, caused the death of a large percentage of neurons. However, what we needed was only a 20 % reduction; therefore, the first step was to establish the dose of DSP-4 toxin to use in order to obtain a 20 % reduction in the number of noradrenergic neurons. Accordingly, we injected intra peritoneally 5 weeks old wild-type mice with different doses of DSP-4 (50, 25, 12.5 and 6.25 mg/kg) and vehicle solution and

after 60 days we sacrificed them and counted the number of LC TH-positive cells as described in **2.9** - **2.10.1** - **2.12.1** (**Figure 29**).

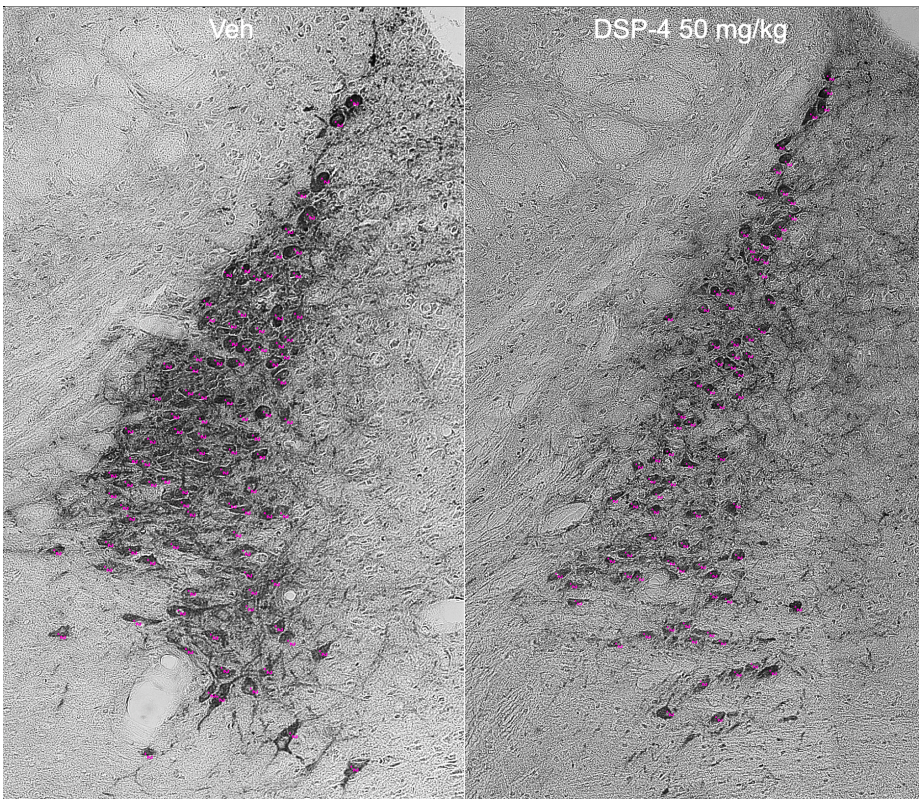

Figure 29: Representative photomicrographs of TH-positive cells count.
Representative photomicrographs of the tyrosine hydroxylase (TH)-positive regions locus coeruleus (LC) of vehicle and DSP-4 50 mg/kg treated mice.

Consistent with expectations, what we obtained was a curve in which the cell count was inversely proportional to the toxin dose (**Figure 30 A**).
Through the simple linear regression model (**Figure 30 B**), we could determine the efficacy of the toxin ($r^2 = 0.9940$; DFn, DFd = 1, 3; $p = 0.0002$) and the equation to derive the right dose of DSP-4:

$$Y = 17.38x - 0.001460$$

Finally, the dose of DSP-4 to be used to obtain 20 % cell death was 14 mg/kg.

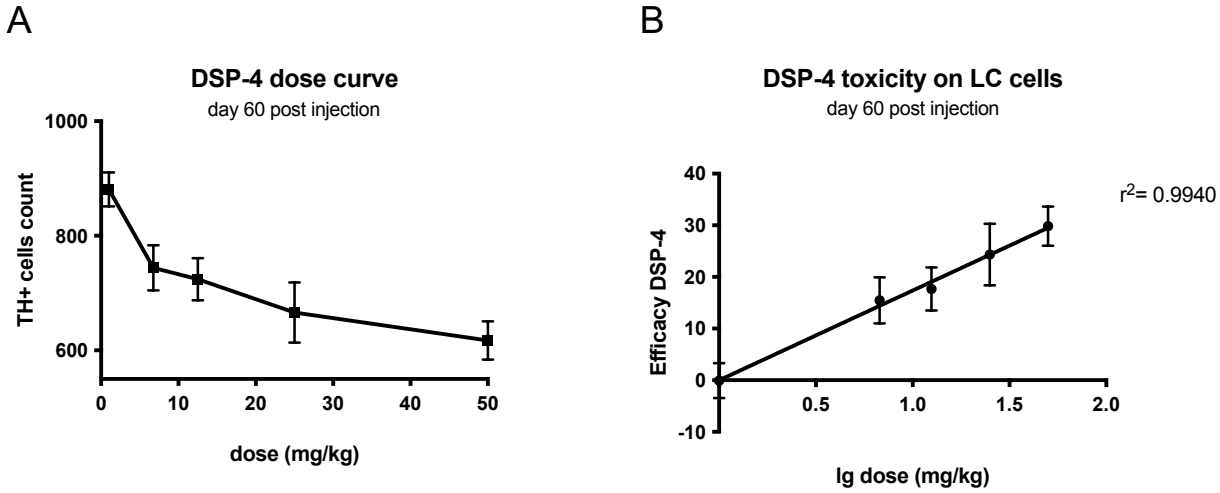

Figure 30: DSP-4 dose seeking curve.
Quantitative stereological analysis of the total number of TH-positive cells in 5 week old animals post treatment with serial concentration of DSP-4 toxin **(A)**. Representation of simple linear regression model on normalized data **(B)** (n = 6 per dose). Shapes represent mean values, and error bars represent standard error of means (SEM).

3.7.2. Age-related working memory and fear learning deficits in C57BL/6J mice

In order to clarify whether a reduced noradrenergic signalling contributes to age-related cognitive deficits, we tested young (3-month-old) and old (20-month-old) C57BL/6J wild-type animals in a battery of models sensitive to both age-related decline and noradrenergic signalling.

Fear learning and extinction were tested in the contextual fear conditioning test (described in detail in **2.8.1**); working memory and attention in the presence or absence of distractors were tested in the 5-CSRTT (described in detail in **2.8.2**).

In the fear conditioning test, we did not find any difference in the baselines of young and old animals. After the fear conditioning protocol, both age groups showed a significant increase in freezing response (Baseline vs Day1: young: $p = 0.0068$; old: $p = < 0.0001$). Nevertheless, our data clearly show that, while for young animals the fear memory seems to be extinct already at day 2, old animals need one additional day to do so (Baseline vs Day2: young: $p = 0.7175$; old: $p = < 0.0001$. Baseline vs Day3: young: $p = 0.9858$; old: $p = 0.0622$) (**Figure 31 A–B**). Overall, our data show that there is a significant difference

between the two age groups in the fear memory extinction and thus that aging plays a key role in this phenomenon (Age: $F_{(1, 18)} = 12.18$; $p = 0.026$. Time: $F_{(4, 72)} = 28.87$; $p = < 0.0001$. Time x age: $F_{(4, 72)} = 8.111$; $p = < 0.0001$).

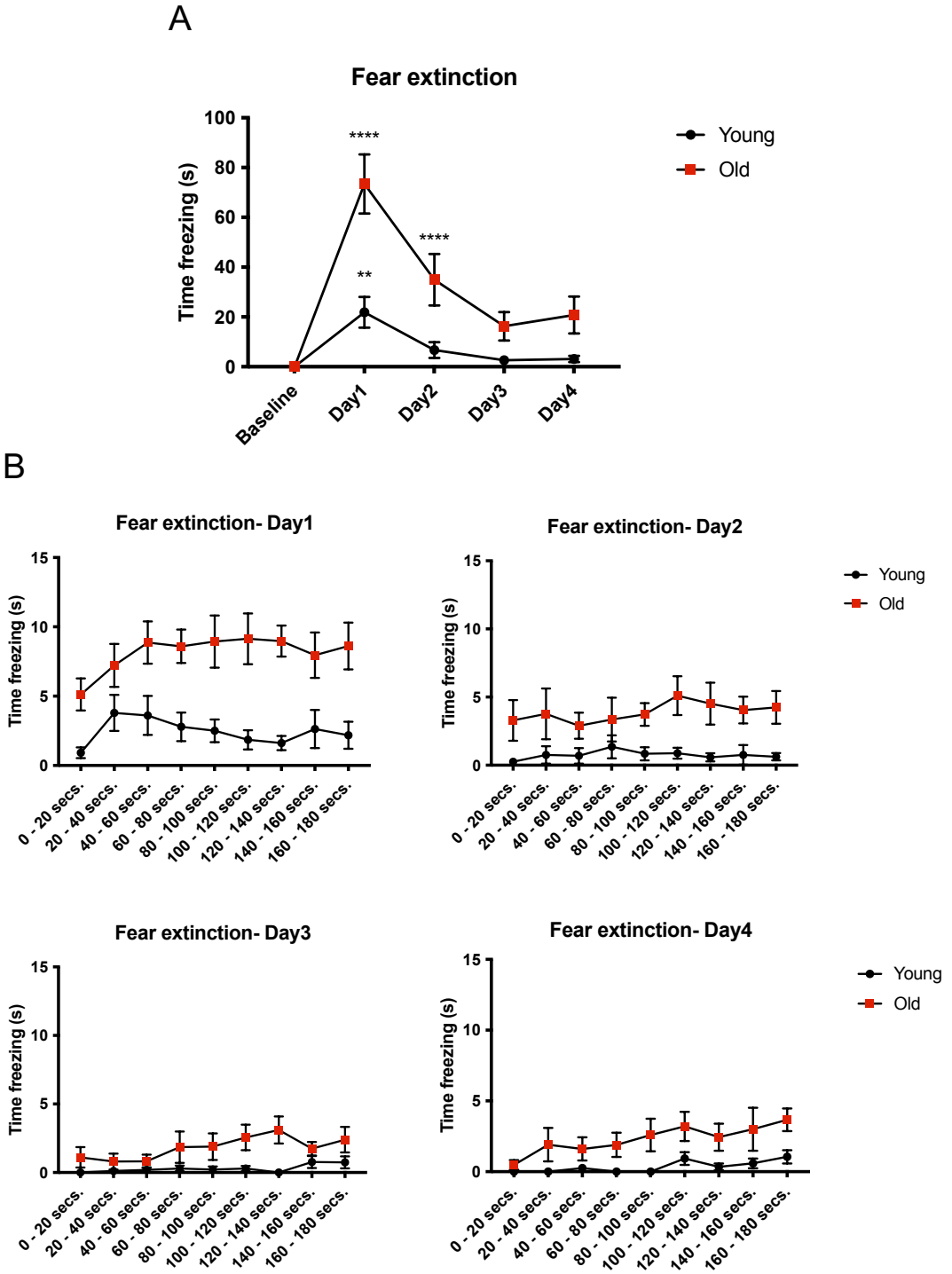

Figure 31: Fear extinction in young and old in C57BL/6J mice.
Analysis of time freezing (s) in the fear extinction process of young and old C57BL/6J mice. * refers to the comparison between the baseline and the day of fear extinction analyzed. **** $p < 0.0001$; ** $p = 0.0068$ according to Dunnett's multiple comparisons test (n = 10 per age group). Shapes represent mean values; error bars represent standard error of means (SEM).

With regards to the 5-CSRTT test, we could detect a striking significant difference between young and old animals in terms of learning capacity: none of the old animals could reach the last phase of the test during the whole duration of the behavior, while the 75 % of the young could (Log-rank (Mantel-Cox) test p = 0.0005) (**Figure 32 A**).

Nevertheless, we tested attention in both groups in the presence or absence of distractors in the phase the single animals were the last week of test. Despite the presence of the distractor, our data clearly show a prominent age effect: old animals perform much worse compared to young controls in terms of correct answers (**Figure 32 B**) and incorrect answers (**Figure 32 C**) (Correct answers: distractor: $F_{(1, 20)} = 7.420$; p = 0.0131. Age: $F_{(1, 20)} = 8.657$; p = 0.0081. Age x distractor: $F_{(1, 20)} = 0.7474$; p = 0.3976) (Incorrect answers: distractor: $F_{(1, 20)} = 0.6438$; p = 0.4318. Age: $F_{(1, 20)} = 48.12$; p = <0.0001. Age x distractor: $F_{(1, 20)} = 5.794$; p = 0.0259) while consequently the omissions were less (**Figure 32 D**) (Omissions: distractor: $F_{(1, 20)} = 8.025$; p = 0.0103. Age: $F_{(1, 20)} = 40.85$; p = <0.0001. Age x distractor: $F_{(1, 20)} = 0.777$; p = 0.3885).

Probably due to the fact that old animals were not able to reach the last phase of the behavior, we could not clearly attest to the effect of the distractor on attention, nonetheless it is clear that in aged animals the overall choice accuracy during the distractor phase was lower compared to young controls (**Figure 32 E**) (-D, +D: p = <0.0001).

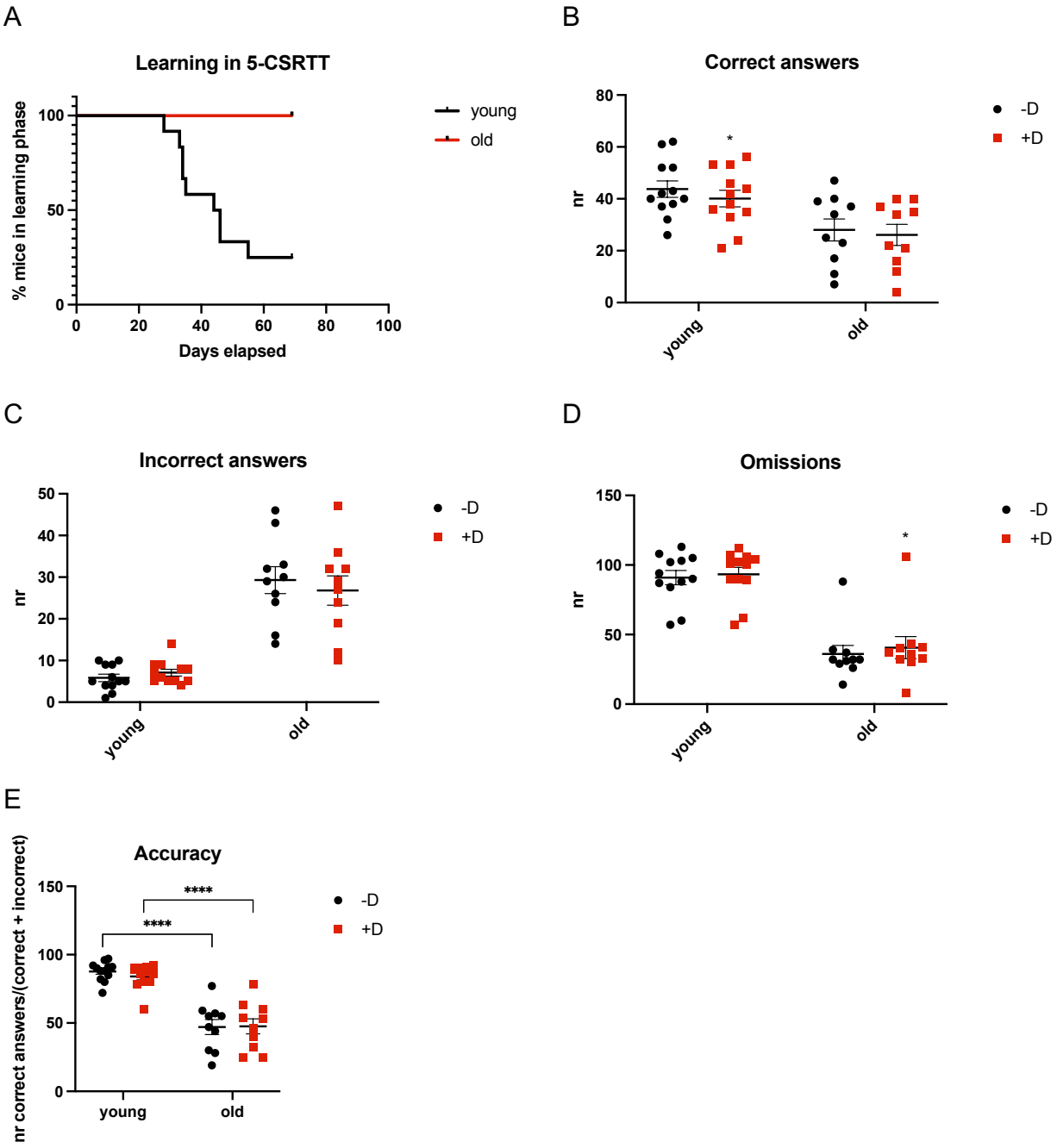

Figure 32: 5-CSRTT in young and old C57BL/6J mice.
Analysis of the leaning capacity of young and old **(A)**, the number of correct **(B)**, incorrect **(C)** and omitted **(D)** answers and the accuracy **(E)** in the presence or absence of distractor (+D, -D). **** $p < 0.0001$, * $p = 0.0298$ **(B)** and 0.0407 **(D)** according to Šídák's multiple comparisons test (n = 10 –12 per age group). Shapes represent mean values **(A)** or single animals **(B–C–D)**; error bars represent standard error of means (SEM).

3.7.3. A reduced number of noradrenergic neurons is responsible for working memory but not fear learning deficits in C57BL/6J mice

As is it possible to see in **Figure 31**, we showed that in aged animals there is an altered extinction of fearful memories. To understand if the age-related neuronal loss in the LC is responsible for this behavior, we injected 4-month-old animals with the DSP-4 toxin (14 mg/kg, see **3.7.1**) and tested them in the contextual fear conditioning (see **2.8.1** and **3.7.2**) together with vehicle injected controls. As it is possible to denote from the **Figure 33**, both DSP-4 and vehicle injected mice show an increase in freezing response right after the fear conditioning protocol (Baseline vs Day1: DSP-4: $p = < 0.0001$; vehicle: $p = < 0.0001$). However, we found no difference between the two groups in the process of fear extinction as both groups seem to extinct the fearful memory from day 2 on (Baseline vs Day2: DSP-4: $p = 0.8474$; vehicle: $p = 0.4811$). So, the lack of a difference between groups indicates that the reduction in noradrenergic neurons is not responsible for the age-related deficit in fear extinction process (Treatment: $F_{(1, 18)} = 0.00183$; $p = 0.9664$. Time: $F_{(4, 72)} = 36.62$; $p = < 0.0001$. Time x treatment: $F_{(4, 72)} = 0.1546$; $p = 0.9303$).

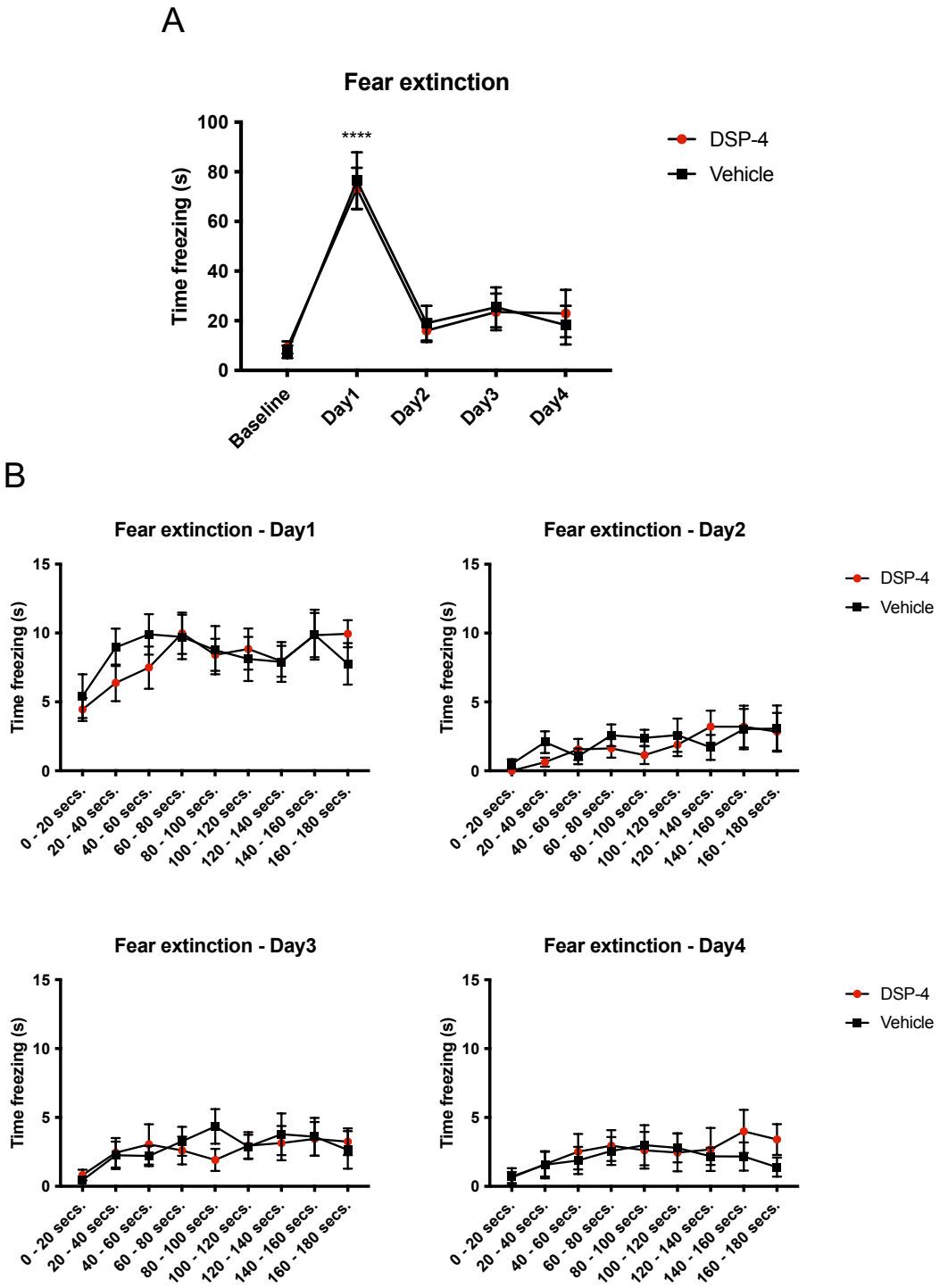

Figure 33: Fear extinction in DSP-4 and vehicle treated mice.
Analysis of time freezing in the fear extinction process of DSP-4 and vehicle injected mice. * refers to the comparison between the baseline and the day of fear extinction analyzed. **** $p < 0.0001$ according to Dunnett's multiple comparisons test (n = 10 per treatment). Shapes represent mean values; error bars represent standard error of means (SEM).

In order to test working memory and attention too, we injected an additional cohort of 4-month-old animals with the DSP-4 toxin (14 mg/kg, see **3.7.1**) and tested them in the 5-CSRTT (see **2.8.2** and **3.7.2**) together with vehicle injected controls. As shown in **Figure 34 A**, we could detect a significant difference between DSP-4 and vehicle injected animals already in terms of learning capacity using Log-rank (Mantel-Cox) test ($p = 0.0432$): DSP-4 animals needed more time to reach the last phase of the test compared to vehicle injected controls. Moreover, our data demonstrate that the distractor has an effect on the number of correct and incorrect responses in both groups but not the treatment per se, indicating that under normal conditions the DSP-4 treated animals performed in a comparable way with vehicle controls. Nevertheless, it is statistically significant the interaction between the distractor and the DSP-4 treatment for both correct and incorrect answers, but not for the omissions (Correct answers: distractor: $F_{(1, 23)} = 31.93$; $p = < 0.0001$. Treatment: $F_{(1, 23)} = 0.9214$; $p = 0.3471$. Treatment x distractor: $F_{(1, 23)} = 9.648$; $p = 0.0050$) (Incorrect answers: distractor: $F_{(1, 23)} = 2.804$; $p = 0.1076$. Treatment: $F_{(1, 23)} = 0.1743$; $p = 0.6802$. Treatment x distractor: $F_{(1, 23)} = 6.382$; $p = 0.0189$) (Omissions: distractor: $F_{(1, 23)} = 4.802$; $p = 0.0388$. Treatment: $F_{(1, 23)} = 1.056$; $p = 0.3147$. Treatment x distractor: $F_{(1, 23)} = 0.1358$; $p = 0.7158$). We found that in presence of the distractor the DSP-4 treated mice showed a poorer choice accuracy compared to vehicle controls which do not seem to be affected by it: DSP-4 treated animals in the presence of the distractor gave significantly fewer correct and more incorrect responses, while omissions were unaffected as in principle they are not influenced by the distractor (Correct answers: vehicle: $p = 0.1306$; DSP-4: $p = < 0.0001$. Incorrect answers: vehicle: $p = 0.7765$; DSP-4: $p = 0.0199$. Omissions: vehicle: $p = 0.3320$; DSP-4: $p = 0.1912$) (**Figure 34 B–C–D**).

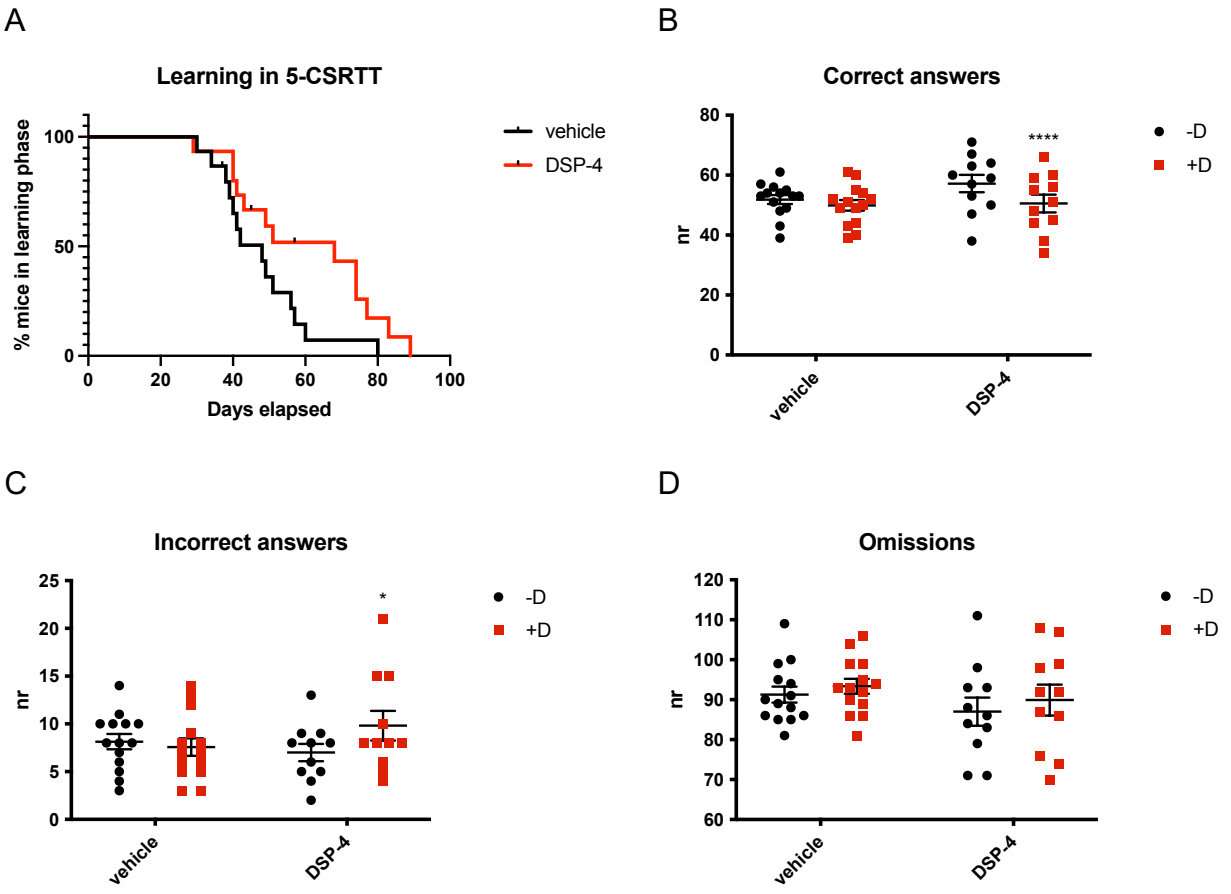

Figure 34: 5-CSRTT in DSP-4 and vehicle treated mice.
Analysis of the leaning capacity of DSP-4 and vehicle injected mice **(A)** and of the number of correct **(B)**, incorrect **(C)** and omitted **(D)** answers in the presence or absence of distractor (+D, -D). **** $p < 0.0001$, * $p = 0.0199$ according to Šídák's multiple comparisons test (n = 11 –15 per treatment). Shapes represent mean values **(A)** or single animals **(B–C–D)**; error bars represent standard error of means (SEM).

In order to confirm the effect of the DSP-4 toxin injection, we sacrificed the animals after the behavioral test and performed a NET staining in prefrontal cortex (PFC) (**Figure 35 A**). As expected, we found a significant decrease of roughly 15 % in the area covered by NET-positive axon terminals in DSP-4 treated animals (**Figure 35 B**).

Therefore, altogether our data support the hypothesis that the age-related reduction of noradrenergic neuronal number is responsible for the working memory and attention deficits occurring in the context of aging.

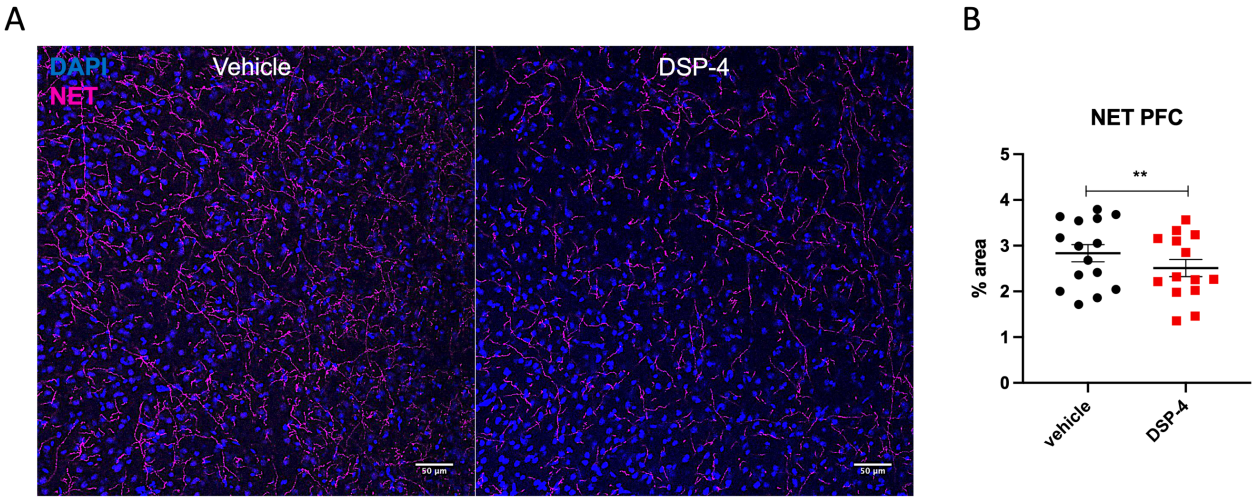

Figure 35: Norepinephrine transporter staining in prefrontal cortex of vehicle and DSP-4 injected animals.
Representative photomicrograph of norepinephrine transporter (NET) staining within prefrontal cortex (PFC) of vehicle and DSP-4 injected animals. Negative controls were stained only with the secondary antibodies. Scalebar: 50 µm **(A)**. Analysis of the area covered by NET-positive axon terminals in the PFC of vehicle and DSP-4 injected animals **(B)**. ** p = 0.0018 according to 2way ANOVA (n = 14 – 15 per treatment). Dots represent single animals; error bars represent standard error of means (SEM).

4. Discussion

The locus coeruleus (LC) is a small nucleus located in the pons of the brainstem which represents the major source of noradrenaline (NE) in the central nervous system. The aim of this study was to shed light on the age-related changes of the LC-NE system, with a special focus on the role played by the endocannabinoid system. The results and their implications are discussed in the following chapter.

4.1. The LC undergoes a process of the age-related neurodegeneration in C57BL/6J mice

It has been widely demonstrated that the LC undergoes structural changes in neurodegenerative diseases such as PD and AD (Braak et al., 2003, 2011), already identifiable in patients with just mild cognitive impairment (Reddy and Oliver, 2019). The neuronal loss in the LC in AD patients is higher than the loss of cholinergic neurons (Ordureau et al., 2015) and also in PD the neuronal loss is more intensive in the LC than in the SN (Hou et al., 2018).

On the contrary, many controversial results emerged regarding changes during physiological aging. Despite a decrease in neuronal numbers have been proposed for decades to be the major cause of a reduced brain function in aging, the magnitude and time course of age-related neuronal loss are still debated (Flood and Coleman, 1988). Nevertheless, a recent in vivo study based on a sophisticated magnetization transfer weighted imaging technique showed an inverted U-shaped pattern between LC signal intensity and age, whereby there is an age-related increase until the age of 60 followed by a decline in signal intensities. This recent finding supports the theory that in humans there is an age-related shrinkage or loss of neuromelanin containing noradrenergic neurons in the LC also in healthy subjects (Liu et al., 2019).

As for mice, controversial results are reported about an age-related change in LC neuronal numbers mostly depending on the mouse strains used: no change (Leslie et al., 1985), decline (Tatton et al., 1991) and even increase (Szot et al., 2009) were reported. These studies, however, were not conducted using a stereological technique, which might explain the inconsistency of the data across the different publications.

Thus, using unbiased stereological counting now we showed a reduced number of neurons in the LC of old C57BL/6J mice compared to young ones (**Figure 8 A**), strongly supporting the evidence of an age-related neurodegeneration of the LC in this mouse line. Interestingly, the number of dopaminergic neurons in the SN and VTA remained unaltered (**Figure 8 B–C**), indicating a particular vulnerability to aging of the LC compared to other brain regions. Our data about the LC are therefore comparable with the data in humans (Liu et al., 2019) pointing out that C57BL/6J mice are a good model for the study of the age-related neuronal loss in this brain region, its mechanism and consequences.

When testing at what stage of life the neurodegenerative process of LC took place, we found a clear decrease in the TH-positive cells number in the age group 7-9-months and that this number remained unchanged until old age (**Figure 9**). Despite aging is considered to be associated with progressive changes in the brain, rather little is known about the changes happening from young adulthood (2-7 months) to middle age (8-12 months). Interestingly, Shoji et al. (2016) conducted a large-scale analysis of age effects on behavior in C57BL/6J wild-type mice using the data from up to 1739 animals from 2 to 12 months of age, diving them into four age groups: 2–3, 4–5, 6–7, and 8–12 months of age. They performed a battery of behavioral tests finding a gradual decrease in motor functions and neuromuscular strength with age, together with an increase in anxiety-like behavior and a decrease in social contacts. In particular, they examined the mice in the startle response/prepulse inhibition test and in the fear conditioning test, both known to be associated with the activity of the noradrenergic system (Fendt et al., 1994; Giustino and Maren, 2018; Kokkinidis and Anisman, 1978; Saitoh et al., 1986). They detected an age effect in the startle response/prepulse inhibition test in the prepulse inhibition (PPI); indeed, 8-12-old-month mice showed a lower startle response compared to all the other age groups. Also for the fear conditioning, 8-12-old-month mice showed a greater freezing behavior during the last phase of the conditioning session and also a higher activity suppression ratio (distance traveled during the first 2 min in the context test/distance traveled during the first 2 min in the conditioning + distance traveled during the first 2 min in the context test), compared to all the other age groups. These data not only indicate an aging effect in the startle response and an impaired contextual fear memory in older animals, but also focus the attention on a time period (8-12 months) which could prove essential in the brain aging process. Furthermore, these data seem consistent with our

findings about the timeline of neurodegeneration in LC, suggesting that possibly the age-related changes of noradrenergic system start as well from middle age.

4.2. A constitutive genetic disruption of CB1r signaling accelerates the age-related loss of noradrenergic LC neurons

We compared the number of LC neurons in old wild-type and Cnr1$^{-/-}$ mice in order to comprehend the importance of CB1r in the survival of this neuronal type which appears to be particularly sensitive to the process of aging. Our data showed that the age-related loss of LC neurons was more pronounced in Cnr1$^{-/-}$ mice, strongly indicating that a constitutive genetic disruption of CB1r signaling exacerbates the age-related loss of noradrenergic LC neurons in C57BL/6J mice (**Figure 10 A**). Therefore, the findings from this study indicate a possible neuroprotective role of the CB1r in the survival of noradrenergic neurons during aging. We could exclude that this difference was due to a developmental effect of the CB1r deletion rather than to a real aging effect on the LC neuronal population since we did not find a genotype effect in LC neuronal numbers comparing young Cnr1$^{-/-}$ mice and age-matched wild-type controls (**Figure 10 D**).
Interestingly, only the number of LC neurons, but not SN or VTA neurons, differed between genotypes, being lower in Cnr1$^{-/-}$ mice than in age-matched wild-type controls (**Figure 10 B–C**). Therefore, on one hand the lower number of LC neurons in Cnr1$^{-/-}$ mice compared to age-matched wild-type controls strongly indicates an important neuroprotective effect of CB1r activity, while, on the other hand, the lack of the same outcome in SN and VTA suggests a particular importance of the CB1r in cell populations where an aging-effect is already existing, like the LC. Our findings are also in line with the previously reported enhanced age-related loss of hippocampal neurons in Cnr1$^{-/-}$ mice (Bilkei-Gorzo et al., 2005). It is important to note, however, that Cnr1$^{-/-}$ mice do not show a general decline in neuronal numbers in old animals although it seems to be restricted to the LC and hippocampus, which are brain areas that show neuronal loss during aging in wild-type animals.

4.3. Aged Cnr1$^{-/-}$ mice show reduced density of noradrenergic axon terminals in the projection areas

The noradrenergic system is well known to be incredibly adaptable. Therefore, we further asked whether the observed decreased neuronal number in Cnr1$^{-/-}$ mice leads to a loss of noradrenergic axons or whether the remaining noradrenergic neurons may be balancing for the loss to maintain the original network with compensatory changes (like increasing arborization by sprouting axonal projections) as observed in Alzheimer's disease patients (Szot et al., 2006).

Our data show that a lower number of noradrenergic neurons is associated with a reduced density of noradrenergic axon terminals in the main projecting areas of LC suggesting a low level of compensation (**Figure 14**). Moreover, we observed that this reduction of NET-positive axons in the function of TH-positive neurons in the LC was more intensive in Cnr1$^{-/-}$ mice compared to wild-type mice, so we hypothesize that in the knock-out line the compensatory rate is even less (if any) than in wild-type animals (**Figure 12**). To further prove that there is no developmental effect in the constitutive CB1r knock-out, we repeated the experiment comparing 3-month-old wild-type and Cnr1$^{-/-}$ animals and we could not find neither a difference between genotypes nor a difference in NET signal based on the brain region analyzed (**Figure 13**). This evidence is also in line with the previously reported data showing that the age-related loss of LC neurons is even more pronounced in Cnr1$^{-/-}$ mice and that this is a true age-related process (**Figure 10 A–D**).

Albayram et al. (2011) reported that in old Cnr1$^{-/-}$ mice, where indeed we found a reduced number of LC neurons, the learning flexibility was also severely impaired. Synaptic plasticity is known to be one of the most important neurochemical foundations of learning and memory. Several lines of evidence have shown that catecholamines control synaptic plasticity and that specifically a decrease in noradrenergic signaling in the efferent regions leads to a reduction in neuroplasticity, which may contribute to the deficits in learning flexibility (Mather et al., 2016; Mather and Harley, 2016; Twarkowski and Manahan-Vaughan, 2016). These evidences reinforce our hypothesis that the CB1r plays a fundamental role not only in the survival of noradrenergic neurons in aging but more generally in the functioning of the noradrenergic system and the behaviors controlled by it.

Another peculiarity of LC neurons is that they broadly innervate vast expanses of the CNS, but very less is known about the innervation pattern. Interesting recent studies hypothesized that LC possess a "functional organization": the LC neurons would not innervate randomly the different projecting areas, but on the contrary they would be organized into clusters with unique efferent regions, a preferred terminal field to innervate (Poe et al., 2020). Therefore, we questioned if also the age-related neurodegeneration of LC and/or the knock-out of the CB1r affected in a specific way a determined cluster or if it was a more widespread process. Our study now suggests that neither aging or the knock-out of the CB1r affect a preferential cluster of neurons since we found similar changes in the density of axon terminals in the efferent regions analyzed, only more pronounced in $Cnr1^{-/-}$ animals. It is important to mention though, that one of the limitations of our (and many other) study is the lack of information about others LC projection areas, for example some key motor structures (cerebellum, inferior olive, or motor cortex), deeply affected by aging too. Therefore, one of the next steps could be to investigate whether the noradrenergic innervation of these efferences is as well influenced by the age-related neurodegeneration of LC and to what extent.

4.4. Lack of a pro-inflammatory profile in the LC of $Cnr1^{-/-}$ mice

In order to explain the protective effect of CB1r activity on noradrenergic neurons, we considered its active role in inflammation and investigated the inflammatory glial profile within the LC of old animals. Indeed, loss of hippocampal neurons in constitutive or GABAergic neuron specific $Cnr1^{-/-}$ mice was associated with an increased pro-inflammatory glial activity in the hippocampus (Albayram et al., 2011). The hypothesis that aging is associated with an increase of inflammation (commonly called "inflammaging", Franceschi et al., 2018) is also strengthened by the data from Evans et al. (2021) showing a prominent microgliosis in both LC and hippocampus from old animals compared to young controls.

However, comparing the LC of old wild-type and $Cnr1^{-/-}$ mice, we could not find any difference in microglial expression of neither Iba1 nor TNFα, general indicators of microglia activation (**Figure 16 B–C**). We could though detect in the LC of $Cnr1^{-/-}$ animals a prominent increase (+66 %) of Iba1-positive microglia density (**Figure 16 A**); however, despite Iba1-positive microglia numbers were enhanced (generally interpreted as a sign

of inflammation), the normal Iba1 and TNFα levels suggested that these microglias were not more pro-inflammatory. To be noted, Hammond et al. (2019) compared the RNA expression profile of more that 76000 individual microglia from mice in the developmental stage and in old age. Their data show that, despite aging may trigger a shift toward a more immunogenic profile, the number of microglia in these states is only a small fraction of the total microglia, suggesting that the vast majority of microglia are unaltered or only slightly altered by aging. Therefore, we ruled out inflammation due to increased pro-inflammatory glial activity as a direct cause for the enhanced loss of LC neurons in Cnr1$^{-/-}$ animals.

4.4.1. Altered microglia morphology and phagocytic activity in the aging LC of Cnr1$^{-/-}$ mice

Despite further studies are needed to get a better idea of the role of microglia in the LC and although we have ruled out inflammation as the cause of the LC age-related neurodegeneration in Cnr1$^{-/-}$ animals, microglia cells seem to be anyway influenced by aging in this brain region and the lack of the CB1r may still be affecting the switching between their activation phenotypes. Therefore, we analyzed the morphology of Iba1-positive microglia in 18-month-old wild-type and Cnr1$^{-/-}$ animals by using the MotiQ plugin, obtaining a 3-dimentional analysis (**Figure 6**).

We could identify some differences between genotypes: Iba1-positive microglia from Cnr1$^{-/-}$ animals seemed to have more branches (and consequently more junctions) compared to wild-type controls, but shorter (**Figure 17**). These evidences are not necessarily attributable to a more pro-inflammatory profile, but more likely to the genetic lack of the CB1r. As shown by Beins et al. (2021), Cnr1$^{-/-}$ animals are not only highly sensitive to stress, but under mild stress they also show altered microglial activation marker expression and morphology compared to wild-type controls. Overall Cnr1$^{-/-}$ mice showed a different stress-induced morphological rearrangement compared to wild-type mice, indicating a crucial role of the endocannabinoid system in the modulation of the neuronal stress-induced immune response through CB1r. Furthermore, among the many functions of the noradrenergic system, it is well known how noradrenaline is involved in the morphological changes of microglia after acute stress through the activation of β adrenoreceptors (Sugama et al., 2019). Recent studies have also shown a clear

interaction between the CB1r activation and the β-adr functionality (Martins et al., 2018); also, data from our lab showed that microglia from Cnr1$^{-/-}$ mice overexpress the gene *Adrb1*, encoding for the β1-adrenoreceptor (Beins et al., 2021). These data support the hypothesis that CB1r activity and noradrenergic signaling in microglia are strictly correlated and that, even if we could not detect a striking pro-inflammatory profile in the LC of old Cnr1$^{-/-}$ mice, these alterations in microglia morphology may still be relevant in the progress of the age-related neurodegeneration of noradrenergic neurons.

To know the morphology of microglia is important because it is generally indicative of their response and function. However, the analysis through a single marker does not provide enough information to link microglia to one of the states described in the literature. Therefore, in order to further understand if microglia had any role in the LC age-related neurodegeneration, we decided to analyze microglia's phagocytic activity around the crucial time point identified at 7-9 months of age (**Figure 9**). We used CD68 as it reflects immune activation and response to tissue damage more than Iba1, which is more indicated for structural studies (Hendrickx et al., 2017). We found that in the LC of both wild-type and Cnr1$^{-/-}$ mice, CD68 signal intensity was higher at 7-9 months compared to 2-3 months (**Figure 19 A**), indicating that at this timepoint, in both genotypes, microglia cells began to show increased phagocytic activity, possibly attributable to the onset of the neuronal death. Moreover, in Cnr1$^{-/-}$ mice the microglia cell body size increased at 7-9 months compared to 2-3 months (**Figure 19 B**) and it was significantly higher in all the age groups analyzed compared to wild-type animals. The density of microglia in the LC area was also increased in Cnr1$^{-/-}$ animals only at 7-9 months compared to 2-3 months animals (**Figure 19 D**). Altogether, this data suggests that in both wild-type and Cnr1$^{-/-}$ mice, at the age of 7-9 months, microglia cells start assuming a phagocytic-like profile, probably due to the onset of neuronal death in the LC. Also, microglia seem more abundant and reactive in Cnr1$^{-/-}$ mice, indicating that probably in these animals the neuronal death rate is already more severe compared to wild-type controls. Also in this case, without more in-depth studies it is difficult to associate the microglia to a specific status described in the literature. However, a new status of microglia associated with aging has recently been discovered: the dystrophic microglia. These cells appear to have lost their primary functions and a classic morphology and have been associated with AD too (Lier et al., 2021). As described by Bilkei-Gorzo et al. (2012), the lack of CB1r induces

changes in cognitive function resembling premature signs of aging. Therefore, we cannot exclude the possibility that the lack of CB1r might also influence the morphology of microglia, directing it precociously towards the dystrophic status.

4.5. Reduced mitophagy in the LC of aged Cnr1$^{-/-}$ mice

The reason why noradrenergic neurons in LC seem to be more vulnerable to aging is still quite debated. Different distinctive features of this cell population have been suggested as responsible for the neuronal loss: high oxidative stress due to the noradrenaline synthesis, high neuronal iron content, autonomous pacemaking activity and a very high axonal arborization size (Chrobak et al., 1985; Hagan, 1983). Overall, the cumulative effect of these factors has been hypothesized to result in a global energetic failure responsible for the cell death (Prado de Carvalho and Zornetzer, 1981). Mitochondria are widely recognized as the main suppliers of cell's energy; indeed, their function is critical in cell types particularly energy demanding such as noradrenergic neurons. Bartova and Birmingham (1976) have shown that THC, a well-known CB1r agonist, could affect mitochondrial functions through mitochondrial NADH-oxidase activity. Subsequently Bénard et al. (2012) showed for the first time that CB1r not only are present on neuronal mitochondria (mtCB1r), but also that their direct activation regulates mitochondrial respiration and energy production. The activation of CB1r on the neuronal membrane seems to decrease firing frequency and protects against depletion of energy sources, whereas activation of mitochondrial CB1r decreases mitochondria activity, thus enabling the coupling between firing activity and energy need of the neurons (Hebert-Chatelain et al., 2016). Therefore, in order to understand the cause of the LC age-related neurodegeneration, we analyzed Phospho-Ubiquitin (Serine 65-phosphorylated ubiquitin, Ser65), a key marker for mitochondrial autophagy (also known as mitophagy) within the LC of wild-type and Cnr1$^{-/-}$ 18-month-old animals. Our results showed a significant decreased Phospho-Ubiquitin signal in Cnr1$^{-/-}$ animals compared to wild-type controls, suggesting a lower mitophagy rate (**Figure 21**). Supporting our hypothesis, Evans et al. (2021) performed a proteome analysis of LC comparing young and old animals; they identified major age-related changes in proteins involved in oxidative phosphorylation, metabolomic pathways and mitochondrial functions, showing in LC of aged animals a proteomic signature of metabolic demand and mitochondrial stress. Moreover, our data

were also in line with the observation that the mitochondria in neurons of Cnr1$^{-/-}$ animals show an aberrant morphology and a reduced mitophagy in hippocampus, which is a brain region subject to age-related changes as well (Kataoka et al., 2020) . Altogether, these evidences on one hand support the hypothesis of a central role of mitochondria in the neurodegenerative process of LC and, on the other hand, underline the importance of CB1r in mitochondrial functionality.

4.6. The protective role of DAGL enzyme in the aging process of the LC

Whether the endocannabinoid system undergoes itself age-related changes is still a rather debated topic. Different studies suggested that CB1r expression and coupling activity decrease in aging (Berrendero et al., 1998; Canas et al., 2009; Romero et al., 1998; Wang et al., 2003), while others focused on the ligand AEA showing a reduction of it in old Cnr1$^{-/-}$ animals (Maccarrone et al., 2001, 2002; Wang et al., 2003). Nevertheless, still many aspects have to be clarified. Here we investigated the age-related changes in diacylglycerol lipase (DAGL) enzyme within noradrenergic neurons. The major pool of 2-arachidonoylglycerol (2-AG), the principal endogenous ligand of CB1r in the central nervous system, is synthetized by DAGL, α and β isoforms; genetic deletion of DAGLα leads to ~ 80 % decrease in 2-AG level in the brain, while a deletion of DAGLβ to ~ 50 % (Gao et al., 2010; Jenniches et al., 2016). Piyanova et al. (2015) showed that 2-AG levels decrease during aging in the hippocampus and that this reduction is due to a decreased DAGLα expression, while DAGLβ does not seem to change. Interestingly, our data show that in the LC the dynamics seem to be again different compared to the hippocampus, since we could detect a well-defined accumulation of DAGLα protein within aged noradrenergic neurons compared to young controls (**Figure 22**). Moreover, we could identify the beginning of this protein buildup from 11-13 months of age on (**Figure 23**), suggesting it to be only subsequent to the onset of the age-related neuronal death, which occurs around 8 months of age (**Figure 9**). We did not find the same in neither SN nor VTA, suggesting once again that this process is occurring only in noradrenergic neurons, a specific neuronal population per se sensitive to aging. The possibility that the antibody we used could give such an artifact was ruled out using DAGLα knock-out samples, negative controls and controls in young animals.

The observation that DAGLα may increase in relation to the onset of neuronal death strengthens the hypothesis that this could be a protective mechanism of the remaining noradrenergic neurons. The noradrenergic system has been extensively described as “adaptable” especially in relation to AD. Recent theories hypothesize that there is a massive adaptation of the noradrenergic system in the early stage of the disease, and that the evolution of it occurs due to an impairment in the system integrity rather than a mere loss of NE input (Gannon and Wang, 2019). Supporting this concept, NE decrease has often been observed mostly in advanced AD; in fact, despite LC is one of the first areas impacted during prodromal AD, in some cases NE remains constant or even elevated at this stage (Kalaria et al., 1989; Ruiz et al., 1993; Szot et al., 2006, 2007). Therefore, being the degeneration not a rapid occurrence but rather a gradual process, LC-NE system can actuate compensatory mechanisms in order to counteract these changes and maintain the homeostasis. There are evidences regarding a compensatory sprouting of the remaining neurons in prefrontal cortex and hippocampus (Szot et al., 2006, 2007), increase in the expression of TH and DβH (Giubilei et al., 2004; Szot et al., 2006, 2007) and reduction in NET, the protein responsible for the re-uptake of extracellular NE (Gulyás et al., 2010). Nevertheless, it is possible that these mechanisms may overcompensate, especially at early stage of the LC neurodegeneration, leading to worsening of the disease. Following this logic, DAGLα increase in aging, via 2-AG-mediated depolarization-induced suppression of excitation (DSE) (Straiker and Mackie, 2005) in the remaining neurons, may be an additional protective system in place to avoid this sustained compensatory overexcitation of the remaining LC neurons, overproduction of NE and, subsequently, cytotoxicity.

Another possible explanation for the increase of DAGLα could be linked to the inflammatory process which characterize the aging LC. Evans et al. (2021) describe the presence of microgliosis and the increase of inflammatory proteins in the LC of old animals compared to young controls. Indeed, in literature it has been extensively shown how 2-AG has neuroprotective and anti-inflammatory properties: it increases after brain injuries and improves the consequent cell death (Panikashvili et al., 2001), it inhibits the production of TNFα (Gallily et al., 2000) IFN-γ (Kaplan et al., 2005) and IL-2 (Ouyang et al., 1998). Therefore, DAGLα increase could represent a supplementary way the neurons

use to produce more 2-AG and cope with the age-related inflammation, in order to restore the homeostasis.

The last hypothetical explanation for an increase in DAGLα could be its role in an intracellular signalling pathway. Since the discovery of a mtCB1r (Bénard et al., 2012), the 2-AG produced by the increased DAGLα could act on mitochondria to decrease the neuronal firing frequency, protects against depletion of energy sources and to reduce ROS production.

In our study, we also investigated whether the DAGLα protein increase was due to an increase in its mRNA expression. We did not find any significant age-related difference in the DAGLα mRNA expression, indicating that what we see on the protein level is likely due to a decreased protein degradation. However, surprisingly, our data showed a significant increase in DAGLβ in the aged LC (**Figure 28**). This result, as the protein data, appears to be opposed of what happens in the hippocampus. Piyanova et al. (2015), in fact, showed that DAGLα mRNA expression is lower in the aged hippocampus compared to young control, while DAGLβ remains unchanged. The role of DAGLβ has been partially neglected in the past, when this isoform was thought to be selectively important in microglia. However, even if the role of DAGLβ is still not fully understood in neurons, Schuele et al. (2021) recently showed that it is present in DG hippocampal neurons almost as abundant as DAGLα, consistently with the founding in the LC where the expression of both isoforms is very much equivalent. Supporting the theory of an important contribution of DAGLβ in aging and in line with the DAGLβ mRNA expression increase in aged LC, Pascual et al. (2013) too reported an eightfold increase in this DAGL isoform in the synaptosome fraction from cerebral cortex of old mice compared to young controls. Unfortunately, we could not investigate the protein level of DAGLβ in LC as there is no a DAGLβ knock-out mouse line that can confirm the specificity of the antibodies on the market for immunohistochemistry.

Altogether these results on one hand support the hypothesis that the endocannabinoid system plays a crucial role in the aging process of the LC, and on the other they underline the fact that, although the LC and the hippocampus are regions both sensitive to aging, the mechanisms involved in the neurodegeneration and compensation processes are

profoundly different and might reflect the different nature and peculiarities of the neuronal types.

4.7. The age-related neurodegeneration of LC neurons is responsible for working memory deficits in old C57BL/6J mice

Aging is known to be associated with a decline of cognitive function such as episodic memory (Levine et al., 2002), working memory (Gazzaley et al., 2005), speed of information processing and task switching, and more generally a decline of attention (Robertson, 2013); furthermore, some studies have proven how aging selectively impairs the process of memory extinction and the capacity to use context to modulate learned responses to threat (Battaglia et al., 2018).

All these aspects have been showed to be heavily regulated by the noradrenergic system. Wang et al. (2011) reported how the age-related decline in working memory was normalized by up-regulating the noradrenergic system, while Giustino and Maren (2018) showed how the LC-NE system modulates Pavlovian conditioning and memory extinction. Therefore, our goal was to clarify whether (and to which extent) the moderate reduction in noradrenergic signalling we found happening with aging contributes to these cognitive deficits.

Our data clearly show that old C57BL/6J experience difficulty extinguishing fearful memory compared to young controls in the contextual fear conditioning test (**Figure 31**); this evidence is also in line with previous studies such as Battaglia et al. (2018) and Shoji et al. (2016). We could also demonstrate that old C57BL/6J show a meaningful impairment in working memory in the 5-CSRTT compared to young controls, linked to a lower choice accuracy (**Figure 32**). Thus, in order to understand the importance of the age-related cell loss identified in **3.1** and how much it contributes to these cognitive deficits, we induced in the LC of young mice the same rate of neurodegeneration that we detected in aging using the DSP-4 toxin (**3.7.1**, **Figure 30**), and tested them in the same battery of models. When performing the contextual fear conditioning test, we could not find any significant difference between DSP-4 treated and vehicle control animals in neither the process of fear learning nor extinction, indicating that the age-related neurodegeneration of LC neurons is not liable for the deficit in fear extinction characteristic of old age (**3.7.3**, **Figure 33**). Yet, when comparing DSP-4 treated and vehicle animals in the 5-CSRTT,

considerable differences emerged. In the first place, DSP-4 treated animals needed significantly more time to learn the task and to reach the last phase of the test compared to vehicle injected animals (**3.7.3**, **Figure 34 A**), indicating an impaired working memory. Once reached the last stage of the test, without any distraction the DSP-4 treated animals were able to perform in a comparable way with vehicle controls. However, interestingly, our data demonstrate that, when a distractor was introduced in the test, the DSP-4 treated mice showed a poorer choice accuracy, giving significantly fewer correct and more incorrect answers compared to controls which did not seem to be disturbed by it (**3.7.3**, **Figure 34 B–C**). In order to verify the effect of the DSP-4 toxin as cause of these differences, we performed a NET staining in prefrontal cortex through which we could detect a clear reduction in the amount of area covered by axon terminals in DSP-4 treated group compared to the vehicle control group (**3.7.3**, **Figure 35**).

Overall, these data clearly demonstrate that even a mild reduction of noradrenergic signalling is capable of influencing choice accuracy in the presence of a distractor and focus the attention on how important the noradrenergic signalling is in task-engagement and performance optimization. LC neurons are, in fact, often described as a “temporary attention filter” as they mediate the optimization of performances by setting the optimal arousal level for task-relevant situations (Aston-Jones and Cohen, 2005). In the presence of salient stimuli LC mediates the release of noradrenaline in the cortex enhancing the stimulus processing and increasing the signal-to-noise ratio (Aston-Jones et al., 1991, 1994; Sara, 2009).

Altogether, our data strengthen our hypothesis that the age-related 20 % reduction in LC neuronal number is directly responsible for the working memory and attention deficits occurring in elderly individuals and open a new window on the comprehension of the role played by the noradrenergic system in aging.

4.8. Conclusions

The locus coeruleus (LC) is a small nucleus in the pons of the brainstem representing the major source of noradrenaline (NE) in the central nervous system. It plays a crucial role in the regulation of numerous cognitive functions, including attention, memory as well as in the sleep–wake states and stress response. Recent evidences showed an age-related loss of noradrenergic neurons in healthy subjects, highlighting that the LC is a brain region

particularly vulnerable to age-related changes. There is a large body of evidence demonstrating that cannabinoid receptor 1 (CB1r) signaling modulates the activity of the LC. The immunoreactivity for CB1r within the LC was localized in somatodendritic structures, axon terminals, glial processes and on noradrenergic axon terminals. Moreover, CB1r deletion caused significant alterations of the electrophysiological properties of noradrenergic neurons such as an increase in LC-NE excitability and input resistance.

The present thesis work aimed to investigate the aging process of LC in C57BL/6J mice and to understand the role of the endocannabinoid system in the survival of these neurons. We found that in C57BL/6J mice the LC goes through an age-related neurodegenerative process beginning at the age of 8 months and that the rate of neuronal loss is higher in mice lacking of the CB1r ($Cnr1^{-/-}$). Accordingly, $Cnr1^{-/-}$ showed a lower noradrenergic innervation in the principal efferent areas of the LC such as cortex and hippocampus. In further support to the hypothesis that the endocannabinoid system plays a key role in the aging of this neuronal type, we found that DAGL enzyme increased with age selectively in noradrenergic neurons, in a timepoint subsequent to the onset of the neurodegenerative process, suggesting a protective role of it in the outlived neurons.

Furthermore, we found that the reduction in LC neurons that we found to be associated with aging is directly responsible for an impaired working memory and a greater distractibility in the execution of attention-required tasks.

4.9. Perspectives

The work discussed in this thesis sheds light on the aging process of the LC and on the role played by the eCBS. However, many questions remain unanswered. First of all, we observed a significant reduction in the number of the age-sensitive LC noradrenergic neurons in old $Cnr1^{-/-}$ mice; so we hypothesized that the increased neuronal loss in the LC of $Cnr1^{-/-}$ mice is a result of an accelerated brain aging due to the lack of neuroprotective effect of CB1r activity. However, we performed our experiments in a constitutive knock-out model which prevents us from establishing whether the protective effect of CB1r signalling on LC neurons is cell autonomous or not. To answer this question, we would need a mouse line with the knock-out of the CB1r selectively on noradrenergic neurons and then compare the onset and severity of neuronal loss in the LC, as well as

the reduction of noradrenergic terminals in the forebrain, between this line, wild-type and $Cnr1^{-/-}$ mice. As an additional control, we could use a CB1r knock-out mouse line and restore the CB1 signalling specifically within LC neurons. If the protective effect of CB1r was cell autonomous, the deletion of CB1r from LC noradrenergic neurons in wild-type animals would lead to a comparable pathology as observed in the constitutive $Cnr1^{-/-}$ mice, while CB1r knock-out mice with LC-specific restoration of CB1 signalling would show similar phenotype as wild-types.

During the thesis work, we tried to establish the mouse lines described above using the Cre/lox system. In detail, we used DBH-Cre mice (mice with the Cre recombinase under the dopamine beta-hydroxylase promoter), $CB1^{flox/flox}$ mice (mice with the Cnr1 gene flanked by two loxP sites; Cre-mediated recombination mediates the deletion of the gene) and $CB1^{STOP}$ mice (mice with a floxed STOP cassette inserted into the 5' UTR of the Cnr1 gene, abolishing its expression; Cre-mediated recombination removes the STOP cassette and rescues CB1 expression). Unfortunately, during the establishment of the mouse lines, we detected a germline expression of the Cre recombinase, which prevented us from obtaining the selective knock-out we were aiming for. To overcome the problem of a transient Cre expression in the germline, our next strategy will be using a Tamoxifen-inducible DBH-Cre line.

Another interesting question that the present thesis has brought up is whether it is possible to protect LC noradrenergic neurons by reversing their age-related changes through an elevation of CB1r signalling. Our lab has previously shown that elevation of the CB1r activity by chronic, low dose of the agonist THC reversed age-related changes in the hippocampus. We now ask whether the elevation of cannabinoid signalling is protective for LC neurons and reverse the expression of age-related genes in aged mice to the level of young mice. Therefore, our goal is to apply a chronic, low dose of THC before the onset of the LC age-related neurodegeneration and then compare the LC neuronal number, the density of the noradrenergic terminals in the forebrain and the transcriptome profile of noradrenergic neurons. To perform the transcriptome profiling, we will use the viral TRAP (translating ribosome affinity purification) technique, an innovative technique that allows to isolate RNA from rare cell populations. To conclude, altogether these experimental approaches may clarify many aspects about the vulnerability of LC neurons as well as the role of the endocannabinoid system in the process of brain aging.

5. Abstract

The locus coeruleus (LC) is a small nucleus located in the pons of the brainstem, representing the major source of noradrenaline (NE) in the central nervous system. Although the LC consists of a relatively low number of noradrenergic neurons, they widely innervate cortex, hippocampus, amygdala, hypothalamus and the brainstem itself. The LC plays a crucial role in the modulation of numerous cognitive functions including attention, memory, the regulation of sleep–wake states and the stress response. The peculiarity of noradrenergic neurons, in fact, is to act as a real attention filter switching from a tonic firing mode, related to a “low attention” stimulus, to a phasic firing mode, in response to relevant “focus-demanding” stimuli. It has been widely demonstrated that the LC undergoes structural changes in neurodegenerative diseases, however very little is known about changes in this region during physiological aging. A recent human in vivo study showed the presence of an age-related neurodegeneration of the LC in healthy adults, confirming this brain region as particularly susceptible to aging. Thus, LC seems to be expressly dependent on the activity of neuroprotective mechanisms to compensate for the factors contributing to its vulnerability: increased oxidative stress, pacemaking activity, high arborization, high load on mitochondria due to the big energetic need. Interestingly, all these factors are influenced by the endocannabinoid system, whose activity is thought to be neuroprotective and to influence aging. Yet, whether the endocannabinoid system has a protective effect on the survival of these neurons during aging is still not known. Thus, the aim of this thesis was to investigate the aging process of the LC and to comprehend the role that the endocannabinoid system plays in it.

We discovered that the LC of C57BL/6J mice goes through an age-related neurodegenerative process, as the number of noradrenergic neurons starts decreasing from 8 months of age, for a total 20 % reduction throughout life. We also found that the rate of neuronal loss was higher in animals lacking of the CB1r ($Cnr1^{-/-}$), indicating a crucial role of this receptor in the survival of noradrenergic neurons. Moreover, a lower number of noradrenergic neurons was associated with a reduced density of noradrenergic axon terminals in the main projecting areas of LC such as cortex and all the hippocampal subregions. Also in this case, the reduction was more severe in $Cnr1^{-/-}$ mice compared to wild-types, suggesting a poorer (if any) compensatory rate. This marked neuronal death

in Cnr1$^{-/-}$ animals was also associated with alterations in microglia morphology and mitophagic activity.

In further support to the hypothesis that the endocannabinoid system plays a key role in the aging process of this neuronal type, we found that DAGL enzyme increased with age selectively in noradrenergic neurons, in a timepoint subsequent to the onset of the neurodegenerative process, suggesting a protective role of it in the outlived neurons.

Furthermore, we investigated whether the age-related reduction in LC neurons that we identified could be directly responsible for the cognitive alterations in working memory, attention and memory extinction characteristic of old age. Our data clearly show that even this mild decrease in noradrenergic signalling can lead to an impairment in working memory and to a greater distractibility in the execution of attention-required tasks.

Overall, our data provide the basics for a better comprehension of the role of the noradrenergic system in brain aging and for a future exploration of the endocannabinoid system's potential as a new valuable therapeutic target.

6. List of figures

7. List of tables

8. References

Albayram O, Alferink J, Pitsch J, Piyanova A, Neitzert K, Poppensieker K, Mauer D, Michel K, Legler A, Becker A, Monory K, Lutz B, Zimmer A, Bilkei-Gorzo A. Role of CB1 cannabinoid receptors on GABAergic neurons in brain aging. Proc Natl Acad Sci U. S. A. 2011; 108(27): 11256–11261

Arnsten AF, Goldman-Rakic PS. Selective prefrontal cortical projections to the region of the locus coeruleus and raphe nuclei in the rhesus monkey. Brain Res 1984; 306(1-2): 9–18

Aston-Jones G, Chiang C, Alexinsky T. Discharge of noradrenergic locus coeruleus neurons in behaving rats and monkeys suggests a role in vigilance. Prog Brain Res 1991; 88: 501–520

Aston-Jones G, Cohen JD. An integrative theory of Locus Coeruleus-Norepinephrine function: adaptive gain and optimal performance. Annu Rev Neurosci 2005; 28: 403–450

Aston-Jones G, Rajkowski J, Kubiak P, Alexinsky T. Locus coeruleus neurons in monkey are selectively activated by attended cues in a vigilance task. J Neurosci 1994; 14(7): 4467–4480

Ativie F, Komorowska JA, Beins E, Albayram Ö, Zimmer T, Zimmer A, Tejera D, Heneka M, Bilkei-Gorzo A. Cannabinoid 1 Receptor Signaling on Hippocampal GABAergic Neurons Influences Microglial Activity. Front Mol Neurosci 2018; 11(295)

Bartova A, Birmingham MK. Effect of delta9-tetrahydrocannabinol on mitochondrial NADH-oxidase activity. J Biol Chem 1976; 251(16): 5002–5006

Battaglia S, Garofalo S, di Pellegrino G. Context-dependent extinction of threat memories: influences of healthy aging. Sci Rep 2018; 8(1): 12592

Beins EC, Beiert T, Jenniches I, Hansen JN, Leidmaa E, Schrickel JW, Zimmer A. Cannabinoid receptor 1 signalling modulates stress susceptibility and microglial responses to chronic social defeat stress. Transl Psychiatry 2021; 11(1): 164

Bénard G, Massa F, Puente N, Lourenço J, Bellocchio L, Soria-Gómez E, Matias I, Delamarre A, Metna-Laurent M, Cannich A, Hebert-Chatelain E, Mulle C, Ortega-Gutiérrez S, Martín-Fontecha M, Klugmann M, Guggenhuber S, Lutz B, Gertsch J, Chaouloff F, López-Rodríguez ML, Grandes P, Rossignol R, Marsicano G. Mitochondrial CB1 receptors regulate neuronal energy metabolism. Nat Neurosci 2012; 15(1): 558–564

Berrendero F, Romero J, García-Gil L, Suarez I, De la Cruz P, Ramos JA, Fernández-Ruiz JJ. Changes in cannabinoid receptor binding and mRNA levels in several brain regions of aged rats. Biochim Biophys Acta 1998; 1407(3): 205–214

Berridge CW, Waterhouse BD. The locus coeruleus–noradrenergic system: modulation of behavioral state and state-dependent cognitive processes. Brain Res Rev 2003; 42(1): 33–84

Bilkei-Gorzo A. The endocannabinoid system in normal and pathological brain ageing. Philos Trans R Soc B Biol Sci 2012a; 367(1607): 3326-3341

Bilkei-Gorzo A, Albayram O, Draffehn A, Michel K, Piyanova A, Oppenheimer H, Dvir-Ginzberg M, Rácz I, Ulas T, Imbeault S, Bab I, Schultze JL, Zimmer A. A chronic low dose of Δ9-tetrahydrocannabinol (THC) restores cognitive function in old mice. Nat Med 2017; 23(6): 782–787

Bilkei-Gorzo A, Drews E, Albayram Ö, Piyanova A, Gaffal E, Tueting T, Michel K, Mauer D, Maier W, Zimmer A. Early onset of aging-like changes is restricted to cognitive abilities and skin structure in Cnr1-/- mice. Neurobiol Aging 2012b; 33(1): 200.e11-200.e22

Bilkei-Gorzo A, Racz I, Valverde O, Otto M, Michel K, Sarstre M, Zimmer A. Early age-related cognitive impairment in mice lacking cannabinoid CB1 receptors. Proc Natl Acad Sci 2005; 102(43): 15670–15675

Braak H, Thal DR, Ghebremedhin E, Del Tredici K. Stages of the Pathologic Process in Alzheimer Disease: Age Categories From 1 to 100 Years. J Neuropathol Exp Neurol 2011; 70(11): 960–969

Braak H, Del Tredici K., Rüb U, de Vos RAI, Jansen Steur ENH, Braak E. Staging of brain pathology related to sporadic Parkinson's disease. Neurobiol Aging 2003; 24(2): 197–211

Brailoiu GC, Oprea TI, Zhao P, Abood ME, Brailoiu E. Intracellular Cannabinoid Type 1 (CB1) Receptors Are Activated by Anandamide. J Biol Chem 2011; 286(33): 29166–29174

Breton-Provencher V, Drummond GT, Sur M. Locus Coeruleus Norepinephrine in Learned Behavior: Anatomical Modularity and Spatiotemporal Integration in Targets. Front Neural Circuits 2021; 15: 1–11

Canas PM, Duarte JMN, Rodrigues RJ, Köfalvi A, Cunha RA. Modification upon aging of the density of presynaptic modulation systems in the hippocampus. Neurobiol Aging 2009; 30(11): 1877–1884

Castillo PE, Younts TJ, Chávez AE, Hashimotodani Y. Endocannabinoid signaling and synaptic function. Neuron 2012; 76(1): 70–81

Chevaleyre V, Heifets BD, Kaeser PS, Südhof TC, Castillo PE. Endocannabinoid-mediated long-term plasticity requires cAMP/PKA signaling and RIM1alpha. Neuron 2007; 54(5): 801–812

Chrobak JJ, DeHaven DL, Walsh TJ. Depletion of brain norepinephrine with DSP-4 does not alter acquisition or performance of a radial-arm maze task. Behav Neural Biol 1985; 44(1): 144–150

Devane WA, Hanus L, Breuer A, Pertwee RG, Stevenson LA, Griffin G, Gibson D, Mandelbaum A, Etinger A, Mechoulam R. Isolation and structure of a brain constituent that binds to the cannabinoid receptor. Science 1992; 258(5090): 1946-1949

Devane WA, Dysarz FA 3rd, Johnson MR, Melvin LS, Howlett AC. Determination and characterization of a cannabinoid receptor in rat brain. Mol Pharmacol 1988; 34(5): 605–613

Di Marzo V, Bifulco M, De Petrocellis L. The endocannabinoid system and its therapeutic exploitation. Nat Rev Drug Discov 2004; 3(9): 771–784

Di Marzo V, Stella N, Zimmer A. Endocannabinoid signalling and the deteriorating brain. Nat Rev Neurosci 2015; 16(1): 30–42

Eggan SM, Lewis DA. Immunocytochemical distribution of the cannabinoid CB1 receptor in the primate neocortex: a regional and laminar analysis. Cereb Cortex 2007; 17(1): 175–191

Eljaschewitsch E, Witting A, Mawrin C, Lee T, Schmidt PM, Wolf S, Hoertnagl H, Raine CS, Schneider-Stock R, Nitsch R, Ullrich O. The endocannabinoid anandamide protects neurons during CNS inflammation by induction of MKP-1 in microglial cells. Neuron 2006; 49(1): 67-79

Evans AK, Park HH, Saw NL, Singhal K, Ogawa G, Leib RD, Shamloo M. Age-related neuroinflammation and pathology in the locus coeruleus and hippocampus: beta-adrenergic antagonists exacerbate impairment of learning and memory in aged mice. Neurobiol Aging 2021; 106, 241–256

Fendt M, Koch M, Schnitzler HU. Amygdaloid noradrenaline is involved in the sensitization of the acoustic startle response in rats. Pharmacol Biochem Behav 1994; 48(2): 307–314

Flood DG, Coleman PD. Neuron numbers and sizes in aging brain: Comparisons of human, monkey, and rodent data. Neurobiol Aging 1988; 9(5-6): 453–463

Franceschi C, Garagnani P, Parini P, Giuliani C, Santoro A. Inflammaging: a new immune–metabolic viewpoint for age-related diseases. Nat Rev Endocrinol 2018; 14(10): 576–590

Gallily R, Breuer A, Mechoulam R. 2-Arachidonylglycerol, an endogenous cannabinoid, inhibits tumor necrosis factor-α production in murine macrophages, and in mice. Eur J Pharmacol 2000; 406(1):R5-7

Gannon M, Wang Q. Complex noradrenergic dysfunction in Alzheimer's disease: Low norepinephrine input is not always to blame. Brain Res 2019; 1702: 12–16

Gao Y, Vasilyev DV, Goncalves MB, Howell FV, Hobbs C, Reisenberg M, Shen R, Zhang MY, Strassle BW, Lu P, Mark L, Piesla MJ, Deng K, Kouranova EV, Ring RH, Whiteside

GT, Bates B, Walsh FS, Williams G, Pangalos MN, Samad TA, Doherty P. Loss of retrograde endocannabinoid signaling and reduced adult neurogenesis in diacylglycerol lipase knock-out mice. J Neurosci 2010; 30(6): 2017–2024

Gaoni Y, Mechoulam R. Isolation, Structure, and Partial Synthesis of an Active Constituent of Hashish. J Am Chem Soc 1964; 86(8): 1646–1647

Gaspar P, Berger B, Febvret A, Vigny A, Henry JP. Catecholamine innervation of the human cerebral cortex as revealed by comparative immunohistochemistry of tyrosine hydroxylase and dopamine-beta-hydroxylase. J Comp Neurol 1989; 279(2): 249–271

Gazzaley A, Cooney JW, Rissman J, D'Esposito M. Top-down suppression deficit underlies working memory impairment in normal aging. Nat Neurosci 2005; 8(10): 1298–1300

Ginsberg SD, Hof PR, Young WG, Morrison JH. Noradrenergic innervation of the hypothalamus of rhesus monkeys: distribution of dopamine-beta-hydroxylase immunoreactive fibers and quantitative analysis of varicosities in the paraventricular nucleus. J Comp Neurol 1993; 327(4): 597–611

Giubilei F, Calderaro C, Antonini G, Sepe-Monti M, Tisei P, Brunetti E, Marchione F, Caronti B, Pontieri FE. Increased lymphocyte dopamine beta-hydroxylase immunoreactivity in Alzheimer's disease: compensatory response to cholinergic deficit? Dement Geriatr Cogn Disord 2004; 18(3-4): 338–341

Giustino TF, Maren S. Noradrenergic Modulation of Fear Conditioning and Extinction. Front Behav Neurosci 2018; 12(43): 1–20

Gulyás B, Brockschnieder D, Nag S, Pavlova E, Kása P, Beliczai Z, Légrádi A, Gulya K, Thiele A, Dyrks T, Halldin C. The norepinephrine transporter (NET) radioligand (S,S)-[18F]FMeNER-D2 shows significant decreases in NET density in the human brain in Alzheimer's disease: a post-mortem autoradiographic study. Neurochem Int 2010; 56(6-7): 789–798

Hagan J, Alpert JE, Morris RG, Iversen SD. The effects of central catecholamine depletions on spatial learning in rats. Behav Brain Res 1983; 9(1): 83–104

Hammond TR, Dufort C, Dissing-Olesen L, Giera S, Young A, Wysoker A, Walker AJ, Gergits F, Segel M, Nemesh J, Marsh SE, Saunders A, Macosko E, Ginhoux F, Chen J, Franklin RJM, Piao X, McCarroll SA, Stevens B. Single-Cell RNA Sequencing of Microglia throughout the Mouse Lifespan and in the Injured Brain Reveals Complex Cell-State Changes. Immunity 2019; 50(1): 253-271.e6

Hebert-Chatelain E, Desprez T, Serrat R, Bellocchio L, Soria-Gomez E, Busquets-Garcia A, Pagano Zottola AC, Delamarre A, Cannich A, Vincent P, Varilh M, Robin LM, Terral G, García-Fernández MD, Colavita M, Mazier W, Drago F, Puente N, Reguero L, Elezgarai I, Dupuy JW, Cota D, Lopez-Rodriguez ML, Barreda-Gómez G, Massa F, Grandes P, Bénard G, Marsicano G. A cannabinoid link between mitochondria and memory. Nature 2016; 539(7630): 555–559

Heifets BD, Castillo PE. Endocannabinoid signaling and long-term synaptic plasticity. Annu Rev Physiol 2009; 71:283-306

Hendrickx DAE, van Eden CG, Schuurman KG, Hamann J, Huitinga I. Staining of HLA-DR, Iba1 and CD68 in human microglia reveals partially overlapping expression depending on cellular morphology and pathology. J Neuroimmunol 2017; 309: 12–22.

Herkenham M, Lynn AB, Little MD, Johnson MR, Melvin LS, de Costa BR, Rice KC. Cannabinoid receptor localization in brain. Proc Natl Acad Sci U S A 1990; 87(5): 1932-1936

Hou X, Fiesel FC, Truban D, Castanedes Casey M, Lin WL, Soto AI, Tacik P, Rousseau LG, Diehl NN, Heckman MG, Lorenzo-Betancor O, Ferrer I, Arbelo JM, Steele JC, Farrer MJ, Cornejo-Olivas M, Torres L, Mata IF, Graff-Radford NR, Wszolek ZK, Ross OA, Murray ME, Dickson DW, Springer W. Age- and disease-dependent increase of the mitophagy marker phospho-ubiquitin in normal aging and Lewy body disease. Autophagy 2018; 14(8): 1404-1418

Howlett AC, Barth F, Bonner TI, Cabral G, Casellas P, Devane WA, Felder CC, Herkenham M, Mackie K, Martin BR, Mechoulam R, Pertwee RG. International Union of Pharmacology. XXVII. Classification of cannabinoid receptors. Pharmacol Rev 2002; 54(2): 161-202

Jenniches I, Ternes S, Albayram O, Otte DM, Bach K, Bindila L, Michel K, Lutz B, Bilkei-Gorzo A, Zimmer A. Anxiety, Stress, and Fear Response in Mice With Reduced Endocannabinoid Levels. Biol Psychiatry 2016; 79(10): 858-868

Kalaria RN, Andorn AC, Tabaton M, Whitehouse PJ, Harik SI, Unnerstall JR. Adrenergic receptors in aging and Alzheimer's disease: increased beta 2-receptors in prefrontal cortex and hippocampus. J Neurochem 1989; 53(6):1772-1781

Kano M, Ohno-Shosaku T, Hashimotodani Y, Uchigashima M, Watanabe M. Endocannabinoid-mediated control of synaptic transmission. Physiol Rev 2009; 89(1): 309-380

Kaplan BL, Ouyang Y, Rockwell CE, Rao GK, Kaminski NE. 2-Arachidonoyl-glycerol suppresses interferon-gamma production in phorbol ester/ionomycin-activated mouse splenocytes independent of CB1 or CB2. J Leukoc Biol 2005; 77(6): 966-74

Kataoka K, Bilkei-Gorzo A, Nozaki C, Togo A, Nakamura K, Ohta K, Zimmer A, Asahi T. Age-dependent Alteration in Mitochondrial Dynamics and Autophagy in Hippocampal Neuron of Cannabinoid CB1 Receptor-deficient Mice. Brain Res Bull 2020;160: 40-49

Kawamura Y, Fukaya M, Maejima T, Yoshida T, Miura E, Watanabe M, Ohno-Shosaku T, Kano M. The CB1 cannabinoid receptor is the major cannabinoid receptor at excitatory presynaptic sites in the hippocampus and cerebellum. J Neurosci 2006; 26(11): 2991-3001

Kisler K, Nelson AR, Montagne A, Zlokovic BV. Cerebral blood flow regulation and neurovascular dysfunction in Alzheimer disease. Nat Rev Neurosci 2017; 18(7): 419-434

Kokkinidis L, Anisman H. Involvement of norepinephrine in startle arousal after acute and chronic d-amphetamine administration. Psychopharmacology (Berl) 1978; 59(3): 285-292

Leslie FM, Loughlin SE, Sternberg DB, McGaugh JL, Young LE, Zornetzer SF. Noradrenergic changes and memory loss in aged mice. Brain Res 1985; 359(1-2): 292-299

Levine B, Svoboda E, Hay JF, Winocur G, Moscovitch M. Aging and autobiographical memory: dissociating episodic from semantic retrieval. Psychol Aging 2002; 17(4): 677-689

Lier J, Streit WJ, Bechmann I. Beyond Activation: Characterizing Microglial Functional Phenotypes. Cells 2021; 10(9): 2236

Liu KY, Acosta-Cabronero J, Cardenas-Blanco A, Loane C, Berry AJ, Betts MJ, Kievit RA, Henson RN, Düzel E; Cam-CAN, Howard R, Hämmerer D. In vivo visualization of age-related differences in the locus coeruleus. Neurobiol Aging 2019; 74:101-111

Long LE, Lind J, Webster M, Weickert CS. Developmental trajectory of the endocannabinoid system in human dorsolateral prefrontal cortex. BMC Neurosci 2012; 13: 87

López-Otín C, Blasco MA, Partridge L, Serrano M, Kroemer G. The hallmarks of aging. Cell 2013; 153(6): 1194-1217

Maccarrone M, Attinà M, Bari M, Cartoni A, Ledent C, Finazzi-Agrò A. Anandamide degradation and N-acylethanolamines level in wild-type and CB1 cannabinoid receptor knockout mice of different ages. J Neurochem 2001; 78(2): 339-348

Maccarrone M, Bab I, Bíró T, Cabral GA, Dey SK, Di Marzo V, Konje JC, Kunos G, Mechoulam R, Pacher P, Sharkey KA, Zimmer A. Endocannabinoid signaling at the periphery: 50 years after THC. Trends Pharmacol Sci 2015; 36(5): 277-296

Maccarrone M, Valverde O, Barbaccia ML, Castañé A, Maldonado R, Ledent C, Parmentier M, Finazzi-Agrò A. Age-related changes of anandamide metabolism in CB1 cannabinoid receptor knockout mice: correlation with behaviour. Eur J Neurosci 2002; 15(7): 1178-1186

Manaye KF, McIntire DD, Mann DM, German DC. Locus coeruleus cell loss in the aging human brain: a non-random process. J Comp Neurol 1995; 358(1): 79-87

Martins RS, de Freitas IG, Sathler MF, Martins VPPB, Schitine CS, da Silva Sampaio L, Freitas HR, Manhães AC, Dos Santos Pereira M, de Melo Reis RA, Kubrusly RCC. Beta-adrenergic receptor activation increases GABA uptake in adolescent mice frontal cortex: Modulation by cannabinoid receptor agonist WIN55,212-2. Neurochem Int 2018; 120: 182-190

Mather M, Clewett D, Sakaki M, Harley CW. Norepinephrine ignites local hotspots of neuronal excitation: How arousal amplifies selectivity in perception and memory. Behav Brain Sci 2016; 39: e200

Mather M, Harley CW. The Locus Coeruleus: Essential for Maintaining Cognitive Function and the Aging Brain. Trends Cogn Sci 2016; 20(3): 214-226

Matsuda LA, Lolait SJ, Brownstein MJ, Young AC, Bonner TI. Structure of a cannabinoid receptor and functional expression of the cloned cDNA. Nature 1990; 346(6284): 561-564

Mechoulam R, Ben-Shabat S, Hanus L, Ligumsky M, Kaminski NE, Schatz AR, Gopher A, Almog S, Martin BR, Compton DR, et al. Identification of an endogenous 2-monoglyceride, present in canine gut, that binds to cannabinoid receptors. Biochem Pharmacol 1995; 50(1): 83-90

Mechoulam R, Parker LA. The endocannabinoid system and the brain. Annu Rev Psychol 2013; 64: 21-47

Morrison JH, Molliver ME, Grzanna R. Noradrenergic innervation of cerebral cortex: widespread effects of local cortical lesions. Science 1979; 205(4403): 313-316

Mouton PR, Pakkenberg B, Gundersen HJ, Price DL. Absolute number and size of pigmented locus coeruleus neurons in young and aged individuals. J Chem Neuroanat 1994; 7(3): 185-190

Mulder J, Zilberter M, Pasquaré SJ, Alpár A, Schulte G, Ferreira SG, Köfalvi A, Martín-Moreno AM, Keimpema E, Tanila H, Watanabe M, Mackie K, Hortobágyi T, de Ceballos

ML, Harkany T. Molecular reorganization of endocannabinoid signalling in Alzheimer's disease. Brain 2011; 134(Pt 4): 1041-1060

Munro S, Thomas KL, Abu-Shaar M. Molecular characterization of a peripheral receptor for cannabinoids. Nature 1993; 365(6441): 61-65

Navarrete M, Araque A. Endocannabinoids mediate neuron-astrocyte communication. Neuron 2008; 57(6): 883-893

Ohm TG, Busch C, Bohl J. Unbiased estimation of neuronal numbers in the human nucleus coeruleus during aging. Neurobiol Aging 1997; 18(4): 393-399

Ordureau A, Heo JM, Duda DM, Paulo JA, Olszewski JL, Yanishevski D, Rinehart J, Schulman BA, Harper JW. Defining roles of PARKIN and ubiquitin phosphorylation by PINK1 in mitochondrial quality control using a ubiquitin replacement strategy. Proc Natl Acad Sci U S A 2015; 112(21): 6637-6642

Oropeza VC, Page ME, Van Bockstaele EJ. Systemic administration of WIN 55,212-2 increases norepinephrine release in the rat frontal cortex. Brain Res 2005; 1046(1-2): 45-54

Ortega-Gutiérrez S, Molina-Holgado E, Guaza C. Effect of anandamide uptake inhibition in the production of nitric oxide and in the release of cytokines in astrocyte cultures. Glia 2005; 52(2): 163-168

Ouyang Y, Hwang SG, Han SH, Kaminski NE. Suppression of interleukin-2 by the putative endogenous cannabinoid 2-arachidonyl-glycerol is mediated through down-regulation of the nuclear factor of activated T cells. Mol Pharmacol 1998; 53(4): 676-683

Páldy E, Bereczki E, Sántha M, Wenger T, Borsodi A, Zimmer A, Benyhe S. CB(2) cannabinoid receptor antagonist SR144528 decreases mu-opioid receptor expression and activation in mouse brainstem: role of CB(2) receptor in pain. Neurochem Int 2008; 53(6-8): 309-316

Pammer C, Görcs T, Palkovits M. Peptidergic innervation of the locus coeruleus cells in the human brain. Brain Res 1990; 515(1-2): 247-255

Pamphlett R. Uptake of environmental toxicants by the locus ceruleus: a potential trigger for neurodegenerative, demyelinating and psychiatric disorders. Med Hypotheses 2014; 82(1): 97-104

Panikashvili D, Simeonidou C, Ben-Shabat S, Hanus L, Breuer A, Mechoulam R, Shohami E. An endogenous cannabinoid (2-AG) is neuroprotective after brain injury. Nature 2001; 413(6855): 527-531

Pascual AC, Gaveglio VL, Giusto NM, Pasquaré SJ. Aging modifies the enzymatic activities involved in 2-arachidonoylglycerol metabolism. Biofactors 2013; 39(2): 209-220

Piyanova A, Lomazzo E, Bindila L, Lerner R, Albayram O, Ruhl T, Lutz B, Zimmer A, Bilkei-Gorzo A. Age-related changes in the endocannabinoid system in the mouse hippocampus. Mech Ageing Dev 2015; 150: 55-64

Plescher M, Seifert G, Hansen JN, Bedner P, Steinhäuser C, Halle A. Plaque-dependent morphological and electrophysiological heterogeneity of microglia in an Alzheimer's disease mouse model. Glia 2018; 66(7): 1464-1480

Poe GR, Foote S, Eschenko O, Johansen JP, Bouret S, Aston-Jones G, Harley CW, Manahan-Vaughan D, Weinshenker D, Valentino R, Berridge C, Chandler DJ, Waterhouse B, Sara SJ. Locus coeruleus: a new look at the blue spot. Nat Rev Neurosci 2020; 21(11): 644-659

Prado de Carvalho L, Zornetzer SF. The involvement of the locus coeruleus in memory. Behav Neural Biol 1981; 31(2): 173-186

Radley JJ, Williams B, Sawchenko PE. Noradrenergic innervation of the dorsal medial prefrontal cortex modulates hypothalamo-pituitary-adrenal responses to acute emotional stress. J Neurosci 2008; 28(22): 5806-5816

Reddy PH, Oliver DM. Amyloid Beta and Phosphorylated Tau-Induced Defective Autophagy and Mitophagy in Alzheimer's Disease. Cells 2019; 8(5): 488

Robertson IH. A noradrenergic theory of cognitive reserve: implications for Alzheimer's disease. Neurobiol Aging 2013; 34(1): 298-308

Romero-Sandoval EA, Horvath R, Landry RP, DeLeo JA. Cannabinoid receptor type 2 activation induces a microglial anti-inflammatory phenotype and reduces migration via MKP induction and ERK dephosphorylation. Mol Pain 2009; 5: 25

Romero J, Berrendero F, Garcia-Gil L, de la Cruz P, Ramos JA, Fernández-Ruiz JJ. Loss of cannabinoid receptor binding and messenger RNA levels and cannabinoid agonist-stimulated [35S]guanylyl-5'O-(thio)-triphosphate binding in the basal ganglia of aged rats. Neuroscience 1998; 84(4): 1075-1083

Rossi F, Tortora C, Punzo F, Bellini G, Argenziano M, Di Paola A, Torella M, Perrotta S. The Endocannabinoid/Endovanilloid System in Bone: From Osteoporosis to Osteosarcoma. Int J Mol Sci 2019; 20(8): 1919

Rozenfeld R, Devi LA. Regulation of CB1 cannabinoid receptor trafficking by the adaptor protein AP-3. FASEB J 2008; 22(7): 2311-2322

Ruiz J, Martín I, Callado LF, Meana JJ, Barturen F, García-Sevilla JA. Non-adrenoceptor [3H]idazoxan binding sites (I2-imidazoline sites) are increased in postmortem brain from patients with Alzheimer's disease. Neurosci Lett 1993; 160(1): 109-112

Sadikot AF, Parent A. The monoaminergic innervation of the amygdala in the squirrel monkey: an immunohistochemical study. Neuroscience 1990; 36(2): 431-447

Saitoh K, Shaw S, Tilson HA. Noradrenergic influence on the prepulse inhibition of acoustic startle. Toxicol Lett 1986; 34(2-3): 209-216

Sanchez-Padilla J, Guzman JN, Ilijic E, Kondapalli J, Galtieri DJ, Yang B, Schieber S, Oertel W, Wokosin D, Schumacker PT, Surmeier DJ. Mitochondrial oxidant stress in locus coeruleus is regulated by activity and nitric oxide synthase. Nat Neurosci 2014; 17(6): 832-840

Sara SJ. The locus coeruleus and noradrenergic modulation of cognition. Nat Rev Neurosci 2009; 10(3): 211-223

Satoh A, Iijima KM. Roles of tau pathology in the locus coeruleus (LC) in age-associated pathophysiology and Alzheimer's disease pathogenesis: Potential strategies to protect the LC against aging. Brain Res 2019; 1702: 17-28

Scavone JL, Mackie K, Van Bockstaele EJ. Characterization of cannabinoid-1 receptors in the locus coeruleus: relationship with mu-opioid receptors. Brain Res 2010; 1312: 18-31

Schuele LL, Glasmacher S, Gertsch J, Roggan MD, Transfeld JL, Bindila L, Lutz B, Kolbe CC, Bilkei-Gorzo A, Zimmer A, Leidmaa E. Diacylglycerol lipase alpha in astrocytes is involved in maternal care and affective behaviors. Glia 2021; 69(2): 377-391

Schuele LL, Schuermann B, Bilkei-Gorzo A, Gorgzadeh S, Zimmer A, Leidmaa E. Regulation of adult neurogenesis by the endocannabinoid-producing enzyme diacylglycerol lipase alpha (DAGLa). Sci Rep 2022; 12(1): 633

Sharma Y, Xu T, Graf WM, Fobbs A, Sherwood CC, Hof PR, Allman JM, Manaye KF. Comparative anatomy of the locus coeruleus in humans and nonhuman primates. J Comp Neurol 2010; 518(7): 963-971

Shoji H, Takao K, Hattori S, Miyakawa T. Age-related changes in behavior in C57BL/6J mice from young adulthood to middle age. Mol Brain 2016; 9: 1-18

Stella N. Endocannabinoid signaling in microglial cells. Neuropharmacology 2009; 56 Suppl 1: 244-253

Straiker A, Mackie K. Depolarization-induced suppression of excitation in murine autaptic hippocampal neurones. J Physiol 2005; 569(Pt 2): 501-517

Sturrock RR, Rao KA. A quantitative histological study of neuronal loss from the locus coeruleus of ageing mice. Neuropathol Appl Neurobiol 1985; 11(1): 55-60

Sugama S, Takenouchi T, Hashimoto M, Ohata H, Takenaka Y, Kakinuma Y. Stress-induced microglial activation occurs through β-adrenergic receptor: noradrenaline as a key neurotransmitter in microglial activation. J Neuroinflammation 2019; 16(1): 266

Szot P, Van Dam D, White SS, Franklin A, Staufenbiel M, De Deyn PP. Age-dependent changes in noradrenergic locus coeruleus system in wild-type and APP23 transgenic mice. Neurosci Lett 2009; 463(1): 93-97

Szot P, White SS, Greenup JL, Leverenz JB, Peskind ER, Raskind MA. Changes in adrenoreceptors in the prefrontal cortex of subjects with dementia: evidence of compensatory changes. Neuroscience 2007; 146(1): 471-480

Szot P, White SS, Greenup JL, Leverenz JB, Peskind ER, Raskind MA. Compensatory changes in the noradrenergic nervous system in the locus ceruleus and hippocampus of postmortem subjects with Alzheimer's disease and dementia with Lewy bodies. J Neurosci 2006; 26(2): 467-478

Tatton WG, Greenwood CE, Verrier MC, Holland DP, Kwan MM, Biddle FE. Different rates of age-related loss for four murine monoaminergic neuronal populations. Neurobiol Aging 1991; 12(5): 543-556

Tham CS, Whitaker J, Luo L, Webb M. Inhibition of microglial fatty acid amide hydrolase modulates LPS stimulated release of inflammatory mediators. FEBS Lett 2007; 581(16): 2899-2904

Theofilas P, Dunlop S, Heinsen H, Grinberg LT. Turning on the Light Within: Subcortical Nuclei of the Isodentritic Core and their Role in Alzheimer's Disease Pathogenesis. J Alzheimers Dis 2015; 46(1): 17-34

Twarkowski H, Manahan-Vaughan D. Loss of Catecholaminergic Neuromodulation of Persistent Forms of Hippocampal Synaptic Plasticity with Increasing Age. Front Synaptic Neurosci 2016; 8: 30

Uchigashima M, Narushima M, Fukaya M, Katona I, Kano M, Watanabe M. Subcellular arrangement of molecules for 2-arachidonoyl-glycerol-mediated retrograde signaling and its physiological contribution to synaptic modulation in the striatum. J Neurosci 2007; 27(14): 3663-3676

Wang L, Liu J, Harvey-White J, Zimmer A, Kunos G. Endocannabinoid signaling via cannabinoid receptor 1 is involved in ethanol preference and its age-dependent decline in mice. Proc Natl Acad Sci U S A 2003; 100(3): 1393-1398

Wang M, Gamo NJ, Yang Y, Jin LE, Wang XJ, Laubach M, Mazer JA, Lee D, Arnsten AF. Neuronal basis of age-related working memory decline. Nature 2011; 476(7359): 210-213

Wang S, Wang Z, Mu Y. Locus Coeruleus in Non-Mammalian Vertebrates. Brain Sci 2022; 12(2): 134

Weinshenker D. Long Road to Ruin: Noradrenergic Dysfunction in Neurodegenerative Disease. Trends Neurosci 2018; 41(4): 211-223

Westlund KN, Craig AD. Association of spinal lamina I projections with brainstem catecholamine neurons in the monkey. Exp Brain Res 1996; 110(2): 151-162

Westlund KN, Coulter JD. Descending projections of the locus coeruleus and subcoeruleus/medial parabrachial nuclei in monkey: axonal transport studies and dopamine-beta-hydroxylase immunocytochemistry. Brain Res 1980; 2(3): 235-264

Wyrofsky RR, Reyes BAS, Van Bockstaele EJ. Co-localization of the cannabinoid type 1 receptor with corticotropin-releasing factor-containing afferents in the noradrenergic nucleus locus coeruleus: implications for the cognitive limb of the stress response. Brain Struct Funct 2017; 222(7): 3007-3023

Wyrofsky RR, Reyes BAS, Zhang XY, Bhatnagar S, Kirby LG, Van Bockstaele EJ. Endocannabinoids, stress signaling, and the locus coeruleus-norepinephrine system. Neurobiol Stress 2019; 11: 100176

Zimmer A, Zimmer AM, Hohmann AG, Herkenham M, Bonner TI. Increased mortality, hypoactivity, and hypoalgesia in cannabinoid CB1 receptor knockout mice. Proc Natl Acad Sci U S A 1999; 96(10): 5780-5785

9. Acknowledgements

A PhD is never just the data you get, just a title. My PhD is the people who made it possible, who turned such an achievement into a path towards personal growth.

An initial thanks goes to Prof. Dr. Andreas Zimmer for giving me the chance to work in an environment of scientific (besides human) excellence. Thanks also to Prof. Dr. Mauro Maccarrone, Prof. Dr. med. Michael Heneka and Prof. Dr. Gaia Tavosanis for being part of my thesis committee, for the encouragement and the rewarding scientific discussions through the years.

Of all the special people who have been a part of my journey, the biggest thanks goes certainly to Dr. Andras Bilkei-Gorzo as he truly represented for me what a *Doktorvater* (literally, doctor father) is supposed to be: a constant support and a kindness that is seldom found in the world we are used to live in. Thanks for teaching me everything I know and for believing in me. Without his guidance, none of this would have been possible.

Thanks to Dr. Este Leidmaa for always being a focal point of positivity and hope.

Thanks to my PhD teammates, Lena, Joanna, Bolanle Fatimat and Michela for the practical and emotional support throughout all the way.

Thanks also to Anne, Edda and Kerstin for all the help I have received.

Thanks to all my students for giving me the chance to see myself in a new light.

Thanks to my best friend Teresa for being always on my side, reminding me that distance is only a number and that true friendship doesn't understand math. Watching each other grow up and see the women we are becoming is an amazing gift.

Thanks also to the family I choose here in Bonn: Alberto, Mario and Federica. You taught me that, although not feeling alone is sometimes the most difficult challenge, we win together and we always will.

Thanks to Simone for being a brotherly ever-present friend, willing to listen and support me at every step of the way.

Thanks to Nina and Nora for turning a house into a safe and lovely place, into my home.

Finally, thanks to the family that can be here, my mother Mariella, my brother Claudio, my grandparents Teresa and Annino, and thanks to the family that can't, my father Rolando: it's all for and thanks to you.

10. List of publications

Gargano A, Beins E, Zimmer A, Bilkei-Gorzo A. **Lack of Cannabinoid Receptor Type-1 Leads to Enhanced Age-Related Neuronal Loss in the Locus Coeruleus.** Int J Mol Sci 2020; 22(1): 5. https://doi.org/10.3390/ijms22010005

Nocchi L, Portulano C, Franciosa F, Doleschall B, Panea M, Roy N, Maffei M, **Gargano A**, Perlas E, Heppenstall PA. **Nerve growth factor-mediated photoablation of nociceptors reduces pain behavior in mice.** Pain 2019; 160(10): 2305-2315. http://dx.doi.org/10.1097/j.pain.0000000000001620